SANDIA REPORT

SAND2011-7287
Unlimited Release
Printed July, 2011

Summary Compilation of Shell Element Performance versus Formulation

S.W. Key, N.L. Breivik, M.W. Heinstein and J.D. Hales

Prepared by
Sandia National Laboratories
Albuquerque, New Mexico 87185 and Livermore, California 94550

Sandia National Laboratories is a multi-program laboratory managed and operated by Sandia Corporation, a wholly owned subsidiary of Lockheed Martin Corporation, for the U.S. Department of Energy's National Nuclear Security Administration under Contract DE-AC04-94AL85000.

Approved for public release; further dissemination unlimited.

Sandia National Laboratories

Issued by Sandia National Laboratories, operated for the United States Department of Energy by Sandia Corporation.

NOTICE: This report was prepared as an account of work sponsored by an agency of the United States Government. Neither the United States Government, nor any agency thereof, nor any of their employees, nor any of their contractors, subcontractors, or their employees, make any warranty, express or implied, or assume any legal liability or responsibility for the accuracy, completeness, or usefulness of any information, apparatus, product, or process disclosed, or represent that its use would not infringe privately owned rights. Reference herein to any specific commercial product, process, or service by trade name, trademark, manufacturer, or otherwise, does not necessarily constitute or imply its endorsement, recommendation, or favoring by the United States Government, any agency thereof, or any of their contractors or subcontractors. The views and opinions expressed herein do not necessarily state or reflect those of the United States Government, any agency thereof, or any of their contractors.

Printed in the United States of America. This report has been reproduced directly from the best available copy.

Available to DOE and DOE contractors from
U.S. Department of Energy
Office of Scientific and Technical Information
P.O. Box 62
Oak Ridge, TN 37831

Telephone: (865) 576-8401
Facsimile: (865) 576-5728
E-Mail: reports@adonis.osti.gov
Online ordering: http://www.osti.gov/bridge

Available to the public from
U.S. Department of Commerce
National Technical Information Service
5285 Port Royal Rd
Springfield, VA 22161

Telephone: (800) 553-6847
Facsimile: (703) 605-6900
E-Mail: orders@ntis.fedworld.gov
Online ordering: http://www.ntis.gov/help/ordermethods.asp?loc=7-4-0#online

SAND2011-7287
Unlimited Release
Printed July, 2011

Summary Compilation of Shell Element Performance versus Formulation

Samuel W. Key
FMA Development, LLC
1005 39th Ave. NE
Great Falls, MT 59404

Nicole L. Breivik
Solid Mechanics Department
Martin W. Heinstein
Computational Solid Mechanics and Structural Dynamics Department
Sandia National Laboratories
P.O. Box 5800
Albuquerque, NM 87185-0836

Jason Hales
Idaho National Laboratory
P.O. Box 1625
Idaho Falls, ID 83415

Abstract

This document compares the finite element shell formulations in the Sierra Solid Mechanics code. These are finite elements either currently in the Sierra simulation codes Presto and Adagio, or expected to be added to them in time. The list of elements are divided into traditional two-dimensional, plane stress shell finite elements, and three-dimensional solid finite elements that contain either modifications or additional terms designed to represent the bending stiffness expected to be found in shell formulations. These particular finite elements are formulated for finite deformation and inelastic material response, and, as such, are not based on some of the elegant formulations that can be found in an elastic, infinitesimal finite element setting. Each shell element is subjected to a series of 12 verification and validation test problems. The underlying purpose of the tests here is to identify the quality of both the spatially discrete finite element gradient operator and the spatially discrete finite element divergence operator. If the derivation of the finite element is proper, the discrete divergence operator is the transpose of the discrete gradient operator. An overall summary is provided from which one can rank, at least in an average sense, how well the individual formulations can be expected to perform in applications encountered year in and year out. A letter grade has been assigned albeit sometimes subjectively for each shell element and each test problem result. The number of A's, B's, C's, *et cetera* assigned have been totaled, and a grade point average (GPA) has been computed, based on a 4.0-system. These grades, combined with a comparison between the test problems and the application problem, can be used to guide an analyst to select the element with the best shell formulation.

Acknowledgment

The authors would like to thank Nathan Crane for the irregular mesh flat-plate test problem. It is an important discriminator of element performance that was missing from the original test-problem suite. Our interactions with Nathan Crane and the results of his own testing were illuminating. Documenting the work was instrumental is improving the understanding of the existing algorithms and selective modifications made in the formulations to improve the performance of certain shell elements during the documentation phase. For the this we must thank Joseph Jung for requiring the documentation and the financial support for undertaking the initial testing and final documentation.

Contents

1 Shell Element Formulations **13**

1.1 Overview 13

1.2 Shell Element Brief Descriptions 14

1.2.1 2-D Shell Elements 14

1.2.2 3-D Shell Elements 15

2 Testing Perspective **19**

3 Shell Test Suite Results **21**

3.1 Test Problem 1: Cantilever Beam 22

3.2 Test Problem 2: Twisted Beam 27

3.3 Test Problem 3: Point-Loaded Hemisphere 31

3.4 Test Problem 4: Raasch Hook 34

3.5 Test Problem 5: Beam Bent into a Ring 40

3.6 Test Problem 6: Irons Membrane Patch Test 45

3.7 Test Problem 7: Inflated Sphere Patch Test 50

3.8 Test Problem 8: Pinched Cylinder 59

3.9 Test Problem 9: Vibrating Plate 67

3.10 Test Problem 10: Crushed Spherical Shell 73

3.11 Test Problem 11: Element Shape Sensitivity 82

3.11.1 3-D Hexahedral Shell Elements 82

3.11.2 2-D Quadrilateral Shell Elements 87

3.12 Test Problem 12: Thick Shell to Thin Shell Transition 91

4 Evaluation Summary **95**

4.0.1 Overview 95

4.0.2 Comments on Individual Formulations 97

5 Supporting Literature **101**

5.1 Finite Element Formulations 101

5.1.1 ESH8, Simo-Rifai Enhanced Strain Hexahedron 101

5.1.2 K1H8, Key-Gullerud-Koteras Plane-Stress Hexahedron 102

5.1.3 K2H8, Key-Gullerud-Koteras Multi-Stress Hexahedron 103

5.1.4 TSH8, Wing Kam Liu Thick Shell Hexahedron 103

5.1.5 SDH8, Selective Deviatoric Hexahedron 103

5.1.6 KHQ4, Key-Hoff Plane-Stress Quadrilateral 104

5.1.7 KGQ4, Key-Gruda Plane-Stress Quadrilateral 104

5.1.8 NCT3, Node-Centered Plane-Stress Triangle 105

5.1.9 ECT3, Element-Centered Plane-Stress Triangle 107

5.2 Reference Solutions 107

List of Figures

3.1 Test Problem 1, 3-D Solid Hexahedral Mesh 22

3.2 Test Problem 1, 2-D Planar Quadrilateral and Triangular Meshes 23

3.3 Test Problem 1, 3-D Deformed Hexahedral Mesh 24

3.4 Test Problem 1, 3-D Solid Shell Deflection Response 25

3.5 Test Problem 1, 2-D Planar Shell Deflection Response 26

3.6 Test Problem 2, 3-D Hexahedral Shell Mesh 27

3.7 Test Problem 2, 2-D Planar Quadrilateral Mesh 28

3.8 Test Problem 2, 3-D Solid Element Shell Deflection Response 29

3.9 Test Problem 2, 2-D Planar Element Shell Deflection Response 30

3.10 Test Problem 3, 3-D Hexahedral Shell Element Mesh 31

3.11 Test Problem 3, 2-D Planar Shell Meshes 33

3.12 Test Problem 4, 3-D Hexahedral Shell Mesh 34

3.13 Test Problem 4, 3-D Deformed Hexahedral Mesh 35

3.14 Test Problem 4, 2-D Planar Quadrilateral and Triangular Shell Meshes 36

3.15 Test Problem 5, 3-D Solid Hexahedral Shell Mesh 40

3.16 Test Problem 5, 2-D Planar Shell Meshes 43

3.17 Test Problem 5, Final Circular Ring Configuration 43

3.18 Test Problem 5, Intermediate Circular Ring Configuration At 15 ms 44

3.19 Test Problem 6, Solid Hexahedral Irons Patch Test Mesh 45

3.20 Test Problem 6, Shell Quadrilateral and Triangular Meshes 46

3.21 Test Problem 6, ESH8 Displacement u_x Contours 49

3.22 Test Problem 7, Solid Hexahedral Mesh 50

3.23 Test Problem 7, Quadrilateral and Triangular Shell Element Meshes 51

3.24 Test Problem 7, Pressure Distribution for ESH8 57

3.25 Test Problem 7, Pressure Distribution for KHQ4 58

3.26 Test Problem 8, Solid Hexahedral Mesh 59

3.27 Test Problem 8, Deformed Solid Hexahedral Mesh 60

3.28 Test Problem 8, Shell Quadrilateral and Triangular Meshes 61

3.29 Test Problem 8, Hauptman, Schweizerhof, and Doll Results 63

3.30 Test Problem 8, Solid Load-Deflection Curves 64

3.31 Test Problem 8, Shell Load-Deflection Curves 65

3.32 Test Problem 8, Solid Mesh Final Cylinder Configuration 66

3.33 Test Problem 8, Shell Mesh Final Cylinder Configuration 66

3.34 Test Problem 9, Soild Hexahedral Mesh 67

3.35 Test Problem 9, Shell Quadrilateral Mesh 68

3.36 Test Problem 9, Shell Triangular Mesh 70

3.37 Test Problem 9, Solid ESH8 Vibrational Response 71

3.38 Test Problem 9, Shell KHQ4 Vibrational Response 72

3.39 Test Problem 10, Shell Quadrilateral Mesh 73

3.40 Test Problem 10, Sphere Collapsed by Opposing Plattens 74

3.41 Test Problem 10, Solid ESH8 Crushed Sphere Lobe Pattern 76

3.42 Test Problem 10, Solid K1H8 Crushed Sphere Lobe Pattern 76

3.43 Test Problem 10, Solid K2H8 Crushed Sphere Lobe Pattern 77

3.44 Test Problem 10, Solid TSH8 Crushed Sphere Lobe Pattern 77

3.45 Test Problem 10, Solid SDH8 Crushed Sphere Lobe Pattern 78

3.46 Test Problem 10, Shell KHQ4 Crushed Sphere Lobe Pattern 78

3.47 Test Problem 10, Shell KGQ4 Crushed Sphere Lobe Pattern 79

3.48 Test Problem 10, Shell NCT3 Crushed Sphere Lobe Pattern 79

3.49 Test Problem 10, Shell ECT3 Crushed Sphere Lobe Pattern 80

3.50 Test Problem 10, Energy *vs* Deflection for K1H8, KHQ4, KGQ4, and NCT3 . . 81

3.51 Test Problem 11, Solid Hexahedral Mesh 82

3.52 Test Problem 11, Reference Results From Simo and Rifai ESH8 83

3.53 Test Problem 11, Random Axial Nodal Points, One Layer 84

3.54 Test Problem 11, Random Axial Nodal Points, Two Layer 85

3.55 Test Problem 11, TSH8 Wing Kam Liu Thick Shell Results 86

3.56 Test Problem 11, Irregular Quadrilateral Meshes 87

3.57 Test Problem 11, Contours for Regular and Irregular Fine Mesh 89

3.58 Test Problem 11, Contours for Regular and Irregular Fine Mesh 90

3.59 Test Problem 12, Solid Hexahedral Meshes 91

5.1 Quadrilateral Enhanced Strain Modes 101

Chapter 1

Shell Element Formulations

1.1 Overview

The following is a list of the shell element formulations addressed in this summary. The list is divided into traditional two-dimensional, plane stress shell finite elements, and three-dimensional solid finite elements that contain either modifications or additional terms designed to represent the bending stiffness expected to be found in shell formulations. These are finite elements either currently in the Sierra simulation codes Presto and Adagio, or expected to be added to them in time. These particular finite elements are formulated for finite deformation and inelastic material response, and, as such, are not based on some of the elegant formulations that can be found in an elastic, infinitesimal finite element setting.

- 2-D Plane-Stress Formulations

KHQ4	Key-Hoff	4-Node Quadrilateral
KGQ4	Key-Gruda	4-Node Quadrilateral
NCT3	Node Centered	3-Node Triangle
ECT3	Element Centered	3-Node Triangle

- 3-D Multi-Stress Formulations

ESH8	Simo-Rifai Enhanced Strain	3-D Multi-Stress Hexahedron
K1H8	Key-Gullerud-Koteras	2-D Plane-Stress Hexahedron
K2H8	Key-Gullerud-Koteras	3-D Multi-Stress Hexahedron
TSH8	Wing Kam Liu Thick Shell	3-D Multi-Stress Hexahedron
SDH8	Selective Deviatoric	3-D Multi-Stress Hexahedron

The following table, Table 1-1, relates these element formulations to what is currently available in the Sierra applications Presto and Adagio. The table includes current and future key words for those formulations expected to be implemented.

TABLE 1-1: Presto/Adagio Formulation Keywords

Name	Section type	Formulation keyword	Status
KHQ4	`Shell Section`	`Formulation = KH_Shell`	Wrk
KGQ4	`Shell Section`	`Formulation = KG_Shell`	Nyi
NCT3	`Shell Section`	`Formulation = NC_Shell`	Nyi
ECT3	`Shell Section`	`Formulation = EC_Shell` (default)	Wrk
ESH8	`Solid Section`	`Formulation = Enhanced_Strain`	Wrk
K1H8	`Solid Section`	`Formulation = HexShell`	Brk
K2H8	`Solid Section`	`Formulation =`	Tbd
TSH8	`Solid Section`	`Formulation = ThickShell`	Wrk
SDH8	`Solid Section`	`Formulation = Selective_Deviatoric`	Wrk
		`Deviatoric Parameter = <value>`	Wrk

(Wrk = Working; Brk = Broken; Nyi = Not yet implemented; Tbd = To be determined)

1.2 Shell Element Brief Descriptions

1.2.1 2-D Shell Elements

All of the following 2-D shell finite elements at each vertex node have three translational degrees of freedom and three rotational degrees of freedom, that is, translational movement along the three x, y, z-coordinate axises u_x, u_y, and u_z, respectively, and rotational degrees of freedom ω_x, ω_y, and ω_z about the x,y,z-coordinate axises, respectively, following a *right-hand rule*. For transient dynamic applications, velocities and accelerations are also included for all of these degrees of freedom.

KHQ4: Key-Hoff 4-node quadrilateral. The Key-Hoff finite element is based on a Mindlin-Reissner transverse shear shell theory and a bi-linear interpolation of displacements and rotations at the four vertex nodal points. To obtain the membrane and bending stress resultants that drive the equations of motion, a one-dimensional numerical integration in the thickness direction is used; plane-stress constitutive models are evaluated at each numerical quadrature location. The element contains a classical transverse shear correction factor of 5/6. When the finite element becomes thin (the element's aspect ration L/t becomes large[2]), the transverse shear correction factor becomes a 'Lagrange multiplier' that depends on the element's aspect ratio L/t and limits the build up of transverse-shear strain energy that would otherwise cause the element to lock.

KGQ4: Key-Gruda 4-node quadrilateral. The KGQ4 Key-Gruda plane-stress 4-node quadrilateral shell finite element is a formulation that employs the hexahedral solid shell internals of the K1H8 solid 8-node finite element. However, it escapes the need to use nettlesome

[2] A shell finite element's aspect ratio is defined as $L/t = \sqrt{Area}/thickness$

through-thickness kinematic constraints. In addition, it employs nodal-based common fiber vectors (initially surface normal vectors that have been rotated in time using nodal point rotational rates) in the time-step-by-time-step reconstruction of the internal hexahedral frame. To obtain the membrane and bending stress resultants that drive the equations of motion, a one-dimensional numerical integration in the thickness direction is used; plane-stress constitutive models are evaluated at each numerical quadrature location. The element contains a classical transverse shear correction factor of 5/6. When the finite element becomes thin, the transverse shear correction factor becomes a 'Lagrange multiplier' that depends on the element's aspect ratio L/t and limits the build up of transverse-shear strain energy that would otherwise cause the element to lock. In its current form, the element also uses an areal integration on the middle surface to obtain the bilinear distribution needed for the *constant* bending stress resultant M_{rs} expected by the Mindlin-Reissner transverse shear shell theory.

ECT3: Element Centered 3-node triangle. The Element Centered finite element is based on a Mindlin-Reissner transverse shear shell theory and a linear interpolation of displacements and rotations at the three vertex nodal points. To obtain the membrane and bending stress resultants that drive the equations of motion, a one-dimensional numerical integration in the thickness direction is used *within the finite element*; plane-stress constitutive models are evaluated at each numerical quadrature location. The element contains a classical transverse shear correction factor of 5/6. When the finite element becomes thin (L/t large), the transverse shear correction factor becomes a 'Lagrange multiplier' that depends on on the element's aspect ratio L/t and limits the build up of transverse-shear strain energy that would otherwise cause the element to lock.

NCT3: Node Centered 3-node triangle. The Node Centered finite element is based on a Mindlin-Reissner transverse shear shell theory and a linear interpolation of displacements and rotations at the three vertex nodal points. To obtain the membrane and bending stress resultants that drive the equations of motion, a one-dimensional numerical integration in the thickness direction is used *at each nodal point*; plane-stress constitutive models are evaluated at each numerical quadrature location. The element contains a classical transverse shear correction factor of 5/6. The element does not exhibit shear locking and, therefore, does not contain any other factors for large values of L/t.

1.2.2 3-D Shell Elements

All of the following finite elements at each vertex node have three translational degrees of freedom, that is, translational movement along the three x, y, z-coordinate axises u_x, u_y, and u_z, respectively. For transient dynamic applications, velocities and accelerations are also included for all of these degrees of freedom.

ESH8: Simo-Rifai Enhanced Strain, 8-node, 3-D multi-stress hexahedron. The Simo-Rifai 3-D multi-stress hexahedral element is based on a tri-linear interpolation of displacements at the eight vertex nodal points. Improved bending characteristics are obtained from internal

enhanced strain modes. The enhanced strain modes are statically determined based on minimum strain-energy. The element is rather shape sensitive.

K1H8: Key-Gullerud-Koteras 8-node, 2-D plane-stress hexahedron. The Key-Gullerud-Koteras 2-D plane-stress hexahedral element is based on a tri-linear interpolation of displacements at the eight vertex nodal points. The bending characteristics are derived from a Mindlin-Reissner transverse shear shell theory. *Plane-stress constitutive relations are used.* The equations of motion are driven by the mean stress, the linear variation of lateral stress through the thickness, and a linear variation in transverse shear stress components in the in-plane directions of the element. Plane-stress constitutive models require the use of independently specified through-thickness kinematic constraints at each corner of the element.

K2H8: Key-Gullerud-Koteras 8-node, 3-D multi-stress hexahedron. The Key-Gullerud-Koteras 3-D multi-stress hexahedral element is based on a tri-linear interpolation of displacements at the eight vertex nodal points. The bending characteristics are derived from a Mindlin-Reissner transverse shear shell theory. *Three-dimensional constitutive relations are used.* The equations of motion are driven by the mean stress, the linear variation of lateral stress through the thickness, and a linear variation in transverse shear stress components in the in-plane directions of the element, plus a bi-linear variation of stress normal to the middle-plane of the element, that is, in the thickness direction. Classical plane-stress results are obtained as a limiting condition to the extent allowed by boundary conditions and and interactions between adjacent layers. In explicit transient dynamic simulations, the critical time step can depend on the thickness dimension.

TSH8: Liu Thick Shell 8-node, 3-D multi-stress hexahedron. The Liu Thick Shell 3-D multi-stress hexahedral element is based on a tri-linear interpolation of displacements at the eight vertex nodal points. It is an 'almost' mean-strain finite element to which has been added a selected number of additional strain modes gotten from a Taylor series expansion about the center of the element. In its published form, a decimated $2 \times 2 \times 2$ Gauss numerical quadrature is proposed that, however, gives an artificially skewed response; a full $2 \times 2 \times 2$ Gauss quadrature is to be preferred. The element is rather shape sensitive. Note: All results presented here using this finite element utilize two finite elements in the thickness direction unless otherwise noted. The bending response for a single layer is about a factor of 2 too soft.

SDH8: Selective Deviatoric 8-node, 3-D multi-stress hexahedron. The Selective Deviatoric 3-D multi-stress hexahedral element is based on a tri-linear interpolation of displacements at the eight vertex nodal points. The element uses reduced integration, that is, only a mean quadrature bulk strain is computed and used followed by only using a mean-quadrature pressure for the equations of motion. The element is not necessarily tuned for bending; it was conceived as an element using physically based hour-glass control and to that end contains a parameter that allows the non-mean quadrature deviatoric stress components to be scaled down. The element has *no preferred orientation* that can be associated with in-plane membrane behavior, out-of-plane bending behavior, or transverse shear behavior – concepts and terms common with shell formulations. It is included here only to document its behavior in

beam bending and shell bending applications.

Chapter 2

Testing Perspective

The underlying purpose of the tests here is to identify the quality of both the spatially discrete finite element gradient operator and the spatially discrete finite element divergence operator. (If the derivation of the finite element is proper, the discrete divergence operator is the transpose of the discrete gradient operator.)

Though used here, explicit central difference time integration is not being tested here and is, in fact, counted upon to not be a factor in any of the results reported here. Discrete explicit central difference time integration is a technology that goes back to the origins of computational mechanics in the 1940's and is now well understood and has been routinely implemented in any number of finite difference and finite element codes over the past 70 years. A number of the test problems use vibrational results to differentiate one finite element from another, but the frequency content (usually close to a first mode response) is very low compared to the highest frequencies that the temporal integration can handle accurately.

The material models used are either elastic or perfectly-plastic, both of which use simple, reliable incremental integration schemes. Coupled with the tiny step sizes dictated by the conditionally stable explicit central difference temporal integration scheme, the material integration algorithms are more accurate than the gradient/divergence operators being tested. While some of the test problems have decidedly non-infinitesimal strains and rotations, they are not large enough to bring into question the the suitability of the invariant stress flux algorithms or their implementation.

Several of the test problems involve no more than infinitesimal strains and displacements, and might easily bring into question whether they are useful test problems for finite elements intended for simulations that require large deformations and strains. But, what is significant is the identification of the reduced capabilities that come from a departure from a regular mesh lined up with the coordinate system. In this regard, the Irons Patch Test is very significant even though it is routinely used with small displacements. It examines how well a small collection (five to fifteen) of very irregularly shaped finite elements can reproduce a uniform strain state. The irregularity of the finite elements used in the Irons Patch Test is typical of what would occur to a regular mesh under large deformations. The Irons Patch Test is the opposite to asking the question of how well can a refined uniform mesh approximate a complex solution (a less significant question).

The Irons Patch Test is fundamental; it is a go/no-go test. If a finite element fails to reproduce the uniform strain/stress state, then the discrete gradient calculation is defective. The next step after the first-order uniform strain Irons Patch Test is a second-order linear strain Irons Patch Test. The second-order linear strain test can reveal the shape sensitivity of the element; one of the test problems utilizes this concept.

Chapter 3

Shell Test Suite Results

Throughout the following plots for the individual shell test problems, the same color coding for the overlayed curves will be used.

- 2-D Plane-Stress Formulations

Green	KHQ4	Key-Hoff	4-Node Quadrilateral
Magenta	KGQ4	Key-Gruda	4-Node Quadrilateral
Blue	NCT3-table	Node Centered	3-Node Triangle
Gray	NCT3-tuned	Node Centered	3-Node Triangle
Red	ECT3	Element Centered	3-Node Triangle

- 3-D Multi-Stress Formulations

Black	ESH8	Simo-Rifai enhanced strain	3-D Multi-Stress Hexah
Green	K1H8	Key-Gullerud-Koteras	2-D Plane-Stress Hexah
Blue	K2H8	Key-Gullerud-Koteras	3-D Multi-Stress Hexah
Red	TSH8	Wing Kam Liu Thick Shell	3-D Multi-Stress Hexah
Gray	SDH8	Selective Deviatoric	3-D Multi-Stress Hexah

Note that 'NCT3-table' refers to tuning parameters obtained internally from a tabulated-function interpolation of tuning-parameters *vs* aspect-ratio based on five selected shell test problems, while 'NCT3-tuned' refers to tuning parameters identified for the individual test problem for which the results are being plotted.

3.1 Test Problem 1: Cantilever Beam

Test Problem Statement. The beam, pictured in Figure 3.1, has a length of 10 inches, a depth of 1 inch, and a width of 0.5 inches. The boundary conditions are those of a cantilevered beam, namely, zero displacement and zero rotation at the root (far end), Figure 3.1.

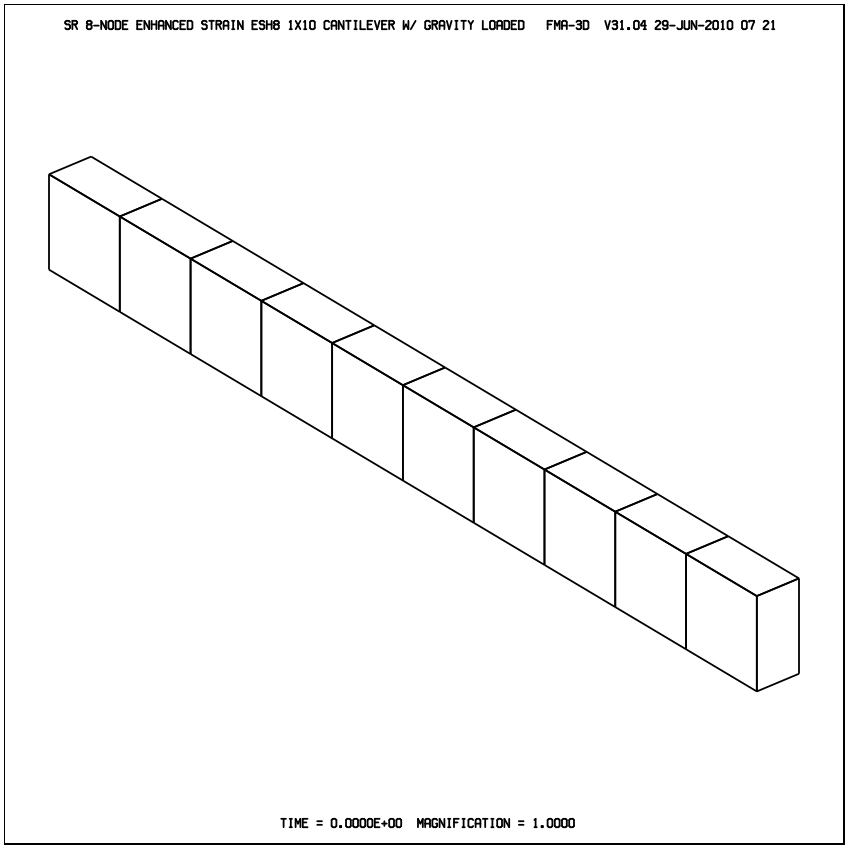

Figure 3.1. Beam mesh consisting of a single strip of ten 8-node hexahedral solid elements.

The loading is a constant gravity loading of 600 g's applied at time equal to zero. (A "1 g" gravity loading equals a body force in $\text{lb}_\text{f}/\text{in}^3$ of $\rho \times 386$ in/sec^2.)

The material is elastic with a Young's modulus of $E = 1.0 \times 10^{+6}$ psi, a Poisson's ratio of $\nu = 0.25$, and a density of $\rho = 2.61 \times 10^{-4}$ lb_f-sec^2/in^4.

Shown in Figure 3.2 are the shell finite element meshes used. The triangular shell element mesh has a symmetry boundry condition along one edge that removes an otherwise asymmetric and inadequate response generated by this "biased" triangular element pattern.

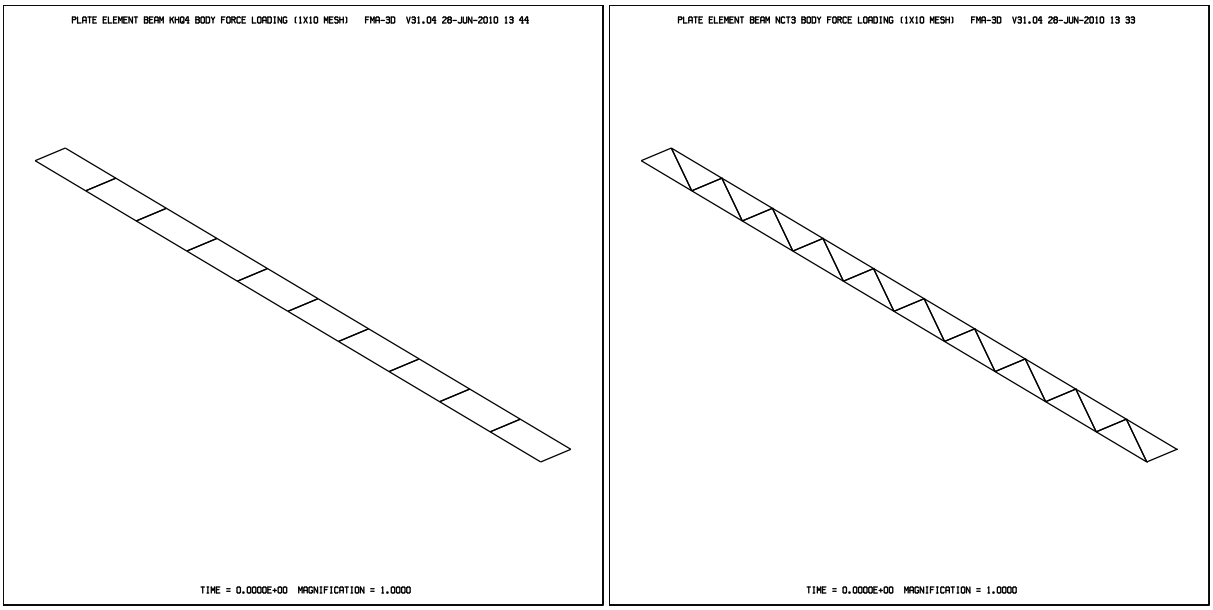

Figure 3.2. Beam mesh consisting of a single strip of 4-node quadrilateral shell elements (left panel); beam mesh consisting of a single strip of 3-node triangular shell elements (right panel). The 1 inch depth dimension is represnted by a 1 inch thickness specification for each shell element.

Test Problem Characteristics. The problem is an elementry one-dimensional bending test, and any finite element that is intended to represent the bending of beams, plates, or shells using a mesh with only one finite element through the thickness needs to provide satisfactory results on this problem. Of course, by their very nature quadrilateral and triangler shell finite elements use only a surface to represent a beam, plate, or shell, and carry the beam depth, plate thickness, or shell thickness as an "internal" geometric parameter.

Test Problem Results. Shown in Figure 3.3 is the $1\times1\times10$ hexahedral solid finite element mesh at both time equal to zero and the time of maximum tip deflection, 5.6 ms.

Shown in Figure 3.4 is the tip deflection *vs* time for the ESH8 Simo-Rifai Enhanced Strain 8-node, solid hexahedron (a solution that matches the 10-element beam reference solution), the K1H8 Key-Gullerud-Koteras 8-node, plane stress hexahedron, the K2H8 Key-Gullerud-Koteras 8-node, multi stress hexahedron, the SDH8 Selective Deviatoric 8-node hexahedron, and the TSH8 Wing Kam Liu Thick-Shell 8-node hexahedron. Note that the ESH8 Simo-Rifai reference solution, a black curve, is overlayed by the K1H8 green curve.

The element rank ordering here is ESH8, K1H8, K2H8, TSH8 with a double layer mesh, SDH8.

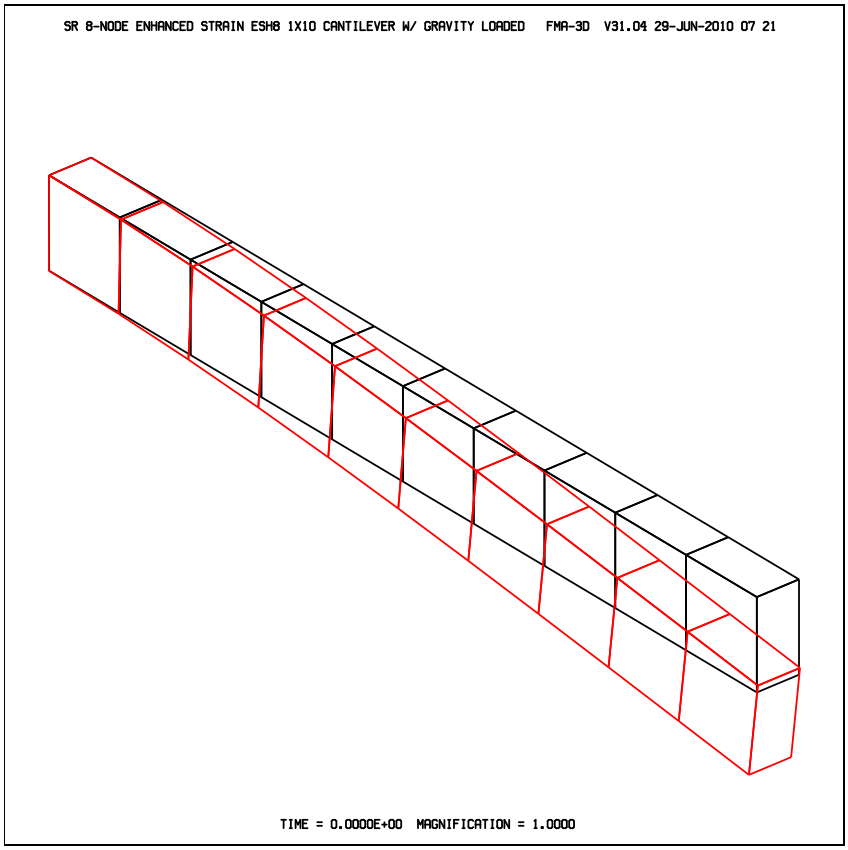

Figure 3.3. Beam mesh consisting of a single strip of 8-node hexahedral solid elements; the peak dynamic deflected shape at 5.6 ms is depicted by the red mesh.

Shown in Figure 3.5 is the tip deflection *vs* time for the KHQ4 Key-Hoff 4-node quadrilateral element, the NCT3 Node-Centered 3-node triangle using hand-tuned parameters of 0.17 and 0.17 for membrane and bending, respectively, the NCT3 Node-Centered 3-node triangle using internal table-look-up tuning parameters, and the ECT3 Element Centered 3-node triangle.

The element rank ordering here is KHQ4, NCT3-tuned, NCT3-table, ECT3. The ECT3 Element Centered 3-node triangle response is the stiffest (lowest amplitude, highest frequency) finite element as expected.

Simulation Notes. For the hexahederal and quadrilateral meshes and associated underlying element isoparameteric coordinates, the bending solution, and the coordinate axises are all aligned. The net result is essentially a one-dimensional test, that is, there are no "off-diagonal" terms that are required to obtain the expected results. Any finite element that fits this descrip-

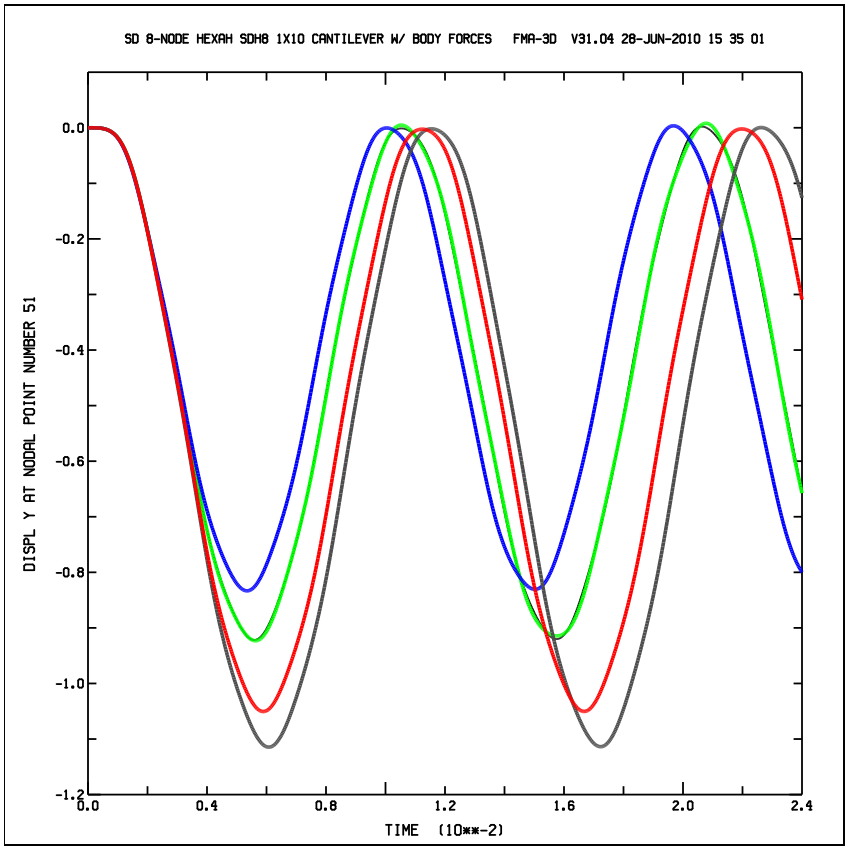

Figure 3.4. Beam vertical tip deflection histories for the 3-D solid finite elements. The solid element ordering by color here is ESH8, K1H8, K2H8, TSH8, SDH8. Note that the ESH8 Simo-Rifai reference solution, a black curve, is overlayed by the K1H8 green curve.

tion (all of them except the triangular elements) and that does not do well on this test problem cannot be expected to do better in a more complex setting.

On the other hand for the simple triangular finite elements here (the NCT3 Node Centered 3-node triangular finite element, and the ECT3 Element Centered 3-node triangular finite element), this test problem is already a complex problem because there is no natural alignments between finite element derivation, local axises or bending solution. For the node centered NCT3 it is even worse because the nodal averaging algorithm is nearly defeated by the one element wide strip mesh. Only through the use of a symmetry plane along one of the lateral edges do the element algorithms have enough information to "find" the beam bending solution. The result portends the advice that triangular shell finite elements should be used only where the narrow dimension of a two-dimensional surface is meshed with several elements.

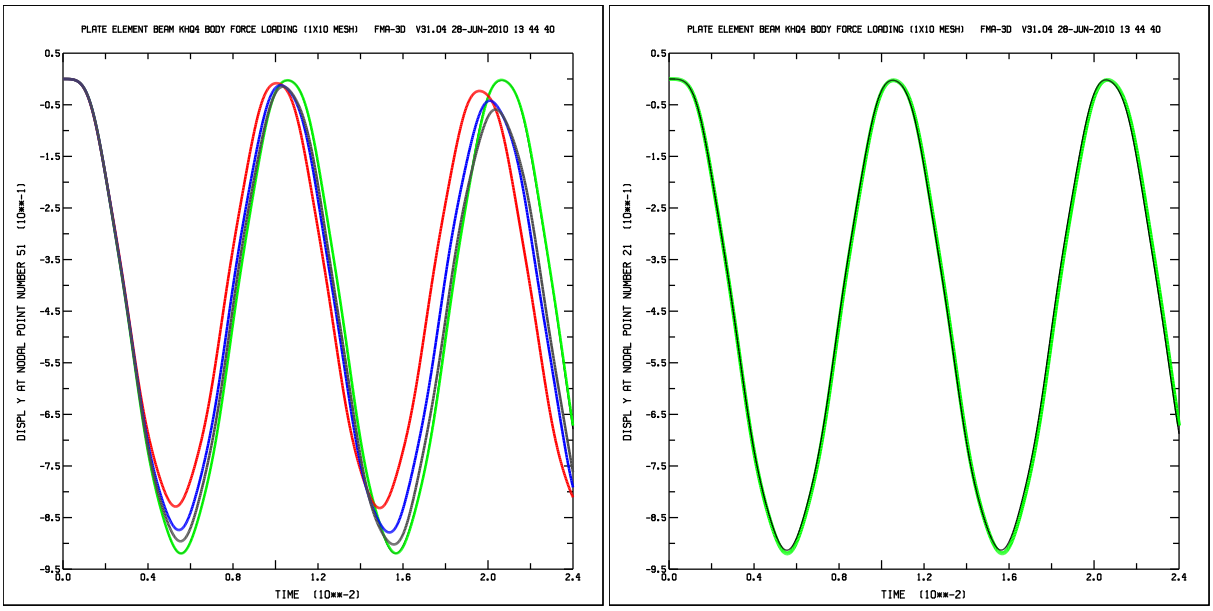

Figure 3.5. In the left panel, beam vertical tip deflection histories for four of the five 2-D shell finite elements. The shell element ordering by color here is KHQ4, NCT3-tuned, NCT3, ECT3. Note that a 10-element beam reference solution, a black curve, is overlayed by the KHQ4 green curve. In the right panel, beam vertical tip deflection histories for the KGQ4 Key-Gruda plane-stress finite element based on K1H8 internals employing surface fiber vectors (initially surface normal vectors that have been rotated in time using nodal point rotational rates) for geometry definition (thin black line) compared to the KHQ4 results (wide green line).

3.2 Test Problem 2: Twisted Beam

Test Problem Statement. The twisted beam, pictured in Figure 3.6, has a length of 12 inches, a depth of 0.32 inchs, and a width of 1.1 inches. The beam's cross-section is rectangular, but rotates by 90-degrees from a horizontal rectangular cross-section to a vertical rectangular cross-section by the time the end of the beam is reached (near end). The boundary conditions are those of a cantilevered beam, namely, zero displacement and zero rotation at the root (far end), Figure 3.6.

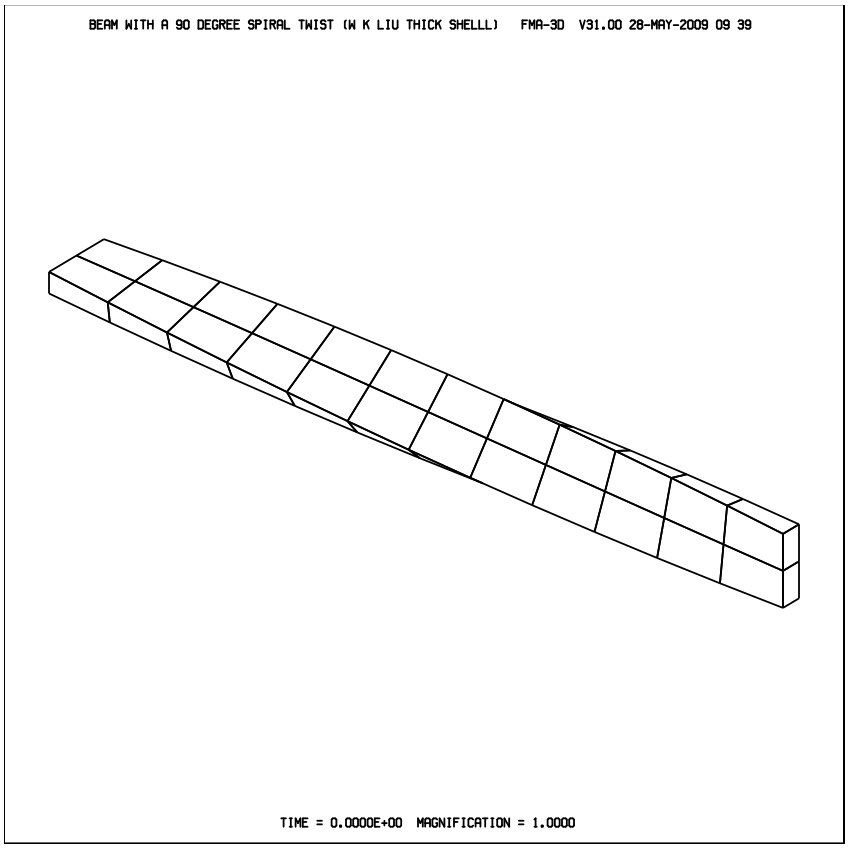

Figure 3.6. Twisted Beam mesh consisting of a $1\times2\times12$ strip of 8-node hexahedral solid elements.

The loading is a constant vertical shear loading of 1.0 lb_f applied uniformly over the beam's cross-section at the tip at time equal to zero, and held constant.

The material is elastic with a Young's modulus of $E = 2.9\times10^{+7}$ psi, a Poisson's ratio of $\nu = 0.22$, and a density of $\rho = 2.5\times10^{-4}$ $\text{lb}_\text{f}\text{-sec}^2/\text{in}^4$.

Shown in Figure 3.6 is the $1\times2\times12$ hexahedral solid finite element mesh at time equal to zero. The small deflections of this test problem do not provide a useful overlayed deformed mesh.

Shown in Figures 3.7 are the shell finite element meshes used. The quadrilateral mesh has 24 finite elements and the triangular mesh has 48 finite elements.

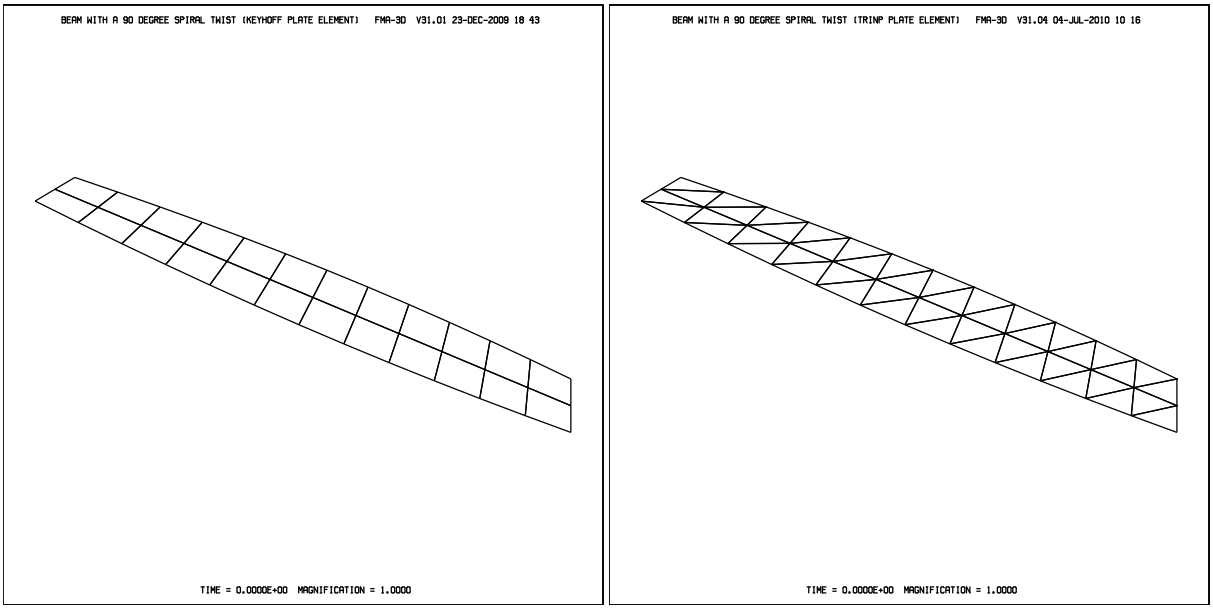

Figure 3.7. Twisted Beam mesh consisting of a double strip of 4-node quadrilateral shell elements (left panel). The 0.32 inch depth dimension is represnted by a 0.32 inch thickness specification for each shell element. Twisted Beam mesh consisting of a double strip of 3-node triangular shell element pairs (right panel)

Test Problem Characteristics. The test problem geometry is a non-planar warped geometry. The significance of the warped geometry is particularly important to the 2-D shell finite elements. At the clamped end of the beam, the solution is classical beam bending. At the loaded end of the beam, the vertical shear load is applied as an in-plane or membrane traction. The geometry assumptions incorporated into the finite element formulation are the determining factor that allows the solution to transition from membrane shear to bending at the root. Early shell finite elements assumed a "flat" geometry and a single fixed orientation of the surface normal vector in their formulation. The result was minimal or no "connection" between the tip load and the clamped support at the other end. Hence, this problem is primarily a test of the geometry constructs incorporated in the finite element's derivation.

Test Problem Results. Shown in Figure 3.8 is the tip deflection *vs* time for the ESH8 Simo-Rifai enhanced strain 8-node, solid hexahedron (reference solution), the K1H8 Key-

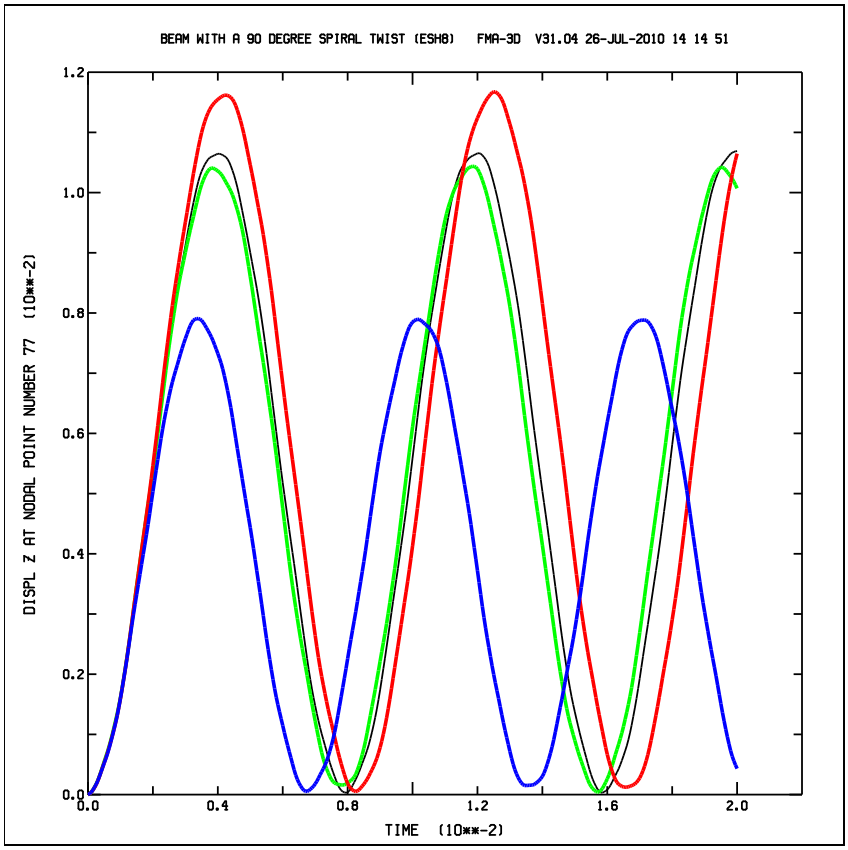

Figure 3.8. Twisted Beam vertical tip deflection histories for the 3-D solid finite elements. The solid element ordering by color here is ESH8, K1H8, TSH8 with a double layered mesh, K2H8, Note that the ESH8 Simo-Rifai reference solution, a black curve, is partially overlayed by the K1H8 green curve.

Gullerud-Koteras 8-node, plane stress hexahedron, the TSH8 Wing Kam Liu Thick-Shell 8-node hexahedron, and the K2H8 Key-Gullerud-Koteras 8-node, multi stress hexahedron. Note that the SDH8 finite element is omitted because of an overly stiff response.

The element rank ordering here is ESH8, K1H8, TSH8 with a double layer mesh, K2H8.

Shown in Figure 3.9 is the tip deflection *vs* time for the KHQ4 Key-Hoff 4-node quadrilateral element, the NCT3 Node-Centered 3-node triangle using the internal table-look-up tuning parameters of 0.2 and 0.2 for membrane and bending, respectively, and the ECT3 Element-Centered 3-node triangle. Note that the ESH8 Simo-Rifai reference solution, a black curve, is nearly overlayed by the KHQ4 green curve.

The element rank ordering here is KGQ4, KHQ4, NCT3, and ECT3.

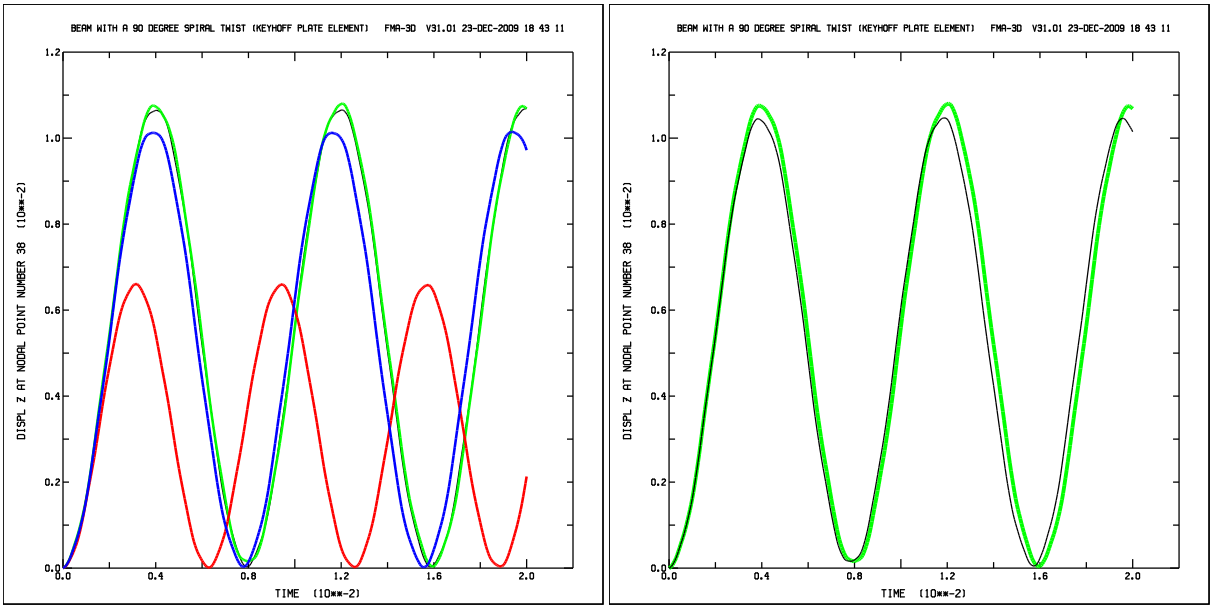

Figure 3.9. In the left panel, twisted Beam vertical tip deflection histories for three of the four 2-D shell finite elements. The shell element ordering by color here is KHQ4, NCT3, ECT3 (left panel). Note that the ESH8 Simo-Rifai reference solution, a black curve, is nearly overlayed by the KHQ4 green curve. In the right panel, twisted Beam vertical tip deflection histories for the KGQ4 Key-Gruda plane-stress finite element based on K1H8 internals employing surface fiber vectors (initially surface normal vectors that have been rotated in time using nodal point rotational rates) for geometry definition (thin black line) compared to the KHQ4 results (wide green line).

3.3 Test Problem 3: Point-Loaded Hemisphere

Test Problem Statement. The hemisphere, pictured in Figure 3.10, has a radius of 10 inches and a thickness of 0.04 inches. The hemisphere is incomplete in that it has an 18-degree polar angle opening at the "top." The hemisphere (half of a sphere) is modeled using a 90-degree sector and symmetry boundary conditions prescribing zero displacement normal to the symmetry plane and restricting the rotation to be around an axis normal to the symmetry plane.

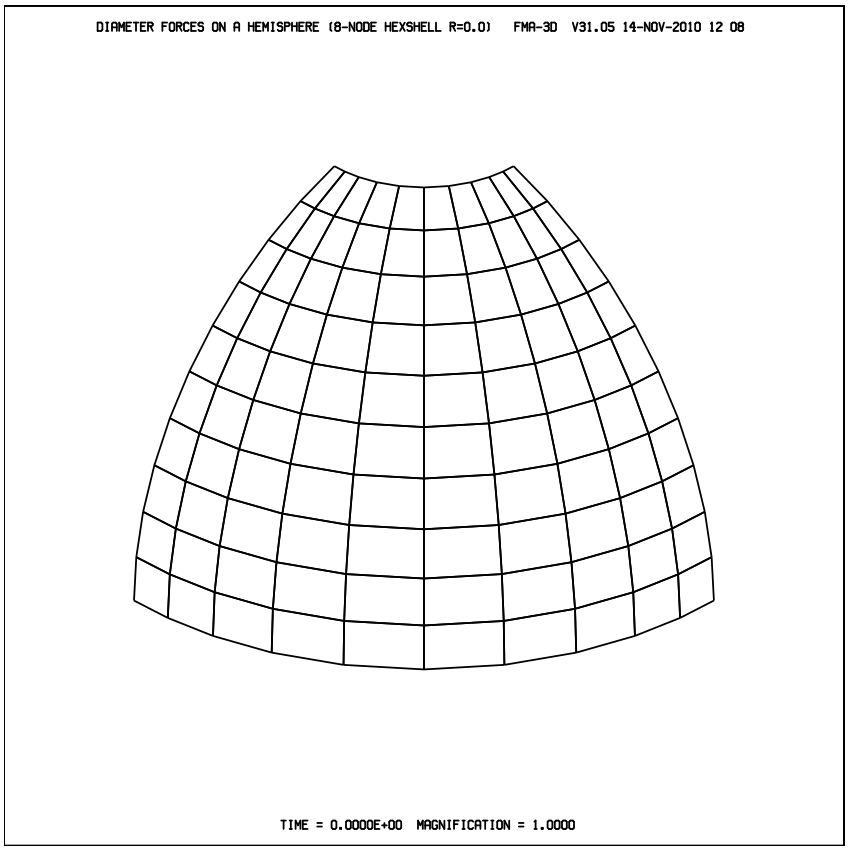

Figure 3.10. Quarter hemisphere mesh consisting of 10×10 8-node hexahedral solid elements.

The loading is four point loads applied normal to the hemisphere's surface at the free edge and 90-degrees apart; they alternate in sign. The amplitude of each point load is 2.0 lb_f. The loading is applied at time equal to zero, and held constant. (For the quarter-symmetry model, the two applied loads are +1.0 and -1.0) The static solution is obtained by damping the velocity at all nodal points.

The material is elastic with a Young's modulus of $E = 6.825\times10^{+7}$ psi, a Poisson's ratio of $\nu = 0.30$, and a density of $\rho = 1.0\times10^{-3}$ $\text{lb}_\text{f}\text{-sec}^2/\text{in}^4$.

Shown in Figure 3.10 is the $1\times10\times10$ hexahedral solid finite element mesh at time equal to zero.

Shown in Figure 3.11 are the shell finite element meshes used at zero load. The quadrilateral mesh has 80 finite elements and the triangular mesh has 160 finite elements, and both are complete hemispheres.

Test Problem Characteristics. The hemisphere is a doublely curved shell with a radius to thickness ratio $R/t = 250$ making it a "thin shell." Hence, with the mesh resolution employed here, the element aspect ratios are also small and, consequently, shear locking will be evidenced by under predicting the deflections if it has not been properly managed in the finite element's derivation.

The meshes used are not particularly irregular and, therefore, shape sensitivity is not tested.

The point loads enter the shell as bending loads, and, diagonally across the elements through the warping resultant component M_{rs}. An inadequate treatment (missing warping stiffness) of the finite element's warping response will produce excessive deflections.

Test Problem Results. The following two tables summarize the static results for the deflections under the point loads. The reference solution is based on an infinitesimal shell calculation, and fails to detect the "stiffening" geometric change (reduced radius of curvature) under the outward deflection u_x under the outward directed point load, and the "softening" geometric change (increased radius of curvature) under the inward deflection u_y under the inward directed point load.

For the multi-stress 3-D solid shell finite elements, the ESH8 Simo-Rifai enhanced strain 8-node, solid hexahedron is overly stiff suggesting that for this very thin element geometry some form of shear-locking is occurring. The K1H8 Key-Gullerud-Koteras 8-node, plane stress hexahedron is predicting deflection amplitudes about 12% higher than the reference result. The K2H8 Key-Gullerud-Koteras 8-node, multi stress hexahedron brackets the reference result, but the amplitude is on average about 3.5% higher. The TSH8 Wing Kam Liu Thick-Shell 8-node hexahedron is the cloest to the reference result, but the amplitude is on average about 1.0% higher. The SDH8 Selective Deviatoric 8-node hexahedron is overly stiff by a factor of 9 as expected.

For the plane-stress 2-D shell elements, KHQ4 and NCT3 both bracket the reference solution. The KGH4 finite element's average deflection is 1.2% lower than the reference solution. The KGQ4 finite element's average deflection is 2.0% lower than the reference solution. The ECT3 is overly stiff by a factor of 4 as expected.

Solid Element Radial Deflections Under Point Loads

Formulation		Geometry	u_x	u_y
ESH8	Simo-Rifai	3-D Stress Hexah	0.0303	-0.0305
K1H8	Key-Gullerud-Koteras	2-D Stress Hexah	0.1043	-0.1056
K2H8	Key-Gullerud-Koteras	3-D Stress Hexah	0.1041	-0.0903
TSH8	W. C. Liu Thick Shell	3-D Stress Hexah	0.0943	-0.0954
SDH8	Selective Deviatoric	3-D Stress Hexah	0.0106	-0.0105
Reference Results (infinitesimal formulation)			0.0940	-0.0940

Shell Element Radial Deflections Under Point Loads

Formulation		Geometry	u_x	u_y
KHQ4	Key-Hoff	4-Node Quad	0.0933	-0.0947
KGQ4	Key-Gruda	4-Node Quad	0.0912	-0.0925
NCT3	Node Centered	3-Node Triangle	0.0931	-0.0956
ECT3	Element Centered	3-Node Triangle	0.0234	-0.0239
Reference Results (infinitesimal formulation)			0.0940	-0.0940

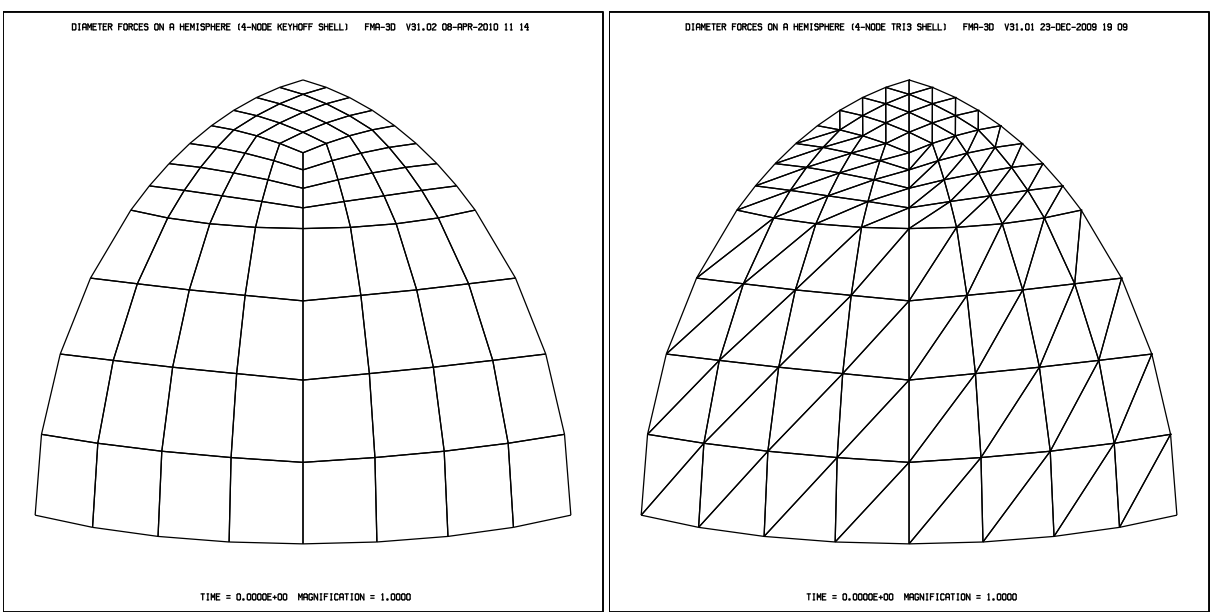

Figure 3.11. Quarter hemisphere meshes consisting of 80 4-node quadrilateral shell elements (left panel), and 180 3-node triangular shell elements(right panel); the 0.04 inch thickness is represented by a 0.04 inch thickness specification for each shell element.

3.4 Test Problem 4: Raasch Hook

Test Problem Statement. The hook, pictured in Figure 3.12, has a thickness of 2.0 inches, a width of 20.0 inches, an initial 60-degree circular arc of radius 14.0 inches completed with a 150-degree circular arc of radius 46.0 inches. The boundary conditions are those of a cantilevered beam, namely, zero displacement and zero rotation at the root (far end), Figure 3.12.

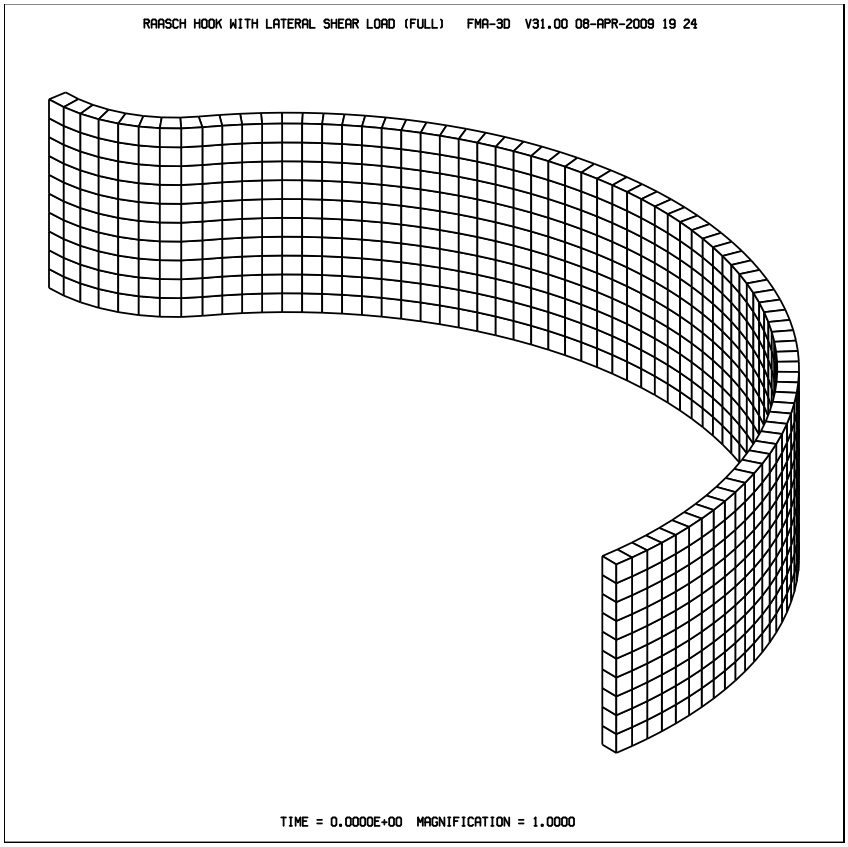

Figure 3.12. Raasch Hook mesh consisting of a $1\times10\times72$ 8-node hexahedral solid elements.

The loading is a vertical in-plane membrane shear traction of 0.05 lb_f/inch along the free-end edge (near end), a total load of 1.0 lb_f. The loading is applied at time equal to zero, and held constant. The vertical static deflection equals 5.027 inches, Kemp, *et al*, [1998]. The static solution is obtained either by damping the velocity at all nodal points, or by examining the initial peak in kinetic energy and, to the extent that the response is dominated by a single mode, the structure is then passing through the static equilibrium state.

The material is elastic with a Young's modulus of $E = 3.3\times10^{+3}$ psi, a Poisson's ratio of $\nu = 0.35$, and a density of $\rho = 2.5\times10^{-6}$ $\text{lb}_\text{f}\text{-sec}^2/\text{in}^4$.

Shown in Figure 3.13 is the $1\times10\times72$ hexahedral solid finite element mesh at both time equal to zero and the static vertical tip deflection of 5.02 inches in red.

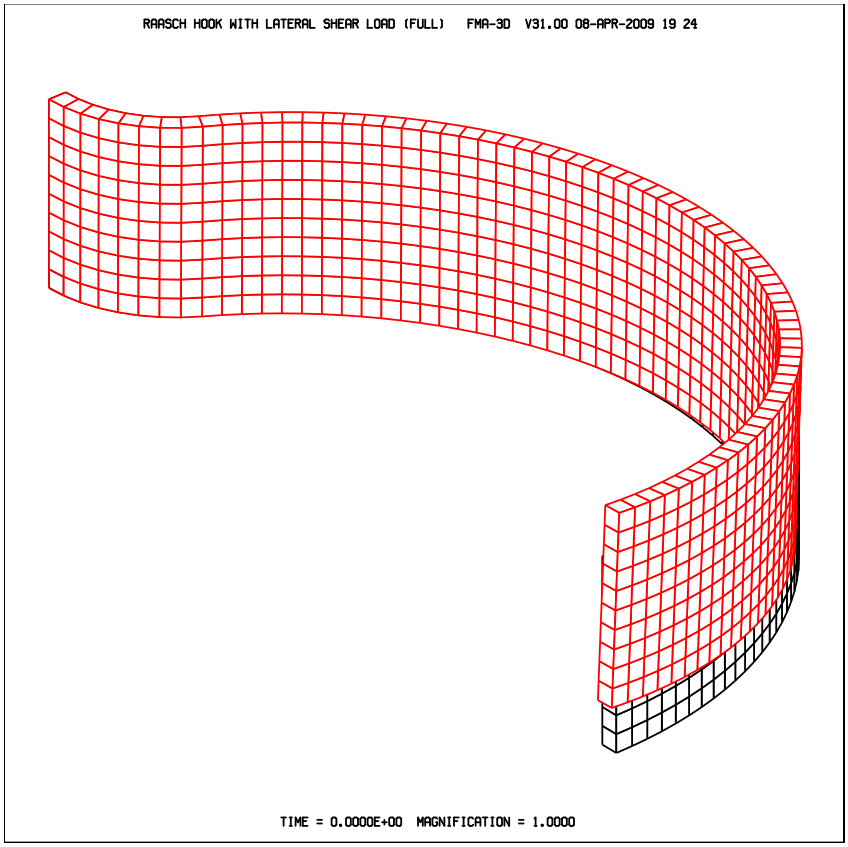

Figure 3.13. Raasch hook mesh consisting of a $1\times10\times72$ 8-node hexahedral solid elements; the static, vertical deflected shape of 5.02 inches is depicted by the red mesh.

Shown in Figure 3.14 are the shell finite element meshes used at zero load. The quadrilateral mesh has 720 finite elements and the triangular mesh has 1440 finite elements.

Test Problem Characteristics. The Raasch hook deformation is primarily a torsional response of the 2.0 inch by 20.0 inch rectangular cross-section where the two circular arches meet near the root. There is a minor secondary overall warping response.

Test Problem Results. That the Raasch Hook is a difficult problem both computationally and theoretically is demonstrated by the number of papers in the literature.

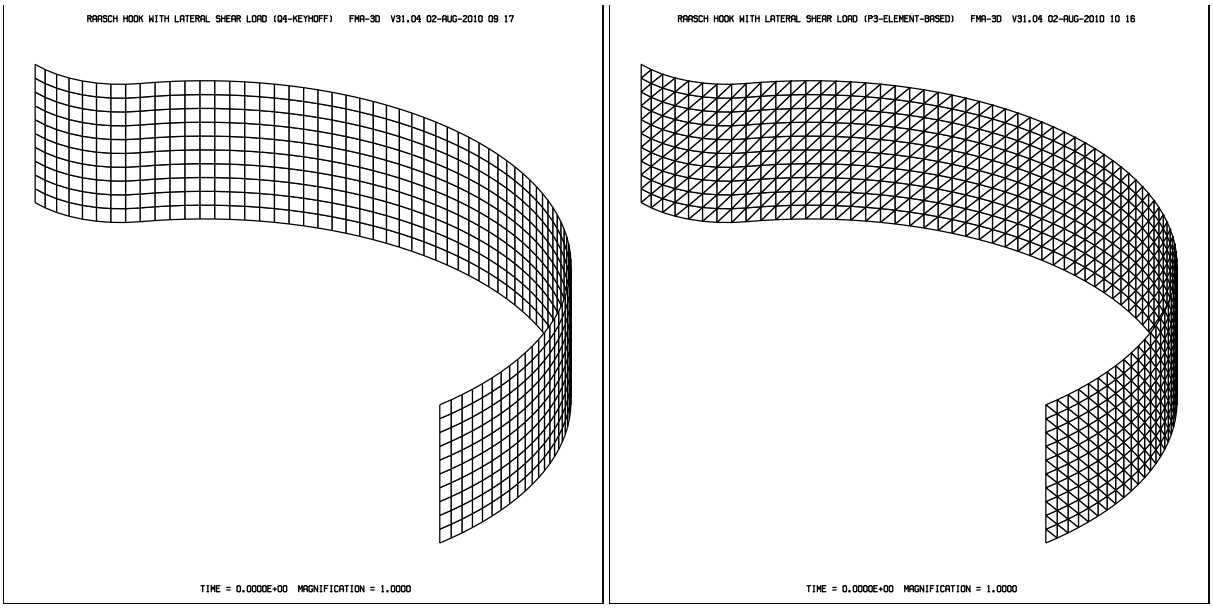

Figure 3.14. Raasch hook mesh consisting of a 10×72 4-node quadrilateral shell elements (left panel). Raasch hook mesh consisting of a 1440 3-node triangular shell elements (right panel).

The work of Schoop, *et al*, [2002], after a detailed investigation assert that the correct answer is 4.7189 inches, but they cite a publication by Wlassow [1964] giving 4.7561 as the solution. The three shell finite elements in Table 4-2, based on the work of Schoop, *et al*, can be expected to produce a deflection of 4.74± inches. The work of Schoop *et al*, [2002], is recommended reading.

Schoop, *et al*,[2000], cite an ABAQUS finely resolved solid finite element solution of 5.035 inches, and Kemp, *et al*, [1998] reports a deflection of 5.027 inches. It would appear that 5.03± is an acceptable value for the solid mesh employed here.

The solid elements, Table 4-1, including the SDH8 Selective Deviatoric 8-node hexahedron, tend to do better on this test problem since all of them have good fidelity with respect to the cylindrical geometry and torsional deformation of the rectangular cross-section.

Table 4-1
Solid Element Tip Deflections Under 1 lb_f Tip Shear Loading

Formulation		Geometry	u_z	t ms
ESH8	Simo-Rifai	3-D Stress Hexah	5.0915	176.0
K1H8	Key-Gullerud-Koteras	2-D Stress Hexah	5.0950	176.0
K2H8	Key-Gullerud-Koteras	3-D Stress Hexah	5.1390	damped
TSH8	W. C. Liu Thick Shell	3-D Stress Hexah	5.0798	176.0
SDH8	Selective Deviatoric	3-D Stress Hexah	5.0424	damped
Reference Results (shells based on solid elements)			5.03±	static

Table 4-2
Shell Element Tip Deflections Under 1 lb_f Tip Shear Loading

Formulation		Geometry	u_z	t ms
KHQ4	Key-Hoff	4-Node Quad	15.278	300.0
KGQ4	Key-Gruda	4-Node Quad	4.9245	damped
NCT3	Node Centered	3-Node Triangle	5.0692	176.2
ECT3	Element Centered	3-Node Triangle	4.5077	165.0
Reference Results (infinitesimal formulation)			4.74±	static

The shell elements, Table 4-2, on the other hand, exhibit quite different results. In particular, the KHQ4 Key-Hoff plane stress 4-node quadrilateral (as it is currently implemented) gives a large value for the vertical deflection, that is, a deflection some 300% above the expected result.

Table 4-3 documents a significant difference in finite element modeling behavior for both the KHQ4 Key-Hoff 4-node quadrilateral shell finite element, and the KGQ4 Key-Gruda 4-node quadrilateral shell finite element. Both of these finite elements in their original form utilize normal vectors constructed at the element verticies to define the extent of the material that lies above and below the reference surface, that is, above and below the meshed 2-D surface. Thus, on a curved surface there is a discrepancy along the element edges because of the slight difference (usually slight but not always) in normal vector orientation from one finite element to the next finite element. The missing part is not really the conceptual gaps and overlaps in the surrounding material, but the difference in rotational velocity ϑ^i obtained by the respective finite elements, namely, $\vartheta^i = \varepsilon^{ijk}\omega_j n_k$, the cross product $\vartheta = \omega \times \mathbf{n}$, where ω_j is the rotational variable carried at the nodal points and n_k is a unit normal vector at the nodal point. The implementation for both of these finite elements was modified to make use of a common fiber vector (initially a surface normal vector that has been rotated in time using nodal point rotational rates) at each nodal point, a one-time, pre-calculation initialization. Each shell element at a node will use the same fiber vector and have the same rotational velocity ϑ^i.

Table 4-3
Solid Element Tip Deflections Under 1 lb_f Tip Shear Loading
Comparison between element-based vertex normals
and nodal-based fiber vectors

Formulation		Geometry	u_z	error
KHQ4	Key-Hoff w/ vertex normals	4-Node Quad	15.278	+322%
KHQ4	Key-Hoff w/ nodal fibers	4-Node Quad	4.256	-10%
Reference Results (infinitesimal formulation)			4.74±	
KGQ4	Key-Gruda w/ vertex normals	4-Node Quad	10.345	+206%
KGQ4	Key-Gruda w/ nodal fibers	4-Node Quad	4.924	-2%
Reference Results (shells based on solid elements)			5.03±	

During the calculation, the orientation of the normal is updated at each time step with a proper orthogonal rotation computed from the nodal rotational velocity ω_i. Likewise, the torque from the divergence of the bending stress resultant is computed with respect to the nodal-based common fiber vector.

For both the KHQ4 and KGQ4 finite elements, the response of the Raasch Hook test problem changes dramatically for the better with nodal-based common fiber vectors. The difference in the before and after results for the Raasch Hook test problem demonstrates the significance of this particular test problem. The results from the modified KGQ4 Key-Gruda shell element are halfway between the results expected for the solid finite elements and the shell theory finite elements, a result that is fitting for the adaptation of the K1H8 Key-Gullerud-Koteras plane stress 8-node hexahedron internals to a 4-node quadrilateral. The results for the modified KHQ4 Key-Hoff are less favorable, but are still a significant improvement over the results from the original implementation.

Simulation Notes. Based on surface contours of the vertical displacement u_z, the actual maximum vertical deflection occurs at the bottom nodal point under the distributed shear load. All of the computed results reported here are for the vertical deflection u_z of the center nodal point under the distributed shear load. The difference is quite minor and my be more due to the finite elements themselves. It is unknown at this time if the analytic solutions all exhibit this behavior. To be slightly conservative, the nodal point halfway between the bottom edge and the top edge was selected.

3.5 Test Problem 5: Beam Bent into a Ring

Test Problem Statement. The beam, pictured in Figure 3.15, has a thickness of 1.0 inch, a width of 3.0 inches, and a length of 36 inches. In addition, a *beam finite element* (depicted by a red dash) has been attached to the solid; the beam cross-section matches the 1 inch by 3 inch dimension of the solid finite elements. The beam finite element is 1 inch in length.

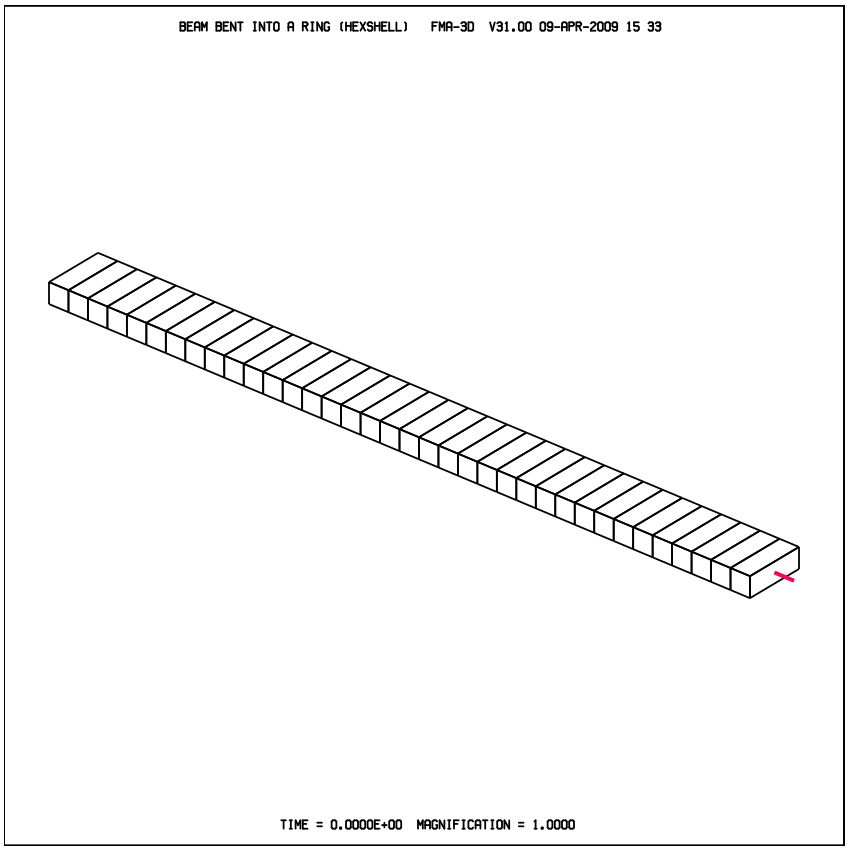

Figure 3.15. Beam mesh consisting of a $1\times1\times36$ 8-node hexahedral solid elements; attached at the free-end (depicted by the red dash) is a 1 inch long beam finite element with a matching cross-section.

The boundary conditions are those of a cantilevered beam, namely, zero displacement and zero rotation at the root (far end), Figure 3.15. The interface between the last solid hexahedral finite element and the single beam finite element is a multipoint constraint (MPC) that ties the translations and rotations of the beam nodal point to those of the 4-nodal points from the hexahedral finite element face on which it lies. At the beams "free-end," the beam's rotational

degrees of freedom are prescribed to be 370-degrees; the final result is pictured in Figure 3.17. The static solution is obtained by damping the velocity at all nodal points.

The material is elastic with a Young's modulus of $E = 1.04\times10^{+7}$ psi, a Poisson's ratio of $\nu = 0.30$, and a density of $\rho = 2.61\times10^{-4}$ lb_f-sec^2/in^4.

Shown in Figure 3.15 is the $1\times1\times36$ 8-node hexahedral solid finite element mesh along with a single beam finite element depicted in red at time equal to zero.

Shown in Figure 3.16 is the two shell finite element meshes used at zero load. The quadrilateral mesh has 36 finite elements and the triangular mesh has 72 finite elements.

Test Problem Characteristics. The beam "bent into a ring" is almost exclusively a bending response. It is a large displacement, finite rotation, finite strain deformation. The final deformation is "zero-dimensional" in that each solid (or shell) finite element along the beam has opposing faces that each rotate 5-degrees to form a 10-degree wedge. The primary test is one of implementation, that is, all of the kinematic variables, strain components, and stress components are in the global x,y,z-coordinate system. Secondarily, the ring will fail to close on itself if the stiffness representation is incorrect. Half way through the dynamic motion the curvature of a portion of the solid finite element beam exceeds the final uniform circular result and, thus, must "unwind" by the time it comes to rest, Figure 3.18. Hence, the implementation, at every location around the ring, must produce what is a *uniform circular result* where each finite element is at a different orientation with respect to the x,y,z-coordinate system, and has undergone a different motion that ranges form nearly uniform in time to a load-unload cycle while traversing an arc in space.

Test Problem Results. In Table 5-1, only three of the solid elements tested came acceptably close to forming a circular ring: the K1H8 Key-Gullerud-Koteras 8-node, plane stress hexahedron; the K2H8 Key-Gullerud-Koteras 8-node, 3-D multi-stress hexahedron; and the SDH8 Selective Deviatoric 8-node hexahedron.

While the double-layer TSH8 Wing Kam Liu Thick-Shell 8-node hexahedron gives the appearance of doing well in Table 5-1, it requires an x,z-symmetry plane to enforce a planar motion and reach a circular shape, but even then, a visible amount of conicity developed. (Without the x,z-symmetry plane, the solution devolves into an out-of-plane double helix configuration.)

The ESH8 Simo-Rifai enhanced strain 8-node, solid hexahedron develops an irregular, non-uniform, not-quite-circular solution just as it reaches closure, and then over-closes. The failure is possibly due to the incremental accumulation of the enhanced strain components.

In Table 5-2, the three shell finite elements all came acceptably close to forming a circular ring. However, all three finite elements relied on a pair of symmetry planes in order to achieve the final result.

Table 5-1
Solid Element Ring Closure Displacements

Formulation		Geometry	u_y	u_z
ESH8	Simo-Rifai	3-D Stress Hexah	-34.23	0.3318
K1H8	Key-Gullerud-Koteras	2-D Stress Hexah	-35.99	0.0002
K2H8	Key-Gullerud-Koteras	3-D Stress Hexah	-36.09	0.0269
TSH8	W. C. Liu Thick Shell	3-D Stress Hexah	-36.16	0.0119
SDH8	Selective Deviatoric	3-D Stress Hexah	-35.95	0.0020
Reference Results			-36.00	0.0

Table 5-2
Shell Element Ring Closure Displacements

Formulation		Geometry	u_y	u_z
KHQ4	Key-Hoff	4-Node Quad	-36.00	0.0149
KGQ4	Key-Gruda	4-Node Quad	-36.00	0.0149
NCT3	Node Centered	3-Node Triangle	-35.95	0.0123
ECT3	Element Centered	3-Node Triangle	-35.90	0.0191
Reference Results			-36.00	0.0

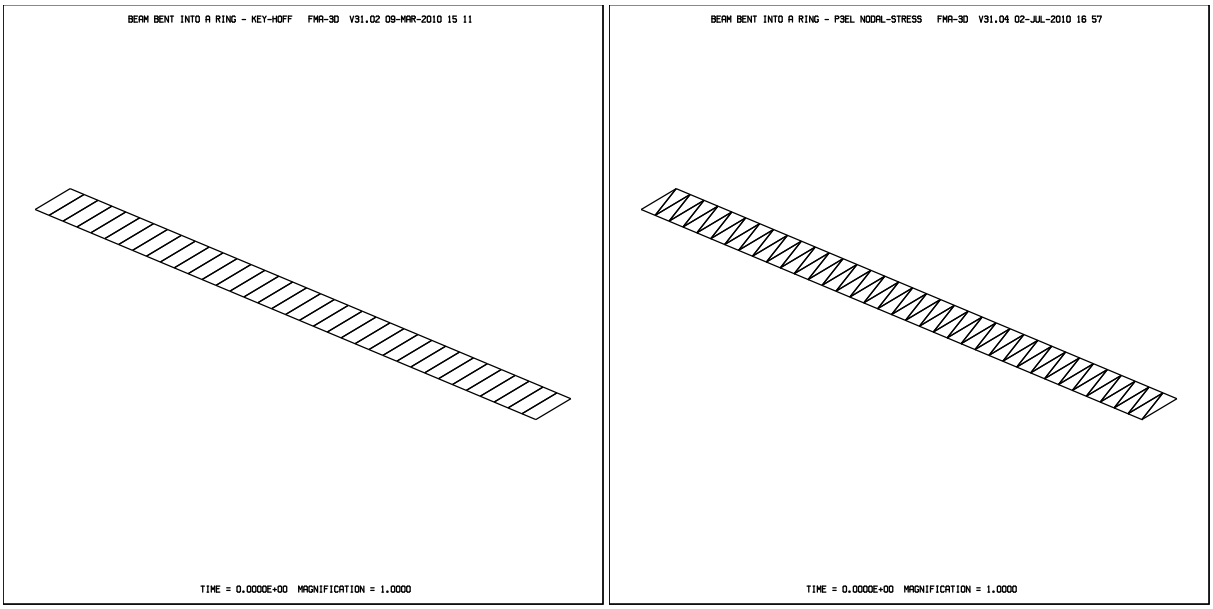

Figure 3.16. Beam mesh consisting of a 1×36 4-node quadrilateral shell elements (left panel);Beam mesh consisting of a 72 3-node triangular shell elements (right panel).

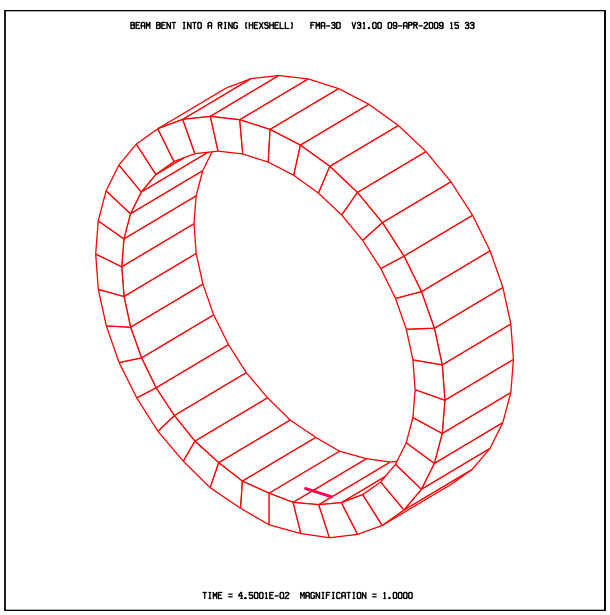

Figure 3.17. Solid finite element mesh closed on itself in the final ring configuration.

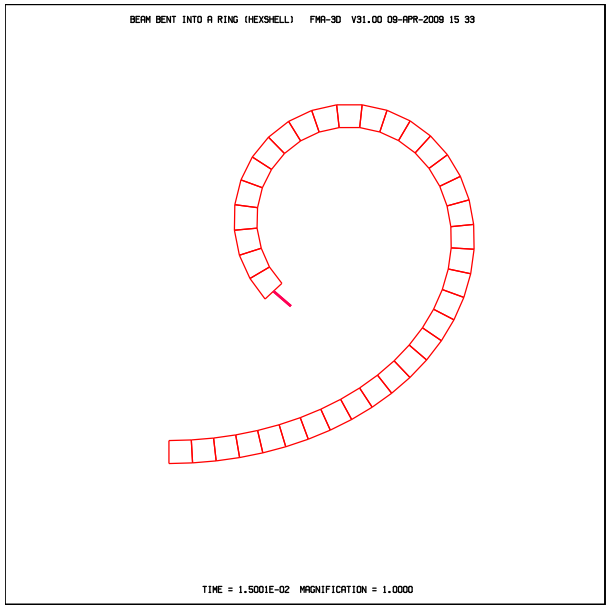

Figure 3.18. Solid finite element mesh at 15 ms during the transition from a straight beam into its final circular ring configuration.

3.6 Test Problem 6: Irons Membrane Patch Test

Test Problem Statement. The rectangular collection of five solid 8-node hexahedral finite elements pictured in Figure 3.19, constitutes an Irons membrane patch test. It is a 1.0 inch square with a thickness of 0.25 inches. Note that the elements are displayed at 80% of their true-size for easier visualization. The white wire-frame mesh is displayed at true-size; both the top and bottom views are shown. Each finite element has a different material number, but all of the finite elements are elastic and have the same material properties. The boundary conditions consist of a prescribed in-plane motion at each of the eight outer vertex nodal points; the normal displacement u_z is zero for all nodal points.

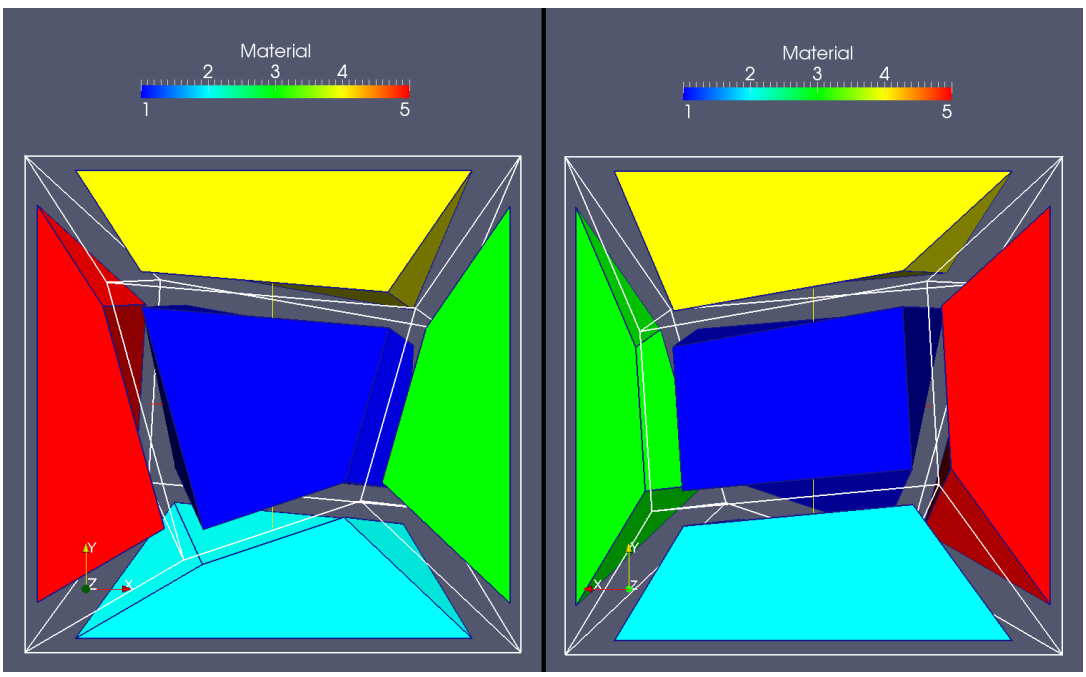

Figure 3.19. Solid mesh consisting of five irregularly shaped 8-node hexahedral solid elements; the finite elements are "shrunk" with respect to the wire frame to aide in visualization. the front side of the mesh is displayed in the left panel, and the obverse is displayed in the right panel.

The Irons membrane patch test for the shell finite elements is pictured in Figure 3.20; for the shell, the 0.25 inch thickness dimension is specified as a geometric parameter.

The material is elastic with a Young's modulus of $E = 1.0\times10^{+6}$ psi, a Poisson's ratio of $\nu = 0.25$, and a density of $\rho = 2.61\times10^{-4}$ $\text{lb}_\text{f}\text{-sec}^2/\text{in}^4$.

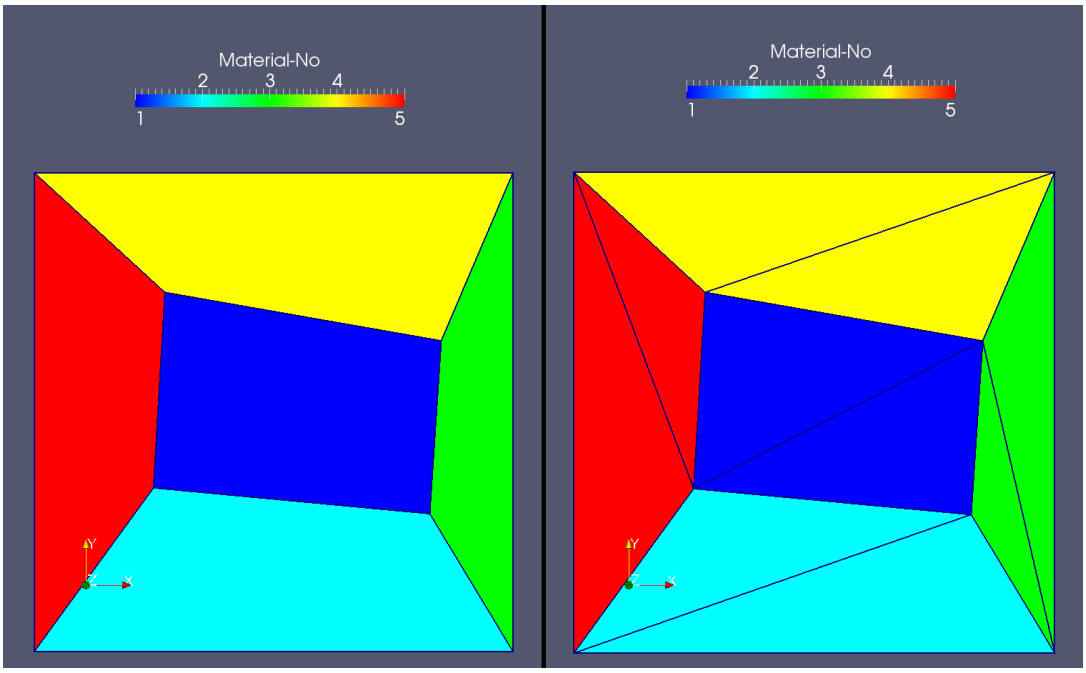

Figure 3.20. Shell mesh consisting of five irregularly shaped 4-node quadrilateral shell elements, and ten irregularly shaped 3-node triangular shell elements.

Test Problem Characteristics. The exact solution to the prescribed linear motion is a constant membrane stress/strain state (uniform over the area and through the thickness) . The object of an Irons patch test is to demonstrate that a geometrically irregular "patch" of finite elements is capable of reproducing the constant stress/strain state, the exact solution to the exterior applied linear displacement field. The internal nodal points must move as part of the solution so as to generate the constant stress/strain state. If the simulation is able to predict the correct constant stress/strain state, the test is passed, otherwise the element formulation is defective. An Irons patch test is closely related to a proof of *linear consistency* for the spatially discrete approximation.

Test Problem Results. Ideally, one would report the direct stress components and the in-plane shear components, however, shell elements for the most part compute with stress components in a local coordinate system, more or less aligned with the element orientation. Thus, to get uniform results for reporting, three geometrically invariant results are used: (1) strain-energy density, (2) pressure, and (3) effective stress. Collectively, these invariants reflect the uniformity or non-uniformity element-to-element as the case may be.

With regard to the two tables, Tables 6-1 and 6-2, it should be noted that the K1H8 Key-Gullerud-Koteras plane-stress 8-node hexahedron has been moved from the solids Table 6-1 to

the shell Table 6-2 since it is based on plane-stress material models and has invariant values that are comparable to results for the shell finite elements.

In Table 6-1, Three of the multi-stress solid elements exhibit acceptably small departures from exact results. However, the TSH8 Wing Kam Liu Thick Shell does however push the test boundaries to between $\pm 1.4\%$ and $\pm 1.6\%$ departures from the reference values. Given the significantly distorted element shapes in the mesh, these departures are acceptable for the membrane response.

In Table 6-2, all five plane-stress formulations have ranges that are quite close to the reference values and reflect finite elements that meet the objectives of the patch test to reproduce a uniform membrane stress/strain state.

Table 6-1
Irons Membrane Patch Test Results
Solid Bending-Formulated Finite Elements
(SED = Strain Energy Density)

Element	Range: SED		Range: p		Range: σ_{eff}	
ESH8	1.788	1.803	1329	1335	1055	1059
K2H8	1.799	1.799	1330	1334	1018	1021
TSH8	1.770	1.825	1325	1338	1043	1078
SDH8	1.789	1.803	1329	1335	1056	1059
Reference	1.800		1333		1057	

Table 6-2
Irons Membrane Patch Test Results
Plane-Stress Finite Elements
(SED = Strain Energy Density)

Element	Range: SED		Range: p		Range: σ_{eff}	
K1H8	1.529	1.531	888	889	1501	1502
KHQ4	1.531	1.532	888	889	1501	1502
KGQ4	1.529	1.535	888	890	1501	1503
NCT3	1.531	1.532	888	888	1501	1502
ECT3	1.529	1.534	887	889	1500	1503
Reference	1.5315		888		1501	

Pictured in Figure 3.21 are the contour results for the linear u_x displacement solution showing that the solution for the interior nodal points moved to reproduce the constant strain solution.

Simulation Notes. The NCT3 Node Centered 3-node triangular shell finite element formulation required that all the elements in the mesh be of one material to get satisfactory uniform

results. The node-centered formulation recognizes material boundaries passing through a nodal point, and maintains two or more one-sided sets of calculations, thus making the five-material model extremely complex.

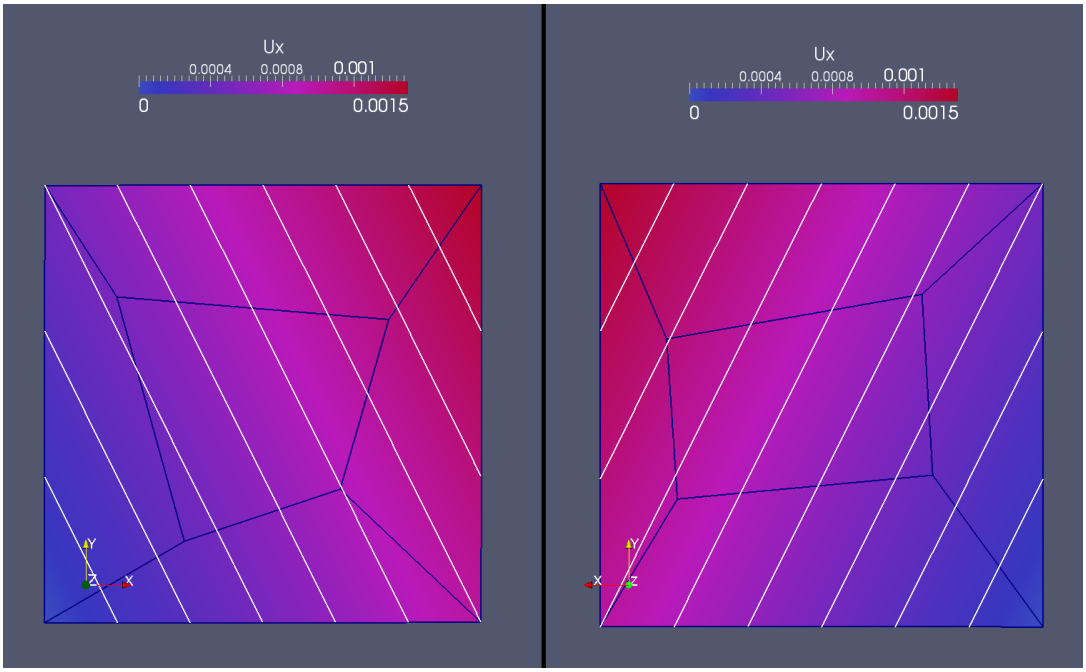

Figure 3.21. Front and back final deformed contours for displacement u_x from the ESH8 Simo and Rifai. Enhanced Strain 8-node hexahedral Irons membrane patch test.

3.7 Test Problem 7: Inflated Sphere Patch Test

Test Problem Statement. The rectangular spherical segment pictured in Figure 3.22, has a thickness of 0.2 inches, and a radius of 10.1 inches. The segment is defined by four planar slices tilted $\pm 15^o$ with respect to the z-axis and passing through the center of the sphere. The boundary conditions along all four edges are symmetry boundary conditions. For the 8-node hexahedral mesh it means that the circumferential displacements along each edge are zero, and, additionally, for the shell elements, rotations along the edge are prescribed to be zero about all three axises. These boundary conditions are compatible with a sphere loaded by either internal or external pressure.

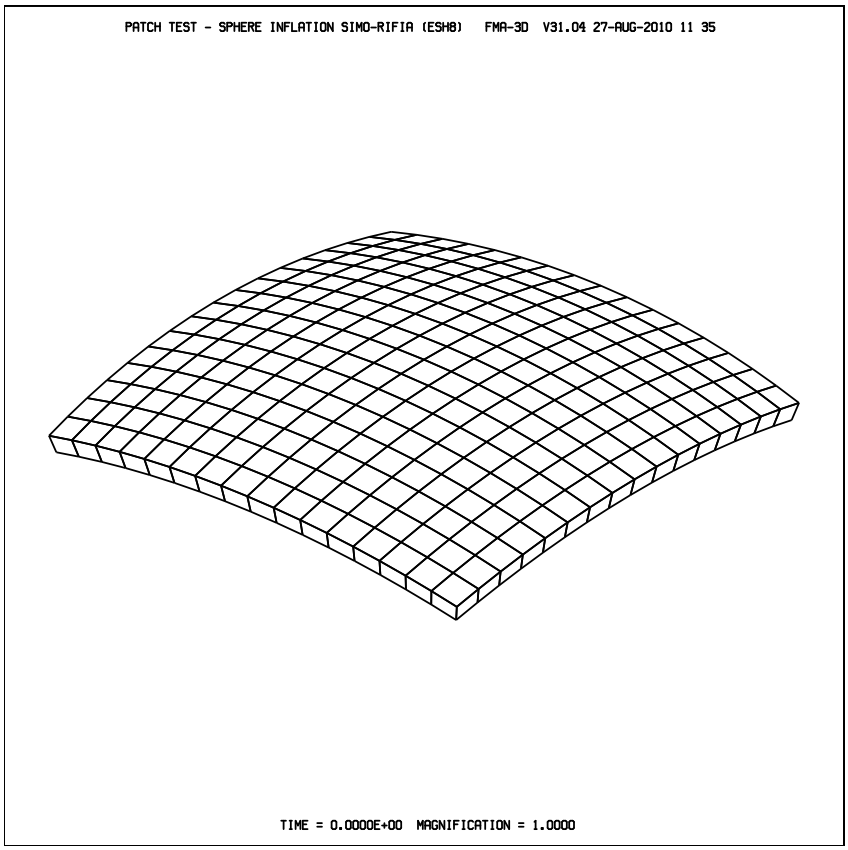

Figure 3.22. The spherical hexahedral solid final mesh consisting of $1\times16\times16$ 8-node hexahedral solid elements for a total of 256 elements; the mesh is a "rectangular" patch of a full sphere.

The loading is an internal pressure $p = 50.0$ psi. The pressure is applied via a cosine-ramp and then held constant. A static solution is obtained with velocity damping applied to each

nodal point.

The material is elastic with a Young's modulus of $E = 1.0\times10^7$ psi, a Poisson's ratio of $\nu = 0.30$, and a density of $\rho = 1.0\times10^{-2}$ $\text{lb}_\text{f}\text{-sec}^2/\text{in}^4$.

Shown in Figure 3.23 are the shell finite element meshes. The quadrilateral mesh has 256 finite elements and the triangular mesh has 512 finite elements.

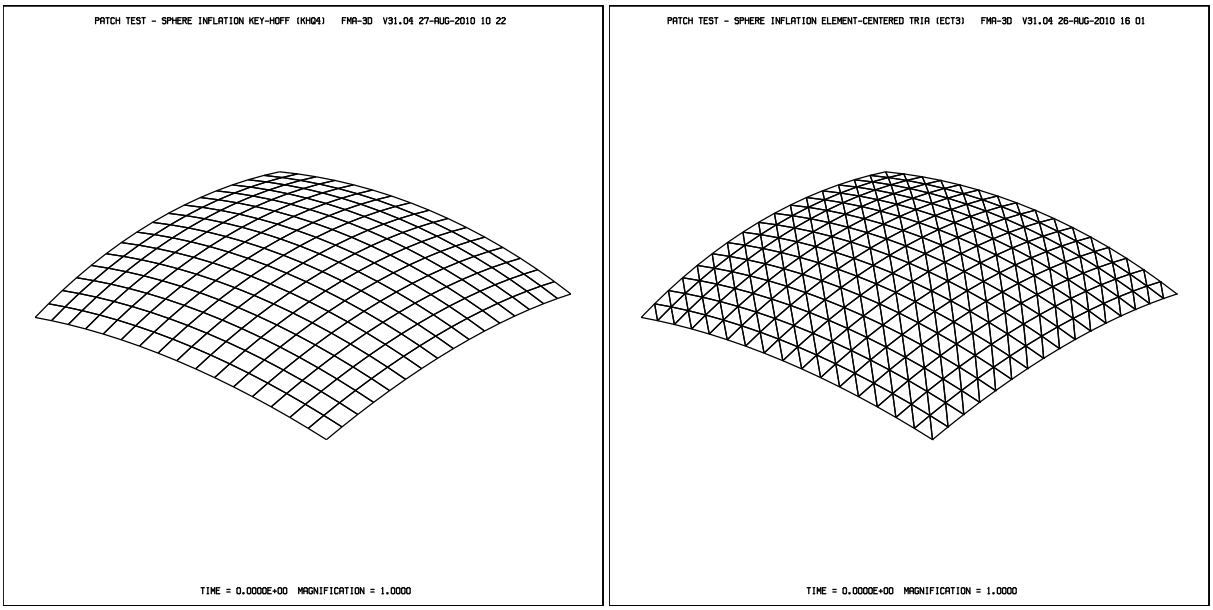

Figure 3.23. The spherical planar quadrilateral final mesh consisting of 16×16 4-node quadrilateral shell elements for a total of 256 elements (left panel), and the spherical planar triangular final mesh consisting of 16×16 3-node triangular shell element pairs for a total of 512 elements (right panel). The meshes are a "rectangular" patch of a full sphere.

Test Problem Characteristics. The test problem geometry is a moderately thin-walled, perfectly spherical shell. Since the finite elements here are linear triangles, bilinear quadrilaterals, and trilinear hexahedral geometries, the curvature of the sphere is represented by the element-to-element change in the normal vector orientation as each edge is crossed. The purpose of this test problem is a two-fold test: (1) to test that the geometric approximation to the curvature is valid, and (2) to test that under mesh refinement the analytic result is obtained.

An ideal elastic thin-walled hollow sphere loaded with internal pressure has an infinitesimal solution. The membrane stress is uniform and the same in all in-plane directions, irrespective of location and material properties that are isotropic, and is given by $\sigma = (Pressure \times Radius)/(2 \times thickness)$. For the pressure and dimensions here, the in-plane or membrane

Table 7-1
Solid ESH8 Mean Quadrature Pressure
Stress Invariant I ($I = \sigma_k^k/3$)

Mesh	Low	Average	High
2×2	817.02	817.02	817.02
4×4	814.23	816.50	818.77
8×8	815.35	816.91	818.48
16×16	816.57	817.01	817.46
Exact	816.88	816.88	816.88

stress is $\sigma = 1262.5$ while the through the thickness direct stress is small and taken to be zero in thin shell theories. The first invariant of the membrane stress ($I = \sigma_k^k/3$) is $I = 841.666\ldots$. The sphere's response is dominated by membrane stretching.

The sphere used here is only moderately thin, and, thus, has a three dimensional stress distribution. However, the solid finite element stress components reported here are *mean quadrature* stress components, that is, volume-averaged stress components. Accordingly, the mean quadrature in-plane direct stress is 1237.577 and the mean quadrature radial stress is -24.505 which gives a mean quadrature pressure of 816.883. The fact that the three-dimensional stress component values match the thin-shell solution to within 2% indicates that the sphere is "moderately thin." A contributing factor to the differences between the shell theory results and the three dimensional solution is the two different radial locations where the internal pressure is applied: for the shell the pressure is applied at a radius of 10.1 and for the three-dimensional solid solution, it is applied at a radius of 10.0.

The use of a sphere under internal pressure is used here as a *patch test*. A sequence of uniform meshes is used and examined for the degree of uniformity in the membrane stress invariant $I = \sigma_k^k/3$. The departure from a uniform stress indicates the departure from satisfying the patch test requirement that a uniform stress be reproduced. The kinematic boundary conditions allow only pure radial motion along each edge; no in-plane motion is permitted. The shell elements have rotational degrees of freedom at each nodal point on the boundary that are prescribed to be zero. These boundary conditions match the motion of the inflation of an ideal thin sphere. It should be noted that because uniform, regular meshes are used, the effect of element distortion on the uniformity of the stress field is not tested.

Test Problem Results. Tables 7-1 through 7-5 tabulate the results for the solid elements. All four of the solid finite elements designed to use three-dimensional material models (ESH8, K2H8, TSH8, and SDH8) replicate the analytic results from the three-dimensional thick-shell solution. Of note are the results from the 2×2 starting mesh – due to the symmetry of the problem and boundary conditions all four elements in the mesh have the same results and the results are very close to the analytic solution. As an example, Figure 3.24 illustrates the near uniformity in the pressure (the first stress invariant) and the strain energy density for the ESH8

Table 7-2
Solid K1H8 Mean Quadrature Pressure
Stress Invariant I ($I = \sigma_k^k/3$)

Mesh	Low	Average	High
2×2	811.55	811.55	811.55
4×4	821.12	821.12	823.68
8×8	813.64	825.39	826.70
16×16	824.52	825.01	825.50
Exact	841.67	841.67	841.67

Table 7-3
Solid K2H8 Mean Quadrature Pressure
Stress Invariant I ($I = \sigma_k^k/3$)

Mesh	Low	Average	High
2×2	817.21	817.21	817.21
4×4	814.62	817.72	820.81
8×8	815.80	817.16	818.53
16×16	816.82	817.20	817.58
Exact	816.88	816.88	816.88

Table 7-4
Solid TSH8 Mean Quadrature Pressure
Stress Invariant I ($I = \sigma_k^k/3$)

Mesh	Low	Average	High
2×2	817.03	817.03	817.03
4×4	814.00	817.56	821.11
8×8	815.20	816.89	818.58
16×16	816.48	817.18	817.89
Exact	816.88	816.88	816.88

Table 7-5
Solid SDH8 Mean Quadrature Pressure
Stress Invariant I ($I = \sigma_k^k/3$)

Mesh	Low	Average	High
2×2	817.21	817.21	817.21
4×4	816.74	817.05	817.36
8×8	816.53	816.97	817.42
16×16	816.76	817.00	817.24
Exact	816.88	816.88	816.88

Table 7-6
Shell KHQ4 Mean Quadrature Pressure
Stress Invariant I ($I = \sigma_k^k/3$)

Mesh	Low	Average	High
2×2	827.26	827.26	827.26
4×4	835.30	840.20	845.10
8×8	839.78	841.23	842.68
16×16	839.73	841.63	843.53
Exact	841.67	841.67	841.67

Table 7-7
Shell KGQ4 Mean Quadrature Pressure
Stress Invariant I ($I = \sigma_k^k/3$)

Mesh	Low	Average	High
2×2	830.92	830.92	830.92
4×4	840.48	838.07	852.24
8×8	845.47	847.50	849.54
16×16	845.94	847.58	849.22
Exact	841.67	841.67	841.67

Table 7-8
Shell NCT3 Mean Quadrature Pressure
Stress Invariant I ($I = \sigma_k^k/3$)

Mesh	Low	Average	High
2×2	823.35	827.54	831.73
4×4	830.61	838.07	845.55
8×8	839.29	841.27	843.25
16×16	838.80	840.88	842.96
Exact	841.67	841.67	841.67

Table 7-9
Shell ECT3 Mean Quadrature Pressure
Stress Invariant I ($I = \sigma_k^k/3$)

Mesh	Low	Average	High
2×2	715.82	799.27	882.72
4×4	794.95	830.83	866.71
8×8	825.03	836.81	848.58
16×16	836.47	841.16	845.81
Exact	841.67	841.67	841.67

Simo-Rifai Enhanced Strain 8-node hexahedron at the finest mesh resolution.

As a second example, the results for K1H8 Key-Gullerud-Koteras plane-stress 8-node hexahedron (a hexahedron that is based internally on a Reissner-Mindlin shell theory), converges to a uniform value of $825.01 \pm 0.05\%$ that is halfway nominally between the thin-shell answer and the three-dimensional elasticity mean-quadrature result, Table 7-2. There is not yet an explanation for this result.

Tables 7-6 through 7-9 tabulate the results for the shell elements. The three shell finite elements KHQ4, NCT3, and ECT3 converge to the thin shell result, and, for example, Figure 3.25 illustrates the near uniformity in the pressure (the first stress invariant) and strain energy density for the KHQ4 Key-Hoff 4-node quadrilateral at the finest mesh resolution.

In Table 7-7, the KGQ4 Key-Gruda plane-stress 4-node quadrilateral using the three-dimensional solid shell K1H8 internals in a reconstructed 8-node hexahedral frame using nodal-based surface unit-fiber vectors (initially surface normal vectors that have been rotated in time using nodal point rotational rates), is converging to a mean quadrature pressure value nearer to $848\pm$ rather than the plane stress result of 841.67. There are two obvious sources of error in this calculation: (1) the nodal-based initial normal vector construction, and (2) the reduced quadrature performed to sample the stress distribution within the finite element's hexahedral volume. The following provides more detail for these two issues:

1. **Surface Normal/Fiber Vectors.** As a practical matter, the surface initial normal vectors at the nodal point are constructed from the mesh by averaging finite element corner normals assembled at the nodal points with area weighting. The construction is a one-time initialization that occurs before the calculation starts. In this test problem, the obvious surface normal is one always aligned with the sphere's radius vector. The reconstructed surface normal vectors with uniform meshing are aligned with the radius vector except at the four corner nodal points where only a single element contributes to the averaging, and along the four boundaries where only two elements share each nodal point. Hence, the *reconstructed* surface normal vector matches the element corner normal and is *not* aligned with the sphere's radius vector, and, similarly, along the four edges. The perturbation to the solution is clear from an element-by-element pressure plot. Ideally, when the mesh is constructed using preprocessor-based mesh generation with surfaces defined geometrically, proper surface normal vectors at the nodal points should be supplied, thereby, avoiding a somewhat *ad hoc* reconstruction of the surface normal vectors with limited accuracy. Note that the initial surface normal vectors are rotated in time using nodal point rotational rates, and, hence, become material fiber vectors characterizing any transverse shear strains that develop during the shell's motion.

2. **Reduced Stress State Sampling.** Since the constant membrane and bending stress resultants are the dominant contributors to the shells response (which includes bilinear contributions from the transverse shear stress components in the finite element's shell theory), a *minimal* volume sampling of the stress field has been implemented, namely, a through-thickness integration to capture the membrane and bending stress combined with a middle-surface areal quadrature to capture the required bilinear variation in the transverse shear stress components. This approach to stress state sampling suffers from incorrectly capturing the true *mean quadrature* values for the constant membrane and bending stress resultants. Ideally for an elastic analyses, an iterated 2-point Gauss quadrature sampling should take place resulting in eight sampling points and a proper capture of the constant mean quadrature membrane and bending stress resultants.

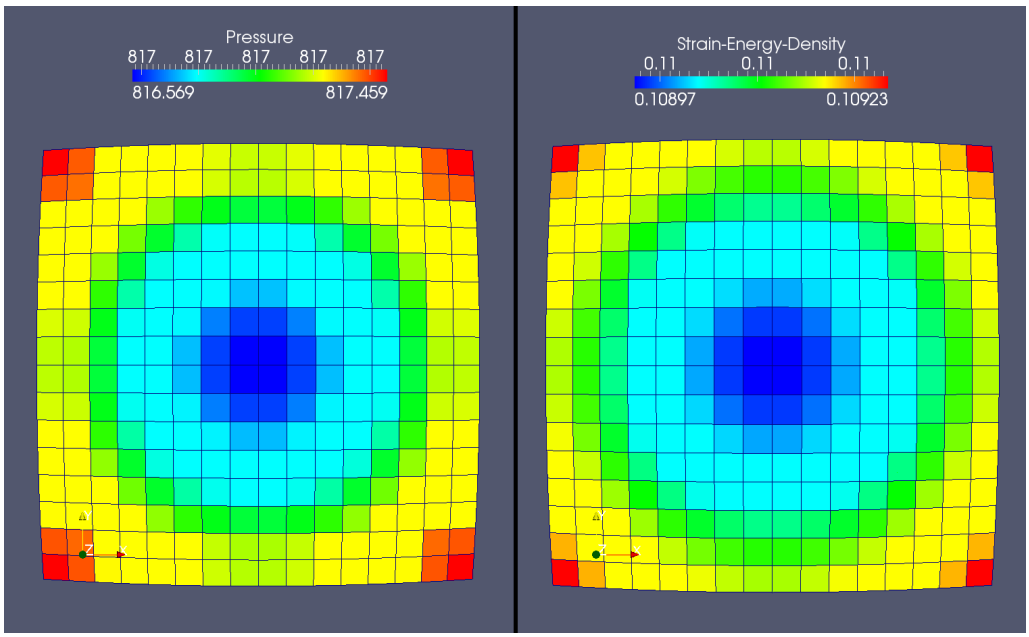

Figure 3.24. ESH8 Simo-Rifai Enhanced Strain 8-node solid element pressure distribution ($817.0 \pm 0.006\%$) and strain-energy density distribution ($0.1090 \pm 0.12\%$).

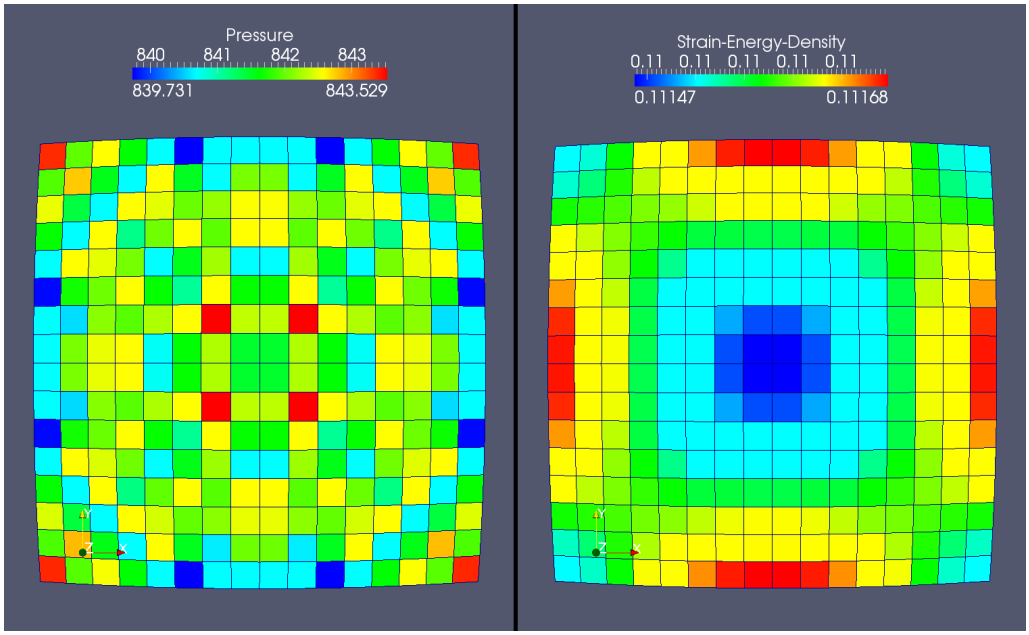

Figure 3.25. KHQ4 Key-Hoff 4-node quadrilateral shell element pressure distribution ($841.63 \pm 0.23\%$) and strain-energy density distribution ($0.1157 \pm 0.09\%$).

3.8 Test Problem 8: Pinched Cylinder

Test Problem Statement. The cylinderical panel, pictured in Figure 3.26, has a thickness of 3.0, a radius of 300.0, and a length of 36.0 units. The cylinderical panel is a 90.0-degree sector from a full cylinder 72.0 units long, that is, the panel is an octant defined by symmetry planes of the full cylinder. The ends of the cylinder are constrained by a "ridgid diaphragm" that requires the cylinder's cross-section to remain cicular as it deforms but does not restrict axial movement or rotation.

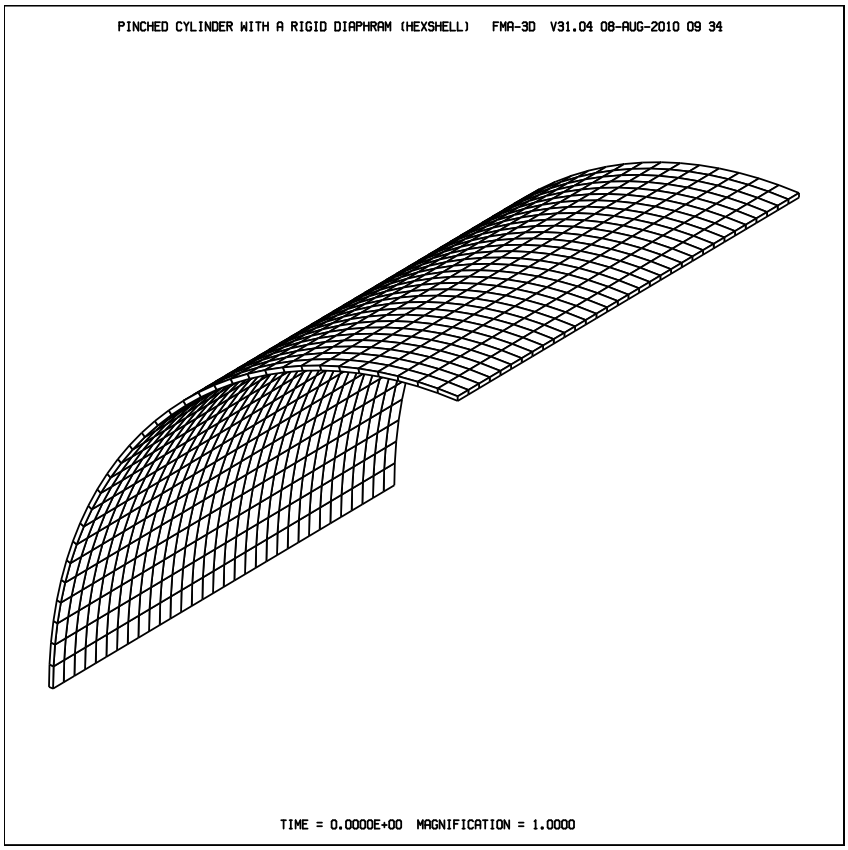

Figure 3.26. Cylinderical panel mesh consisting of a $1\times32\times32$ 8-node hexahedral solid elements; the panel is an octant of a full cylinder.

The loading is a pair of diametrially opposed point-loads applied halfway along the length of the cylinder. Given the complexity of the deformation, the point-loads are imposed via a prescribed motion, Figure 3.27.

The material is elastic-plastic with a bulk modulus of $k = 2500.0$, a shear modulus of $\mu =$

1154.0, a yield stress of $t_y = 24.3$, a linear tangent hardening modulus of $E_t = 272.758$ (plastic hardening modulus of $H = 300.0$), and a density of $\rho = 2.0\times10^{-8}$. The plastic hardening is isotropic.

Shown in Figure 3.28 are the shell finite element meshes used at zero load. The quadrilateral mesh has 1024 finite elements and the triangular mesh has 2048 finite elements.

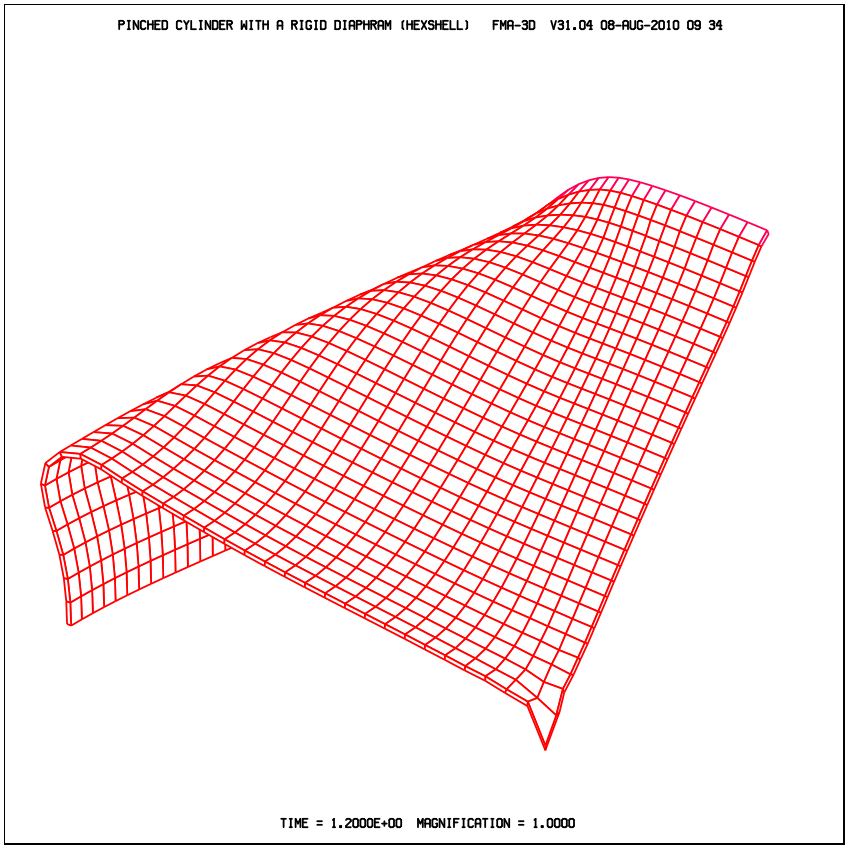

Figure 3.27. Cylinderical panel mesh consisting of a $1\times32\times32$ 8-node hexahedral solid elements; deformed configuration under opposing point loads. (In place of the point load, the deformation is imposed through a surrogate displacement boundary condition of $u_z = 250$.)

Test Problem Characteristics. The cylinder pinched between opposing loads results in a rather extreme motion. The motion is a large displacement, finite rotation, finite strain inelastic deformation that has modest buckling events shifting from one deformation pattern to another as the load increases. Unfortunately, as a test problem there does not exist a definitive answer against which comparisons can be made. Nearly repeatable results from a number of finite element formulations are reported by Hauptman, Schweizerhof and Doll, [2000], where a peak

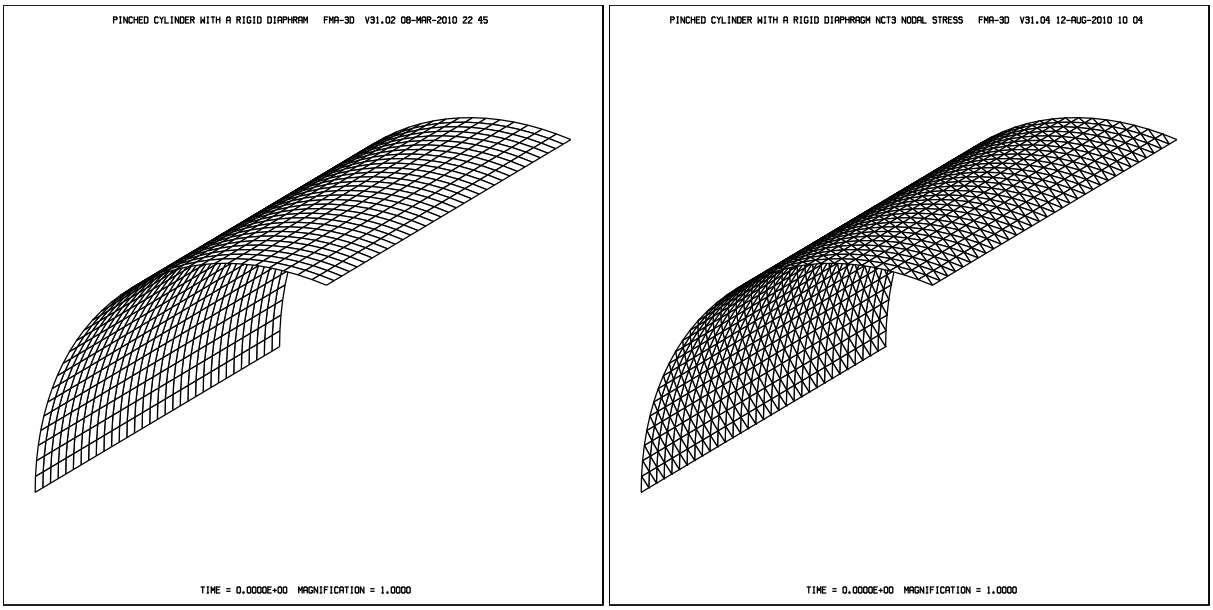

Figure 3.28. Mesh of the cylinderical section consisting of a 32×32 4-node quadrilateral shell elements (left panel), and a mesh of the cylinderical section consisting of a 2048 3-node triangular shell elements (right panel). The cylindrical section is one-eighth of a full cylinder.

load at full deflection of 2500 is shown. There are also results at 3010 and 2485, but during the first 70% of the deflection the reaction forces match, Figure 3.29.

Test Problem Results. In Table 8-1, Only one of the solid elements tested came acceptably close to the final load: the K1H8 Key-Gullerud-Koteras 8-node, plane stress hexahedron. The K2H8 Key-Gullerud-Koteras 8-node, 3-D multi-stress hexahedron, and the ESH8 Simo-Rifai enhanced strain 8-node, solid hexahedron are both on the stiff side by about 20%. The SDH8 Selective Deviatoric 8-node hexahedron is overly stiff as expected.

The double-layer TSH8 Wing Kam Liu Thick-Shell 8-node hexahedron failed early in the calculation as a result of severe hourglassing.

In Table 8-2, Three shell elements came acceptably close to matching the peak force at full deflection reported by Hauptman, Schweizerhof and Doll [2000]: the KHQ4 Key-Hoff 4-node quadrilateral, the KGQ4 Key-Gruda 4-node quadralateral with nodal-based surface fiber vectors, and the NCT3-tuned (0.20) node-centered 3-node triangle. The NCT3-table (0.02) node-centered 3-node triangle is too soft by about 20%. The ECT3 element-centered standard 3-node triangle is overly stiff as expected.

Table 8-1
Solid Element Maximum Force and External Energy
at a Deflection of 250

Formulation		Geometry	F_z	Ext. Eng.
ESH8	Simo-Rifai	3-D Stress Hexah	3161	2.5×10^5
K1H8	Key-Gullerud-Koteras	2-D Stress Hexah	2587	2.1×10^5
K2H8	Key-Gullerud-Koteras	3-D Stress Hexah	2817	2.5×10^5
TSH8	W. C. Liu Thick Shell	3-D Stress Hexah	$*$	$*$
SDH8	Selective Deviatoric	3-D Stress Hexah	3998	4.4×10^5
Reference Results			"2500"	

Table 8-2
Shell Element Maximum Force and External Energy
at a Deflection of 250

Formulation		Geometry	F_z	Ext. Eng.
KHQ4	Key-Hoff	4-Node Quad	2460	2.0×10^5
KHQ4	Key-Gruda	4-Node Quad	2509	2.0×10^5
NCT3-table	Node Centered	3-Node Triangle	2088	1.7×10^5
NCT3-tuned	Node Centered	3-Node Triangle	2551	2.1×10^5
ECT3	Elem't Centered	3-Node Triangle	3070	3.2×10^5
Reference Results			"2500"	

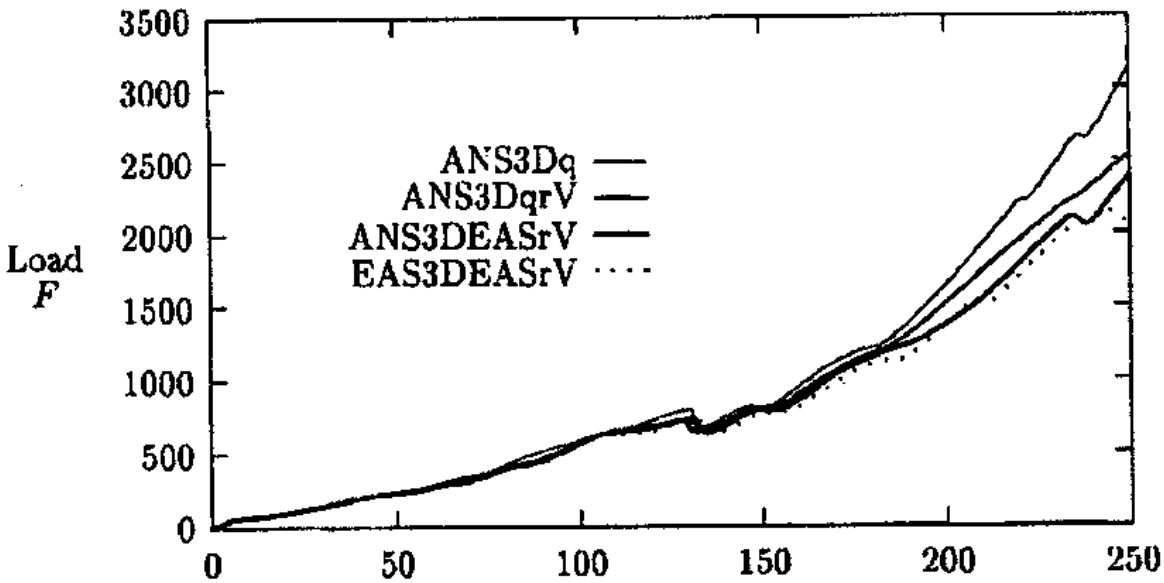

Figure 3.29. Pinched Cylinder Load Deflection Diagram: F_z *vs* u_z at the center point from Hauptman, Schweizerhof, and Doll [2000].

In Figure 3.29 taken from Hauptman, Schweizerhof, and Doll [2000], at a deflection of 135 there is a mild, but notable, buckling event where the deformation pattern shifts. (There are other deformation pattern shifts that take place, as well, for example, at about 240.) In Figure 3.30, two of the solid elements (K1H8, ESH8) exhibit the same buckling event but at a deflection of 160. In Figure 3.31, all of the results exhibit a mild buckling event at a deflection of about 60. Later events are not all uniformly occurring at the same deflection. The difference between the deflections at which the buckling events occur for the KHQ4 element and the two NCT3 elements (NCT3-table and NCT3-tuned) suggest that there are mesh artifacts (quadrilateral *versus* triangular meshes) present in the results. Of note, is the grouping and similarity of results for the three KHQ4, NCT3-table, and NCT3-tuned elements up to a deflection of about 150.

Of particular note is the response predicted by the KGQ4 Key-Gruda plane-stress 4-node quadrilateral using nodal-based suface fiber vectors, Figure 3.31, righthand panel. The KGQ4 finite element naturally reports the maximum deflection force of 2509 that approximates closely the results reported by Hauptman, Schweizerhof and Doll [2000] without the use of tuning parameters required by the NCT3 Nodal Centered 3-node triangles.

Figures 3.32 and 3.33 depict the final deformations ($u_z = \pm 250$) for the solid K1H8 Key-Gullerud-Koteras plane stress 8-node hexahedron and the NCT3-tuned Node-Centered 3-node triangular elements, respectively. The images are constructed by reflecting the original cylin-

derical octant solution to obtain a half-model of the full cylinder. The results for the NCT3-tuned (0.20) triangular shell finite element in Figure 3.33 more nearly matches the final geometric shape reported by Hauptman, Schweizerhof and Doll [2000].

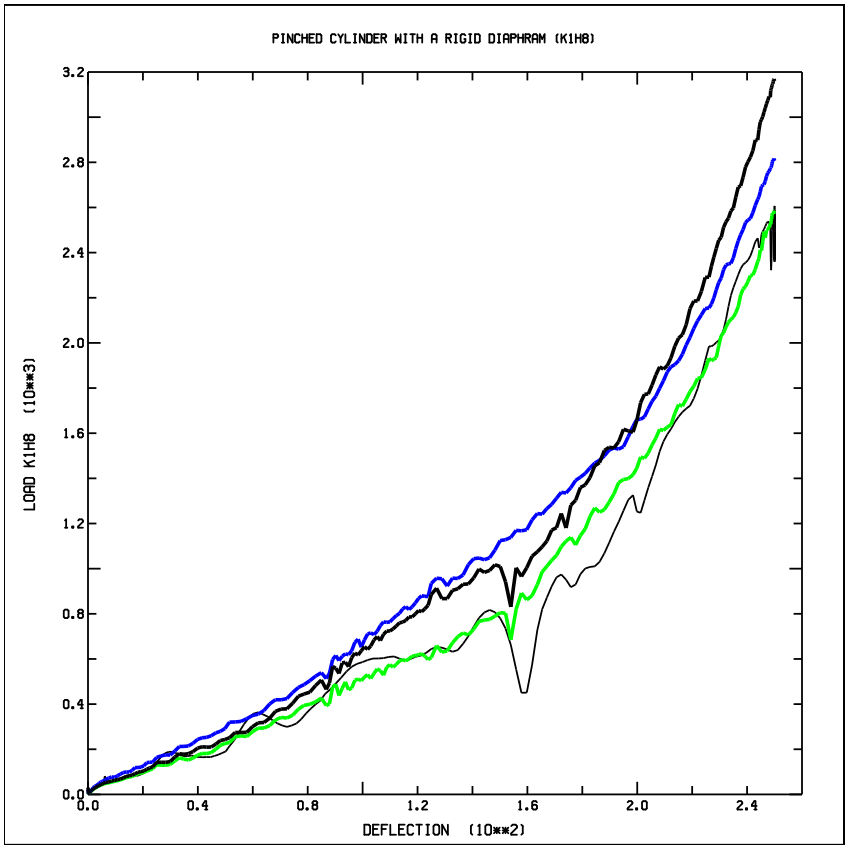

Figure 3.30. Cylinderical panel load *vs* deflection curves for the 3-D solid finite elements. The solid element ordering by color is K1H8, K2H8, and ESH8. Note that the KHQ4 Key-Hoff 4-node quadrilateral solution is the thin black line and has a peak load of 2460 that approximates the results reported by Hauptman, Schweizerhof and Doll [2000].

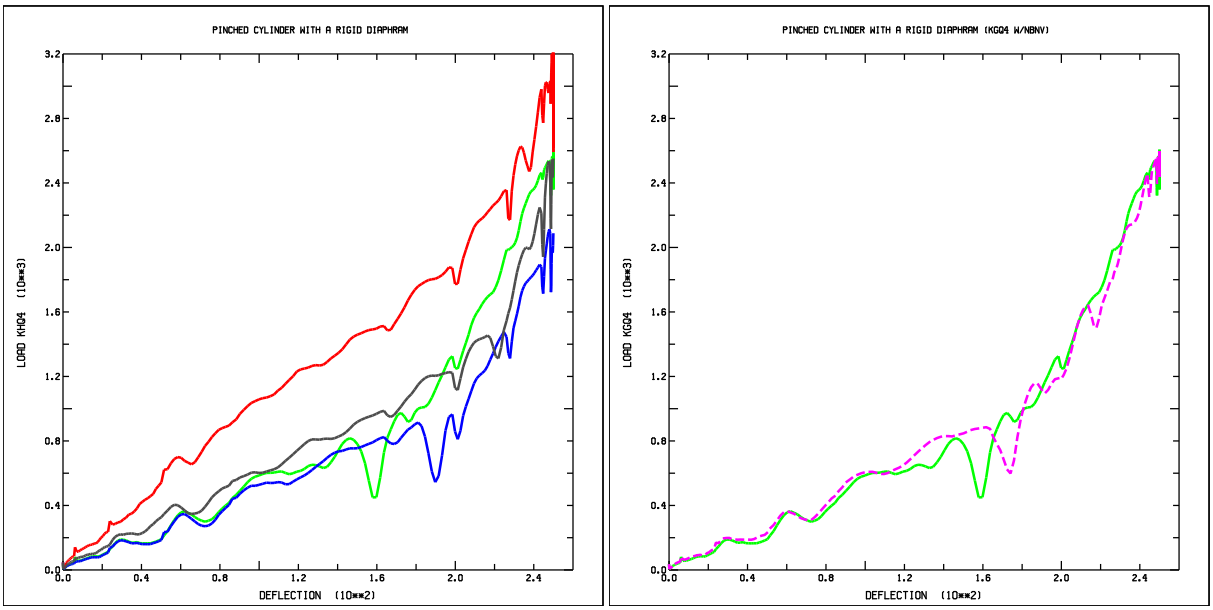

Figure 3.31. Cylinderical panel load *vs* deflection curves for the 2-D shell finite elements. The shell element ordering by color is KHQ4, NCT3-tuned, NCT3-table, and ECT3 (lefthand panel). Cylinderical panel load *vs* deflection curves for the 2-D shell finite elements KHQ4 and KGQ4 (righthand panel). Note that the KGQ4 Key-Gruda 4-node quadrilateral solution is the dashed magenta line and has a peak load of 2509 that approximates closely the results reported by Hauptman, Schweizerhof and Doll [2000].

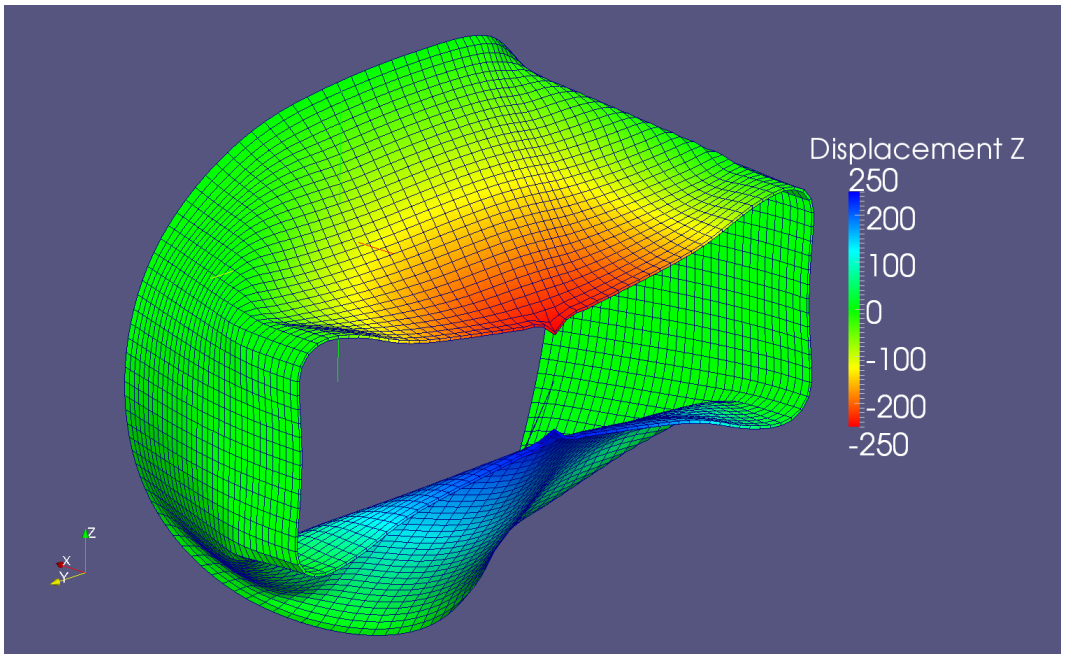

Figure 3.32. Soild finite element mesh using reflections to build a half-model of the final pinched cylinder configuration (K1H8).

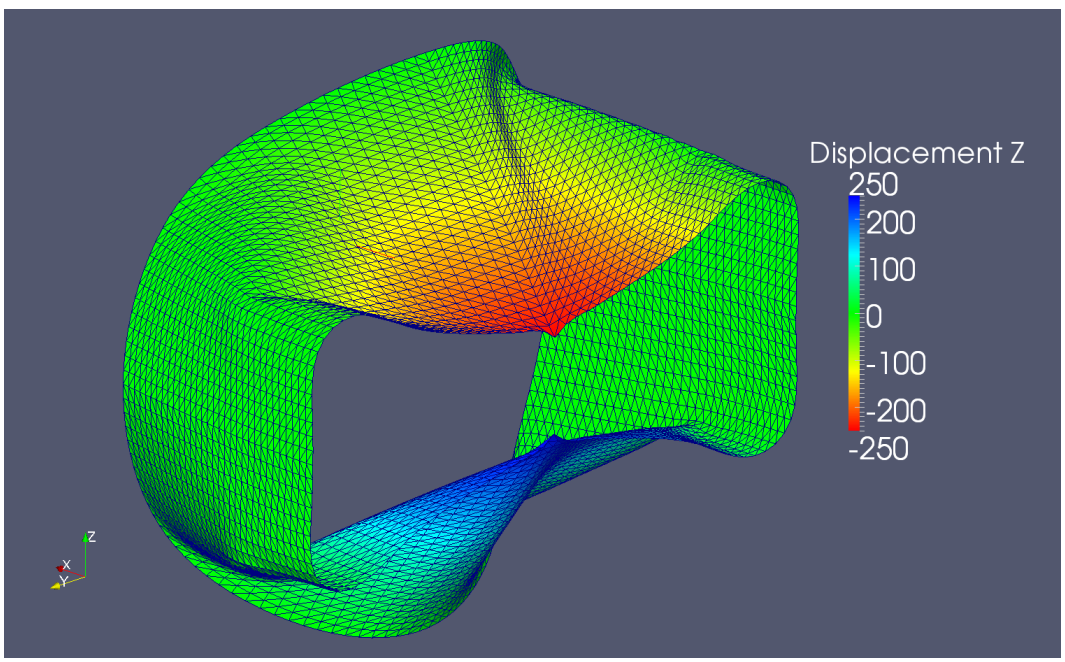

Figure 3.33. Shell finite element mesh using reflections to build a half-model of the final pinched cylinder configuration (NCT3-tuned).

3.9 Test Problem 9: Vibrating Plate

Test Problem Statement. The cantilver plate, pictured in Figure 3.34, has a thickness of 2.0 mm, a length of 100.0 mm, and a width of 50.0 mm. The red configuration of the plate is the final deformed shape. The 25.0 mm edge, far end, is clamped such that no translations are permitted, and, in the case of shell finite elements, no rotations are permitted.

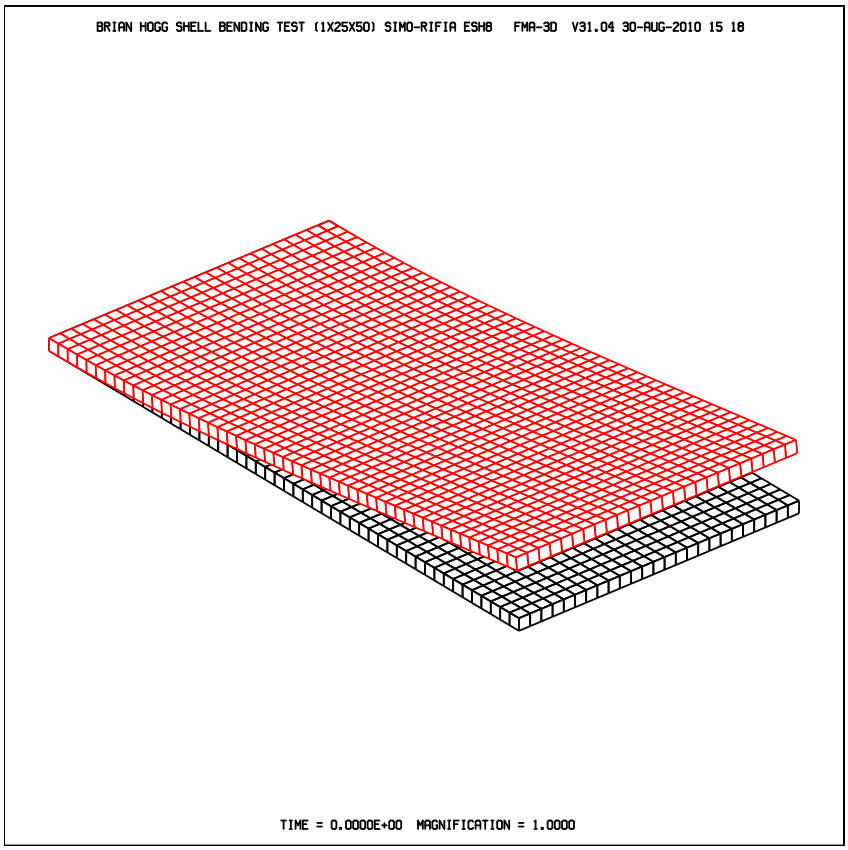

Figure 3.34. Cantilevered plate solid mesh consisting of a $1 \times 25 \times 50$ 8-node hexahedral solid elements; the red configuration of the plate is the final deformed shape.

Shown in Figures 3.35 and 3.36 are the shell finite element meshes. The quadrilateral mesh has 1250 finite elements and the triangular mesh has 2500 finite elements.

The loading is a uniform pressure $p = 0.1066$ MPa applied to the lower surface of the plate. The pressure is increased linearly from $p = 0.0$ MPa at time $t = 0.0$ ms to $p = 0.1066$ MPa at time $t = 100.0$ ms after which the pressure is held constant until time $t = 200.0$ ms. The simulation is complete at time $t = 200.0$ ms.

The material is elastic with a Young's modulus of $E = 1.0 \times 10^2$ GPa, a Poisson's ratio of $\nu = 0.30$, and a density of $\rho = 8.0 \times 10^3$ kg/m^3.

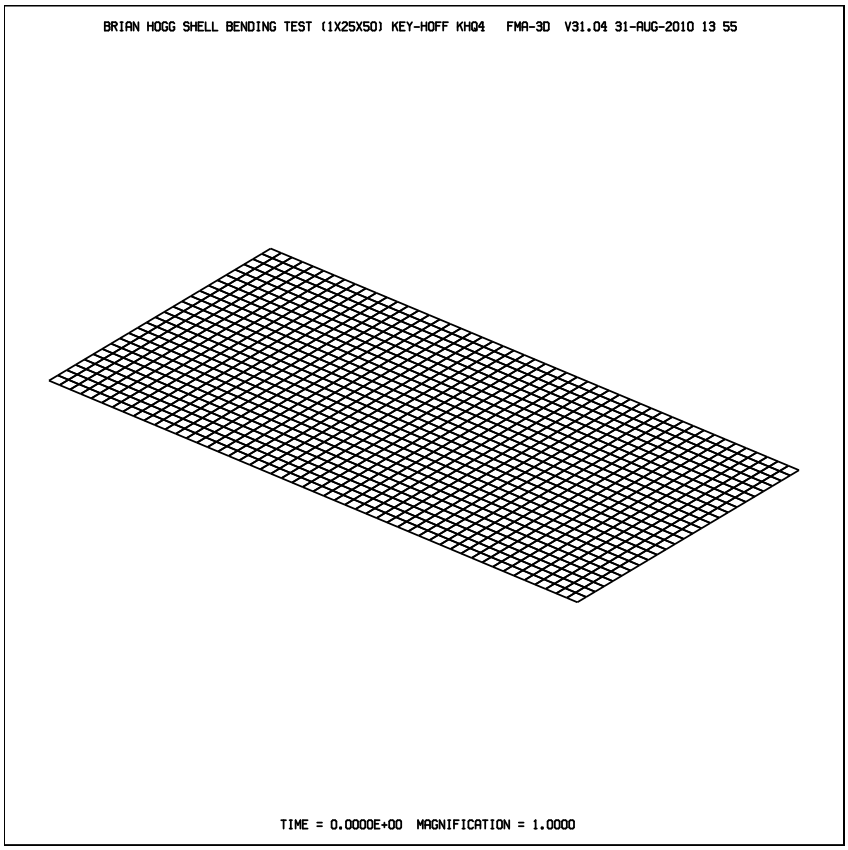

Figure 3.35. Cantilevered plate shell mesh consisting of a 25×50 4-node quadrilateral elements.

Test Problem Characteristics. The test problem geometry is a simple flat plate. The purpose of this test problem is two-fold: (1) to test that the static solution is obtained, namely, an infinitesimal beam-theory "static" deflection of 0.999375 cm, and (2) to test that the element formulation during the portion of the response where the plate is vibrating under load is conservative, that is, both the amplitude and mean of the vibrational response remain constant.

Test Problem Results. In Table 9-1, The following three solid finite elements obtained static deflection results that are within $\pm 7\%$ of the infinitesimal beam-theory result: the ESH8 Simo-Rifia Enhanced Strain 8-node hexahedron, the K1H8 Key-Gullerud-Koteras plane-stress 8-node hexahedron, and the Wing Kam Liu Thick Shell 8-node hexahedron with a double layer

Table 9-1
Brian Hogg Plate Static Deflection
Solid Bending-Formulated Finite Elements

Formulation		Geometry	u_y
ESH8	Simo-Rifai	3-D Stress Hexah	0.9495
K1H8	Key-Gullerud-Koteras	2-D Stress Hexah	0.9468
K2H8	Key-Gullerud-Koteras	3-D Stress Hexah	0.7942
TSH8	W. C. Liu Thick Shell	3-D Stress Hexah	1.0672
SDH8	Selective Deviatoric	3-D Stress Hexah	1.1484
Reference Results			0.9994

Table 9-2
Brian Hogg Plate Static Deflection
Shell Finite Elements

Formulation		Geometry	u_y
KHQ4	Key-Hoff	4-Node Quad	0.9551
KGQ4	Key-Gruda	4-Node Quad	0.9445
NCT3	Node Centered	3-Node Triangle	0.9263
ECT3	Element Centered	3-Node Triangle	0.8660
Reference Results			0.9994

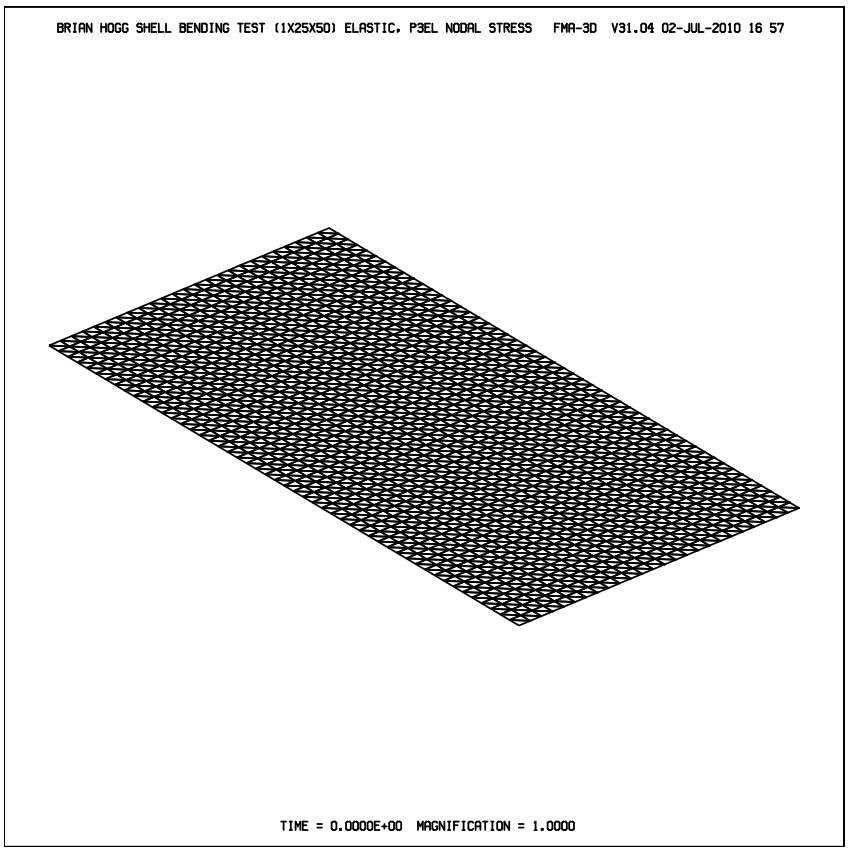

Figure 3.36. Cantilevered plate shell mesh consisting of a 1250 3-node triangular element pairs.

mesh. The K2H8 Key-Gullerud-Koteras multi-stress 8-node hexahedron is 20% too stiff; the SDH8 Selective Deviatoric 8-node hexahedron is 15% too soft.

In Table 9-2, Three of the shell finite elements (the KHQ4 Key-Hoff plane-stress 4-node quadrilateral, the KGQ4 plane-stress 4-node quadrilateral using nodal-based surface unit-normal vectors, and the NCT3 Node Centered 3-node triangle) obtained static deflection results that are within 6% of the infinitesimal beam-theory result. The ECT3 Element Centered plane-stress 3-node triangle is 13% to stiff as expected.

The vibrational response was satisfactory for all of these finite elements. For example, Figure 3.37 is the free-end tip deflection for the ESH8 Simo-Rifia Enhanced strain 8-node hexahedron finite element, and Figure 3.38 is the free-end tip deflection for the KHQ4 Key-Hoff plane-stress 4-node quadrilateral.

Simulation Notes. The "clamped" boundary condition with all three translational degrees

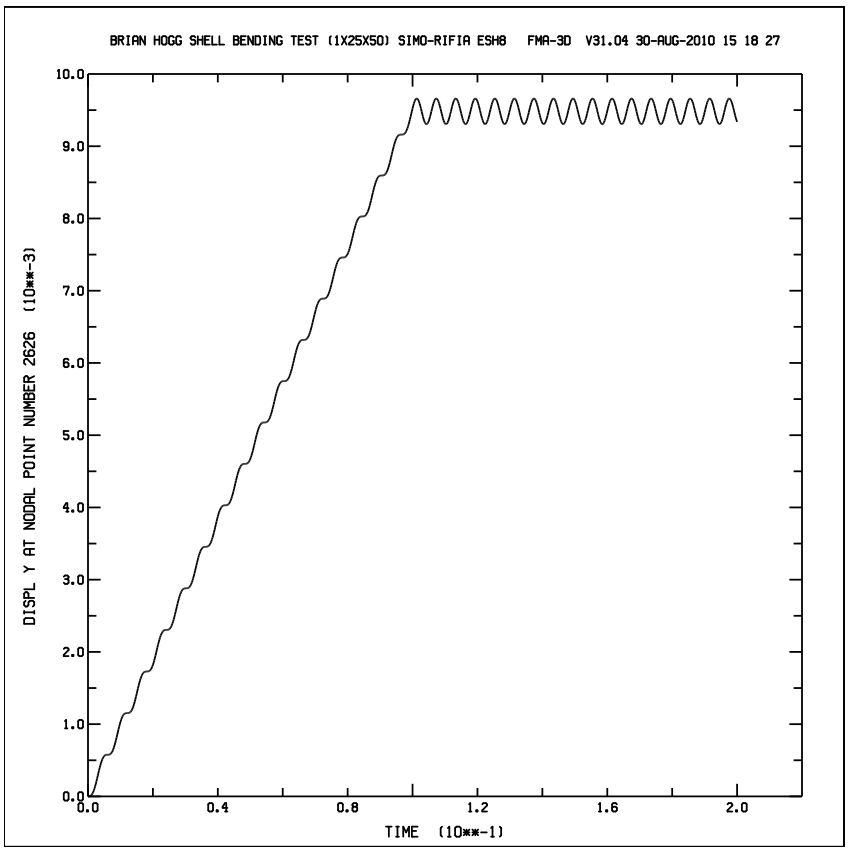

Figure 3.37. Cantilevered plate solid ESH8 Simo-Rifia Enhanced Strain 8-node hexahedral finite element deflected vibrational response.

of freedom set to zero is somewhat restrictive. A second calculation was conducted with the following minimal set of kinematic restraints:

1. The lower line of nodal points along the clamped-end was given a "hinge" boundary condition, namely, if the x-axis is along the length of the plate, the y-axis is normal to the plate, and the z-axis is across the width of the plate, then boundary conditions of nomal movement $u_x = 0$, vertical movement $u_y = 0$, and no restriction on lateral movement u_z were specified, and

2. The upper line of nodal points along the clamped-end was given a $u_x = 0$ boundary condition, and, thus the line of nodal points could move freely both vertically and horizontally.

In spite of the fact the less restrictive boundary conditions that are incorporated into infinitesimal beam theory were used, there was no appreciable difference in the deflection and vibration

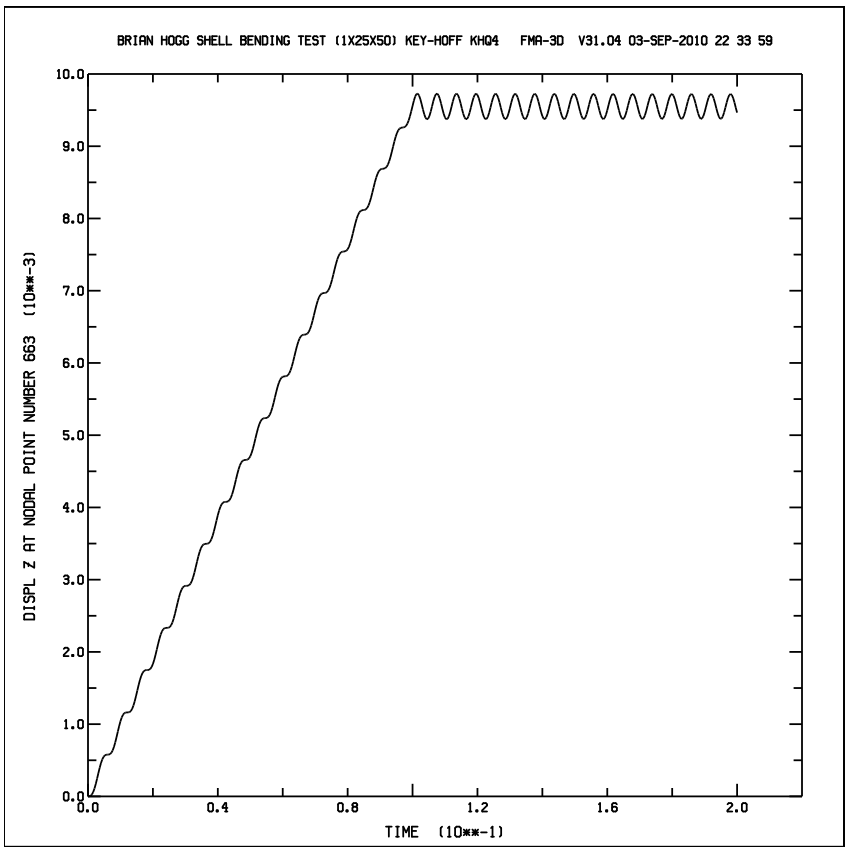

Figure 3.38. Cantilevered plate shell KHQ4 Key-Hoff plane-stress 4-node quadrilateral finite element deflected vibrational response.

results between these two sets of kinematic boundary conditions.

3.10 Test Problem 10: Crushed Spherical Shell

Test Problem Statement. The hollow sphere, pictured in Figure 3.39, has a radius of 114.0 mm and a thickness of 1.52 mm; also pictured are two rigid plattens. The two plattens move toward each other collapsing the sphere on itself.

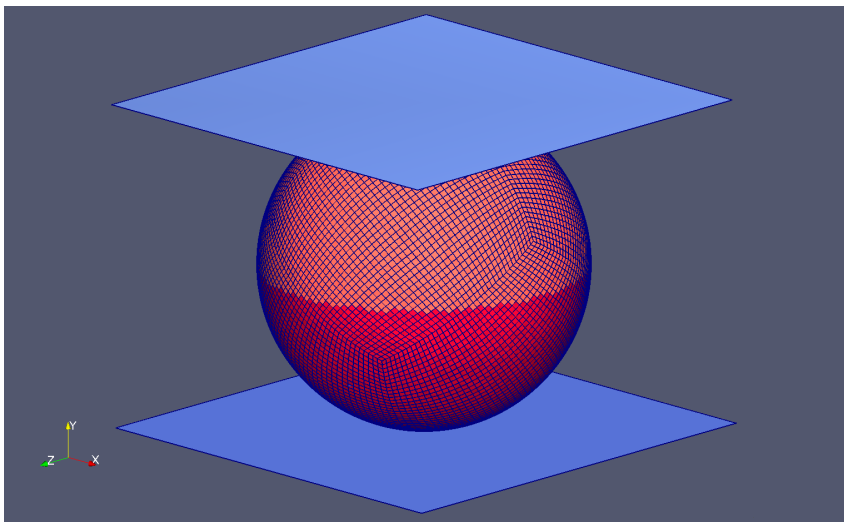

Figure 3.39. Hollow Sphere mesh consisting of 9,602 4-node quadrilateral shell elements. The color change in the sphere represents the top half and lower half side-sets used with the contact algorithms.

The simulation is focused on collapsing or crushing the sphere, Figure 3.40. Each platten is modeled with single 4-node quadrilateral finite element. Rather than appling forces to the plattens, a prescribed motion of the vertex nodes is utilized. There are three contact algorithms running: (1) the top half of the sphere against the upper platten, (2) the bottom half of the sphere against the lower platten, and (3) the top half of the sphere against the bottom half of the sphere. The contact interaction between the sphere and the plattens is frictionless. The crushing of the sphere is completed in a modeled time scale of 20.0 ms. and takes approximately 150,000 time steps for the KHQ4 4-node quadrilateral plate element. The ESH8 Simo and Rifai Enhanced Strain 8-node hexahedral soild element takes approximately 122,000 time steps.

The material is elastic-perfectly plastic with a Young's modulus of $E = 2.0 \times 10^5$ MPa, a Poisson's ratio of $\nu = 0.25$, a yield stress of $\sigma_y = 300$ MPa, a linear hardening tangent modulus of $E_{tan} = 0.0$, and a density of $\rho = 8.0 \times 10^{-9}$.

The solid and shell finite element meshes are visually indistinguishable except for the tri-

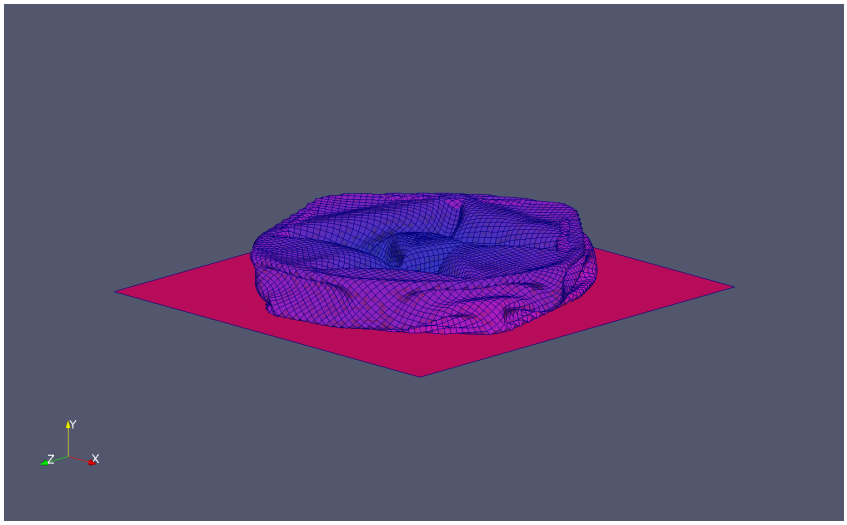

Figure 3.40. Hollow Sphere with an original diameter of 228 mm crushed to 38.12 mm.

angular mesh where each quadrilateral has been subdivided into a pair of triangles.

Test Problem Characteristics. The test problem is a validation calculation as opposed to a verification calculation. The problem parameters have been drawn from experimental results that used 33 common industrial-grade hollow spherical floats, Pepin and Thacker [2003]. Of particular interest is the number of lobes in the buckle pattern that develop as the sphere deforms, namely five lobes and reported to be consistent with the spheres that were crushed experimentally. Secondarily, the force *versus* deflection needed to crush the sphere is an indicator of the quality of the results obtained in the simulation. In the simulations conducted by Pepin and Thacker, three separate material property regions are utilized. Here, only a single set of material properties for the entire sphere are used.

Test Problem Results. The buckling patterns at a nominal platten separation of 90.0 mm, down from the initial 228 mm platten separation, are shown in Figures 3.41 through 3.47. Each finite element tested exhibited a different buckling pattern. One solid and one shell finite element (K1H8 and KGQ4) exhibit a distinct 5-lobe buckling pattern that matches the experimental results of Pepin and Thacker, [2003]. The shell finite element (KHQ4) exhibits a less distinct 5-lobe pattern on one side that appears to be influenced unduly by the pattern of the mesh. Another shell finite element (NCT3) exhibits an unusual, but 5-lobed, buckling pattern in that one lobe is much more advanced in amplitude than the remaining four lobes, a characteristic seen in the buckling pattern on both sides. The total internal energy, dominated by inelastic dissipation, *versus* deflection for these four finite elements is pictured in Figure 3.50

The remaning solid and shell finite elements are notable for their less than impressive re-

sults. Two of the elements (K2H8, ECT3) exhibit minimal or no buckling.

- **ESH8.** In Figure 3.41, the sphere modeled with the Simo and Rifai Enhanced Strain 8-node hexahedron exhibits on both sides either a 6-lobed or a 8-lobed buckling pattern depending on how the amplitudes enter into the count.
- **K1H8.** In Figure 3.42, the sphere modeled with the Key-Gullerud-Koteras plane-stress 8-node hexahedron exhibits a decided 5-lobed buckling pattern on one side and a 4-lobed, maybe a 5-lobed, pattern on the other side.
- **K2H8.** In Figure 3.43, the sphere modeled with the Key-Gullerud-Koteras multi-stress 8-node hexahedron exhibits a zeroth-order buckling pattern.
- **TSH8.** In Figure 3.44, the sphere modeled with the Wing Kam Liu Thick Shell 8-node hexahedron exhibits either a 4-lobed, maybe a 6-lobed, buckling pattern on both sides.
- **SDH8.** In Figure 3.45, the sphere modeled with the Selective Deviatoric 8-node hexahedron exhibits a distinctly uniform 6-lobed buckling pattern on both sides that shows a common mesh configuration preference for each lobe, but does not always develop a lobe at the otherwise prefered mesh configuration.
- **KHQ4.** In Figure 3.46, the sphere modeled with the Key-Hoff 4-node quadrilateral shell exhibits an irregular 5-lobed buckling pattern on one side, and either a 3-lobed or a 7-lobed pattern depending on how the amplitudes enter into the count on the other side.
- **KGQ4.** In Figure 3.47, the sphere modeled with the Key-Gruda plane-stress 4-node quadrilateral using the K1H8 internals on a by time-step reconstructed hexahedral frame that employs surface fiber vectors (initially surface normal vectors that have been rotated in time using nodal point rotational rates) exhibits a near ideal 5-lobed buckling pattern.
- **NCT3.** In Figure 3.48, the sphere modeled with the Node Centered 3-node triangular shell exhibits a 5-lobed buckling pattern with one lobe much more advanced in amplitude than the remaining four lobes on both sides. The "advanced" lobes occur at two different locations when comparing one side to the other side.
- **ECT3.** In Figure 3.49, the sphere modeled with the Element Centered 3-node triangular shell exhibits virtually no buckling under the plattens. (There is a possible 4-lobed buckling pattern around the equator.)

Simulation Notes. The objective of the simulation is to reproduce the collapse response observed when the sphere is crushed in a laboratory test machine. While the test is conducted as rapidly as the test machine can reliably perform, from the perspective of the structure it is still a static test. Computationally, the simulation is conducted using an explicit transient dynamic simulation because the technology utilized has a high level of certainty and reliability for such a complex event, however, there is a trade-off in time scale that must be considered. If

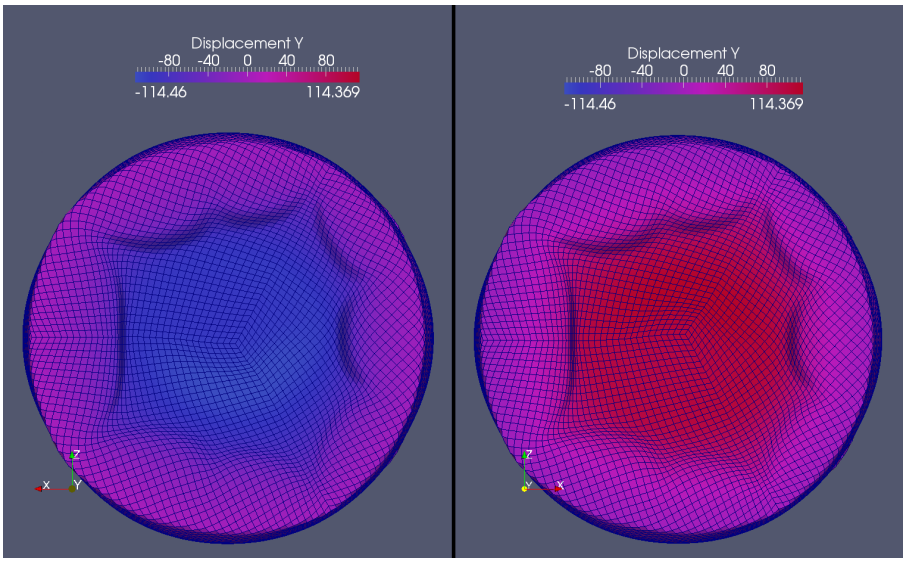

Figure 3.41. ESH8 hollow Sphere with an original diameter of 228 mm crushed to 90± mm. Upper and lower lobe patterns are shown.

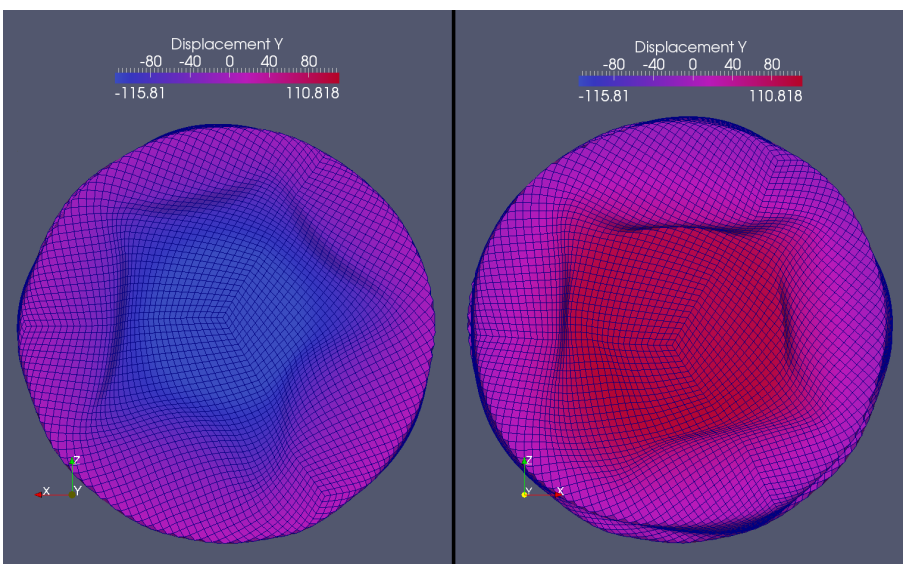

Figure 3.42. K1H8 hollow Sphere with an original diameter of 228 mm crushed to 90± mm. Upper and lower lobe patterns are shown.

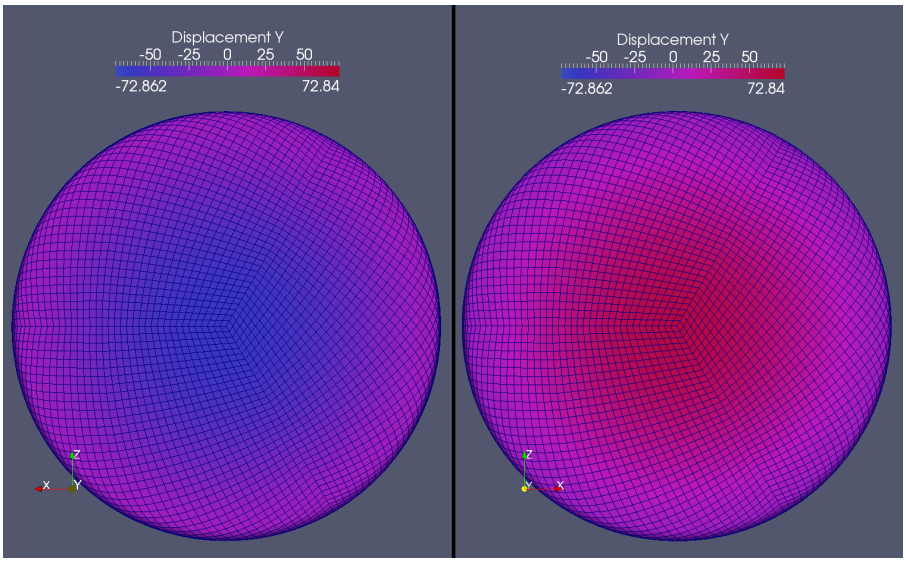

Figure 3.43. K2H8 hollow Sphere with an original diameter of 228 mm crushed to 90± mm. Upper and lower lobe patterns are shown.

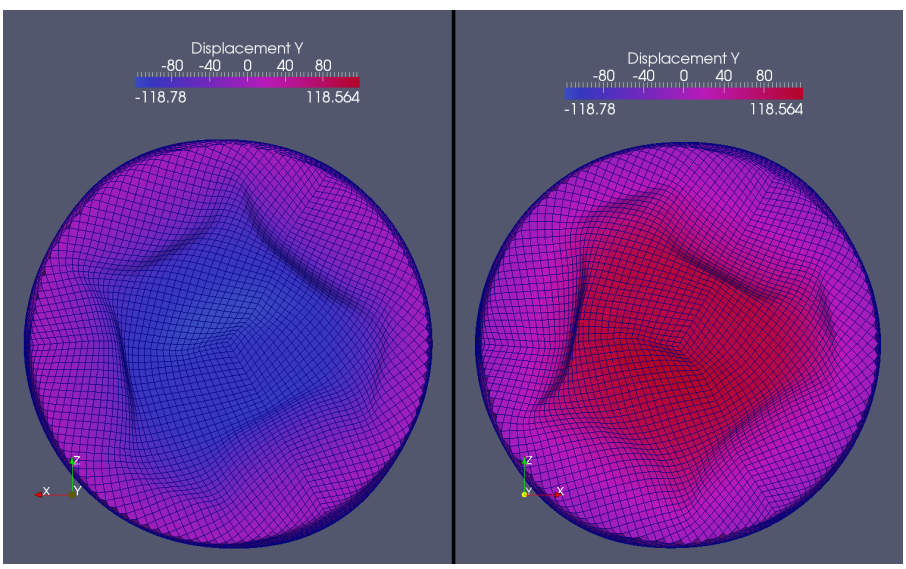

Figure 3.44. TSH8 hollow Sphere with an original diameter of 228 mm crushed to 90± mm. Upper and lower lobe patterns are shown.

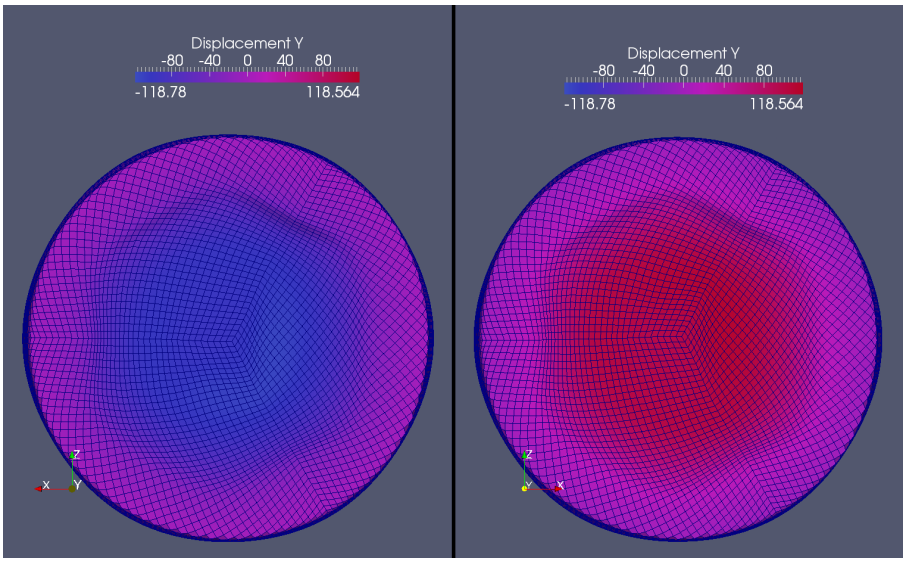

Figure 3.45. SDH8 hollow Sphere with an original diameter of 228 mm crushed to 90± mm. Upper and lower lobe patterns are shown.

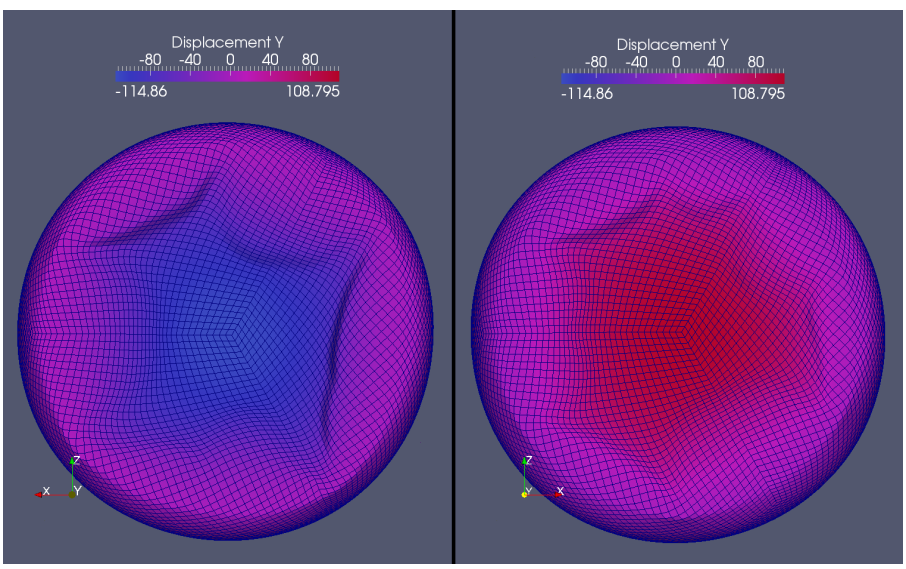

Figure 3.46. KHQ4 hollow Sphere with an original diameter of 228 mm crushed to 90± mm. Upper and lower lobe patterns are shown.

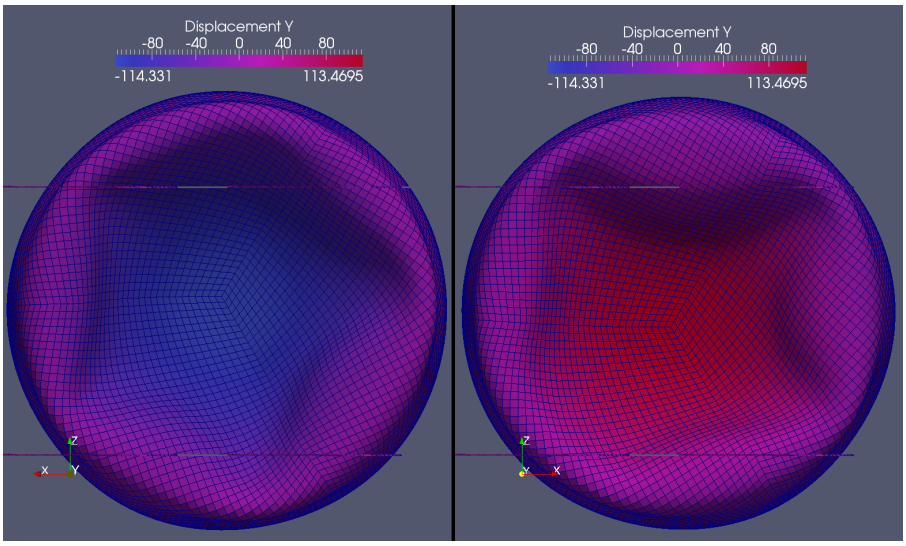

Figure 3.47. KGQ4 hollow Sphere with an original diameter of 228 mm crushed to 90± mm. Upper and lower lobe patterns are shown.

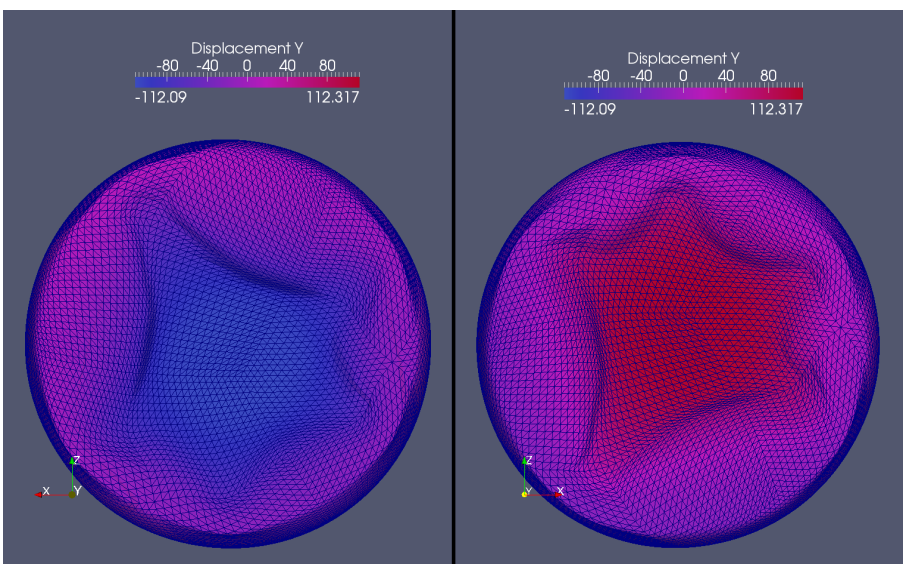

Figure 3.48. NCT3 hollow Sphere with an original diameter of 228 mm crushed to 90± mm. Upper and lower lobe patterns are shown.

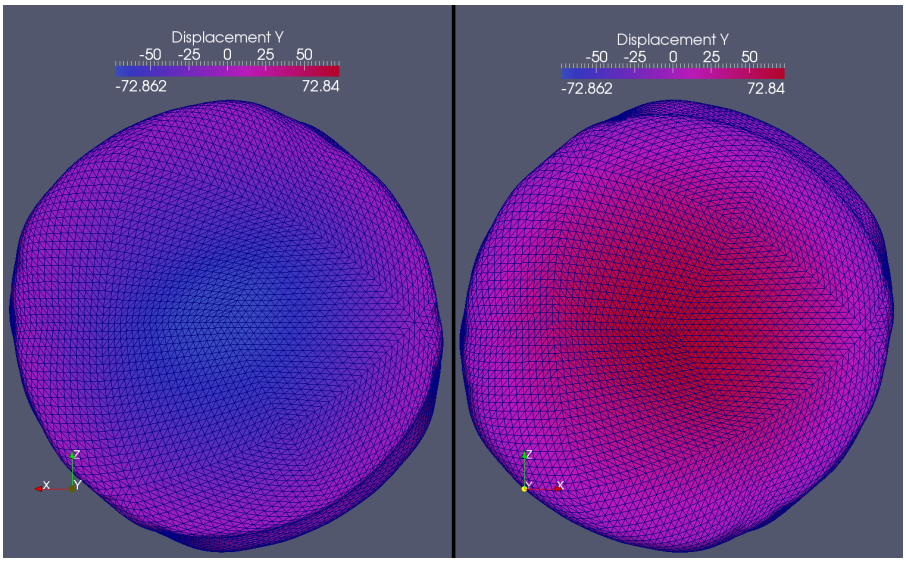

Figure 3.49. ECT3 hollow Sphere with an original diameter of 228 mm crushed to 90± mm. Upper and lower lobe patterns are shown.

the platten movement is simulated at too long a modeled time scale, say, in seconds, then the wall-clock time will be in days, If the platten movement is simulated at too short a modeled time scale, say, in sub-milliseconds, then the wall-clock time will be a few hours, but there will exist in the response true transient dynamic behavior that will be "recorded" in the elastic-plastic history in the material. Here, 20 ms has been selected, and at the time of peak kinetic energy (11 ms), the kinetic energy is 4% of the internal energy.

In the experimental set-up the lower platten is stationary while the upper platten moves downward statically crushing the sperical shell. In the simulation, both plattens move towards each other allowing a more nearly static response compared to one stationary platten and one moving platten producing the same deflection in 20 ms.

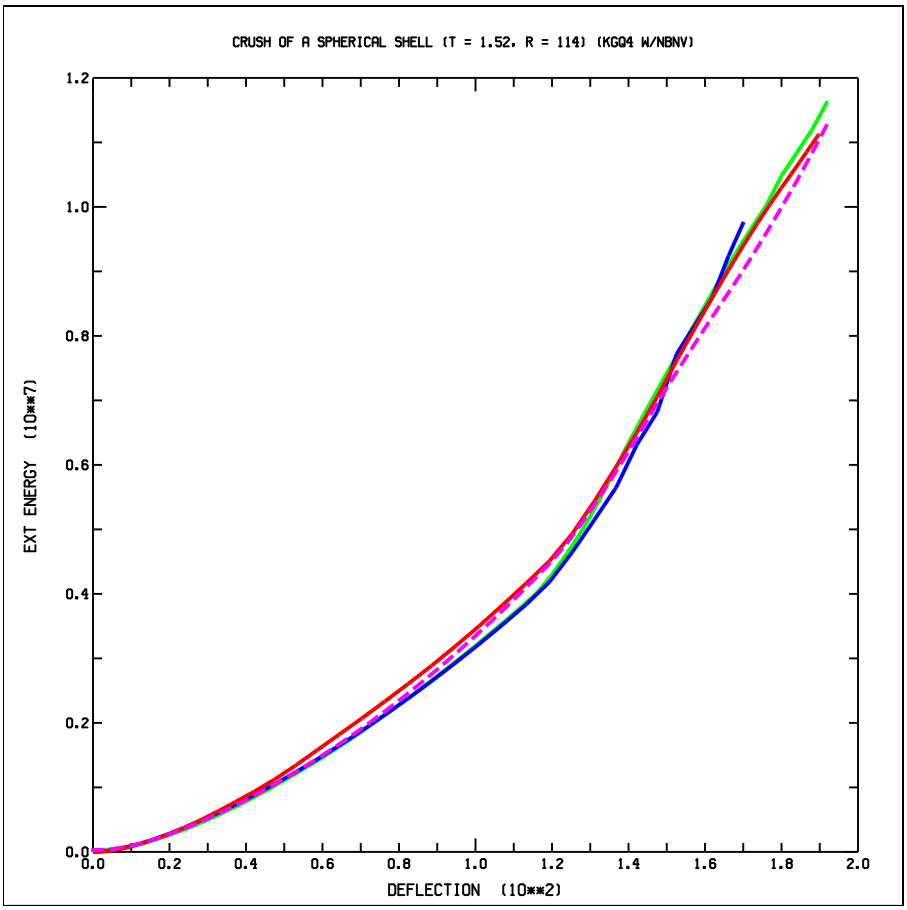

Figure 3.50. External Energy *versus* Deflection for the four finite elements that exhibit one or more 5-lobed buckling patterns: K1H8, KHQ4, KGQ4, and NCT3.

3.11 Test Problem 11: Element Shape Sensitivity

3.11.1 3-D Hexahedral Shell Elements

Test Problem Statement. The beam, pictured in Figure 3.51, has a length of 10 inches, a depth of 1.0 inch, and a width of 1.0 inch. The boundary conditions are those of a cantilevered beam, namely, zero displacement and zero rotation at the root (far end), Figure 3.51.

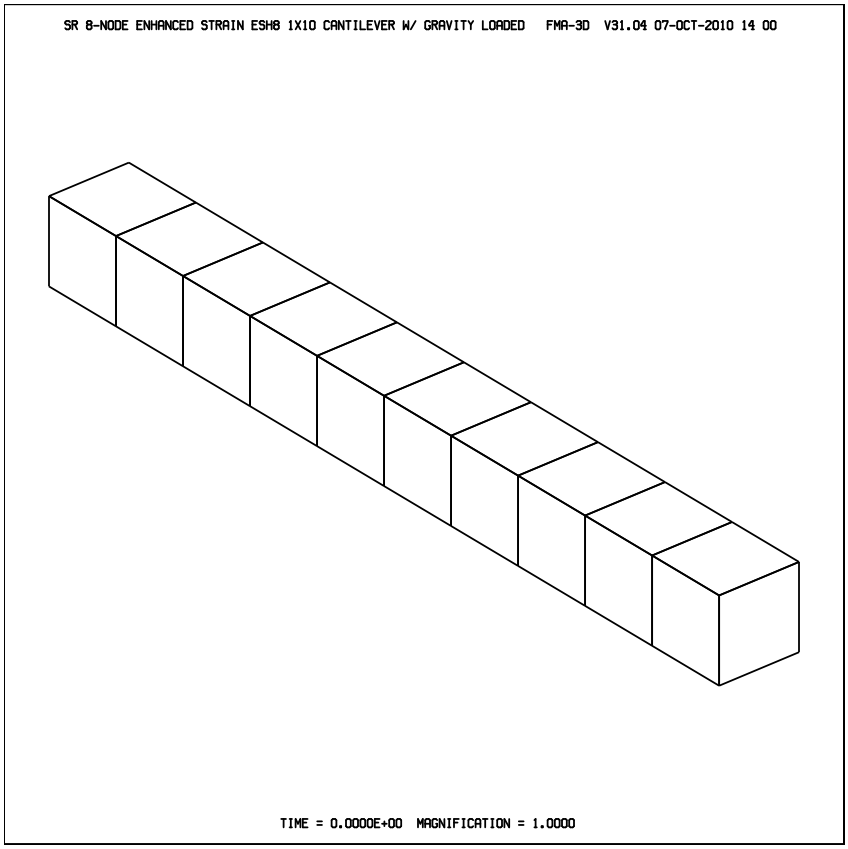

Figure 3.51. Beam mesh consisting of a single strip of ten 8-node hexahedral solid elements.

The loading is a pure bending moment applied to the free end (near end) of the beam. There are concentrated forces at the top two nodal points in 'compression,' and concentrated forces at the bottom two nodal points in 'tension' each with a magnitude of 725 lb_f. The loading is zero at time $t = 0.0$ and is increased in time following a 12.0 ms duration cosine ramp to 725.0 lb_f at which point the concentrated forces are held constant.

The material is elastic with a Young's modulus of $E = 1.0 \times 10^{+6}$ psi, a Poisson's ratio of $\nu = 0.25$, and a density of $\rho = 2.61 \times 10^{-4}$ $\text{lb}_\text{f}\text{-sec}^2/\text{in}^4$.

Test Problem Characteristics. The reference problem is a one-dimensional bending test that has a reference peak tip deflection of 1.0 inch (0.99974) at 11.0 ms (11.040), Figure 3.52. As a test of element shape sensitivity, random axial coordinate positions are introduced, and both change in the peak tip deflection u_y at 11.0 ms and the amplitude of any tip lateral motion u_z from imperfect numerical cross coupling introduced by the irregular mesh are examined. The irregular meshes are pictured in Figures 3.53 and 3.54.

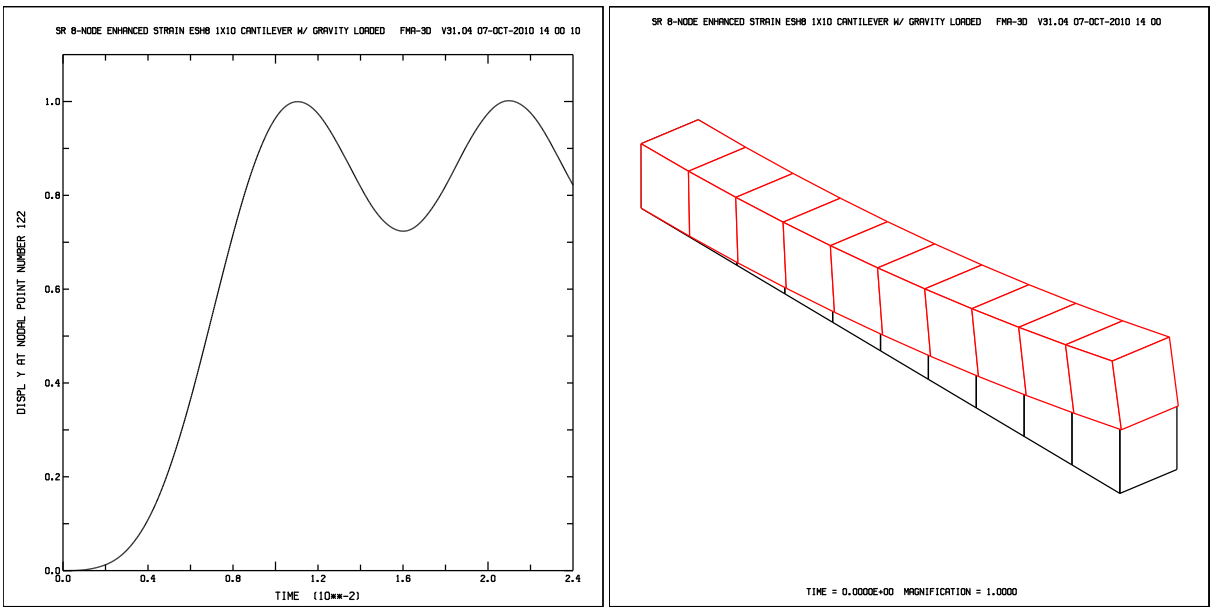

Figure 3.52. The ESH8 reference solutions for the tip displacement u_y *vs* time, left panel, and for the deformed mesh at 11.00 ms, right panel.

The uniform constant bending along the axis introduced by this loading means that all of the finite elements participate equally in the solution as opposed to, say, a tip loaded cantilever beam where the bending deformation is concentrated at the clamped end.

Test Problem Results. The results of the study are tabulated in Table 11-1. Note that δu_y and δu_z are with respect to each element's regular-mesh displacement history, *not* with respect to the ESH8 reference result. As an example, pictured in Figure 3.55 is the uniform mesh and irregular mesh results for the TSH8 Wing Kam Liu Thick Shell 8-node hexahedron.

Viewed as a percentage change in peak tip deflection, the solid finite elements rank as follows: K1H8 (2.7%), ESH8 (6.9%), K2H8 (10.3%), TSH8 (10.6%), and SDH8 (16.4%).

Table 11-1
Beam Tip Deflections Due to a Uniform Axial Bending Resultant
(u_y is the irregular-mesh peak deflection)

Formulation		Geometry	u_y	δu_y	δu_z
ESH8	Simo-Rifai	3-D Stress Hexah	0.9306	-0.0694	-0.0004
K1H8	Key-Gullerud-Koteras	2-D Stress Hexah	0.9684	-0.0271	-0.0566
K2H8	Key-Gullerud-Koteras	3-D Stress Hexah	0.7663	-0.1031	-0.0023
TSH8	W. C. Liu Thick Shell	3-D Stress Hexah	1.0252	-0.1062	-0.0021
SDH8	Selective Deviatoric	3-D Stress Hexah	1.0586	-0.1640	-0.0002
Reference Results (ESH8 formulation)			1.0000	0.0000	0.0000

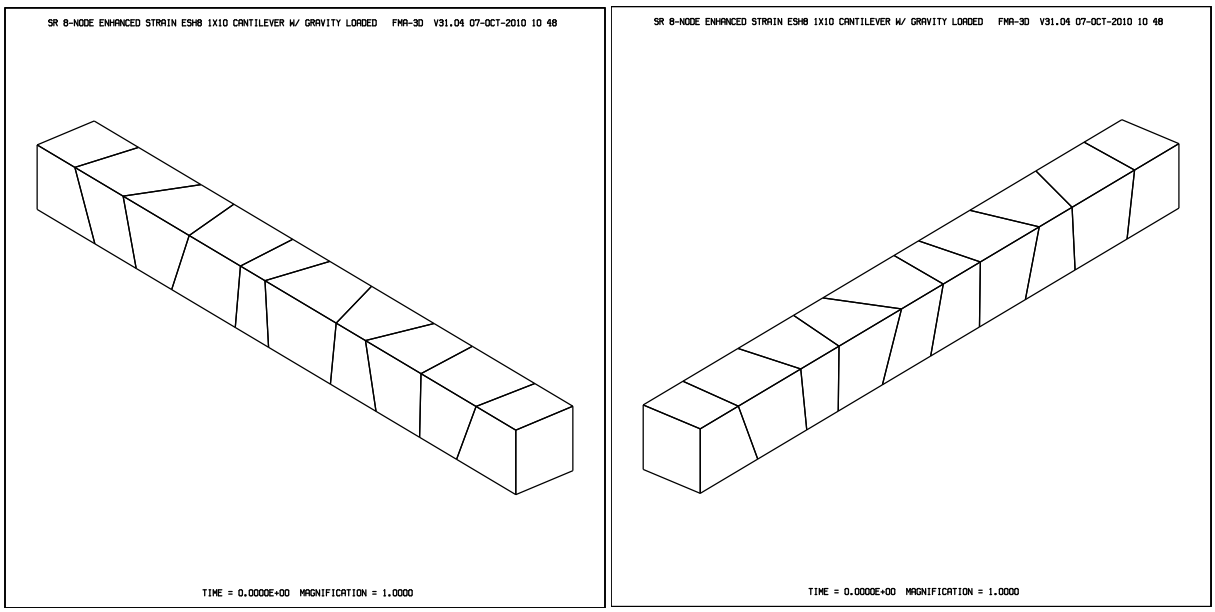

Figure 3.53. The random axial nodal point positions for the the ESH8, K1H8, K2H8, and SDH8 finite elements used to test element shape sensitivity, left-side and right-side views, respectively.

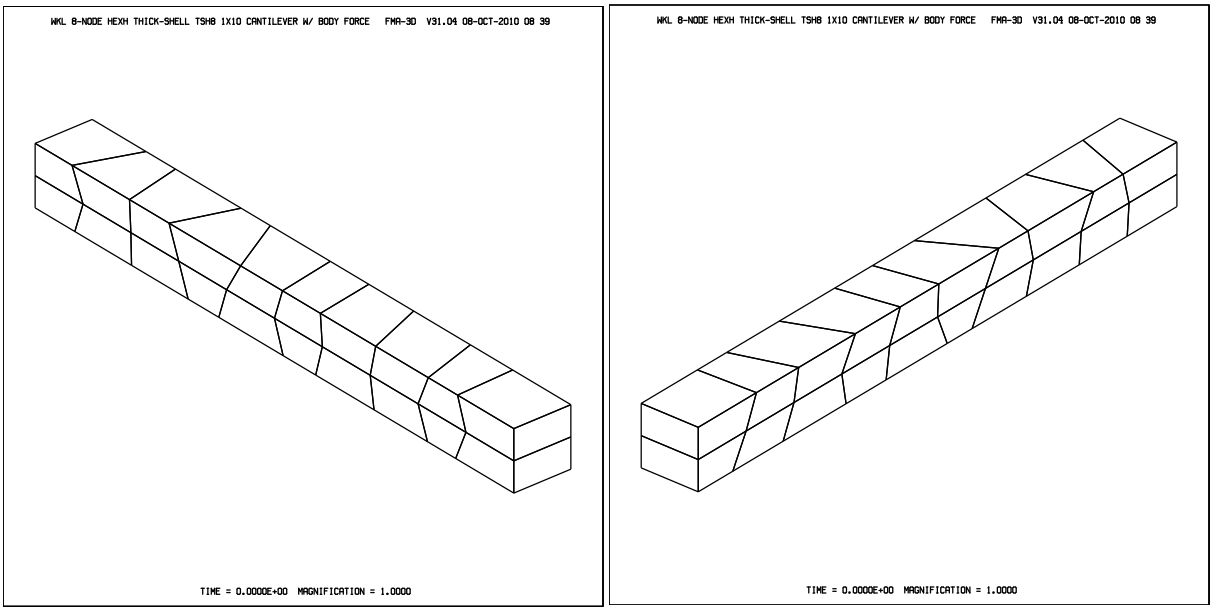

Figure 3.54. The random axial nodal point positions for the the TSH8 finite element used to test element shape sensitivity, left-side and right-side views, respectively.

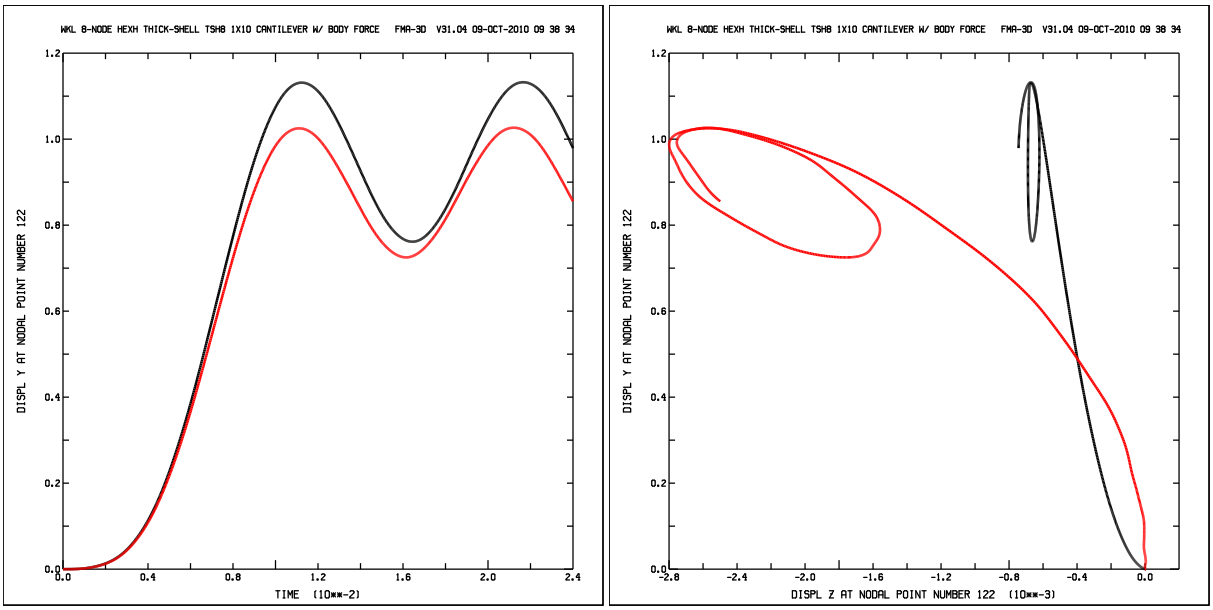

Figure 3.55. TSH8 Wing Kam Liu Thick Shell 8-node hexahedron finite element vertical tip deflection u_y *vs* time t, left panel. and a cross-plot of u_y *vs* lateral tip deflection u_z, right panel; black curves are from the uniform mesh results, and red curves are from irregular mesh results.

3.11.2 2-D Quadrilateral Shell Elements

Test Problem Statement. The square plates, pictured if Figure 3.56, are 4.0 inches by 4.0 inches, with a thickness of 0.01 inch. The boundary conditions are clamped, that is, zero displacement and zero rotation on all four sides. The reference solution comes from a 37×37 uniform mesh.

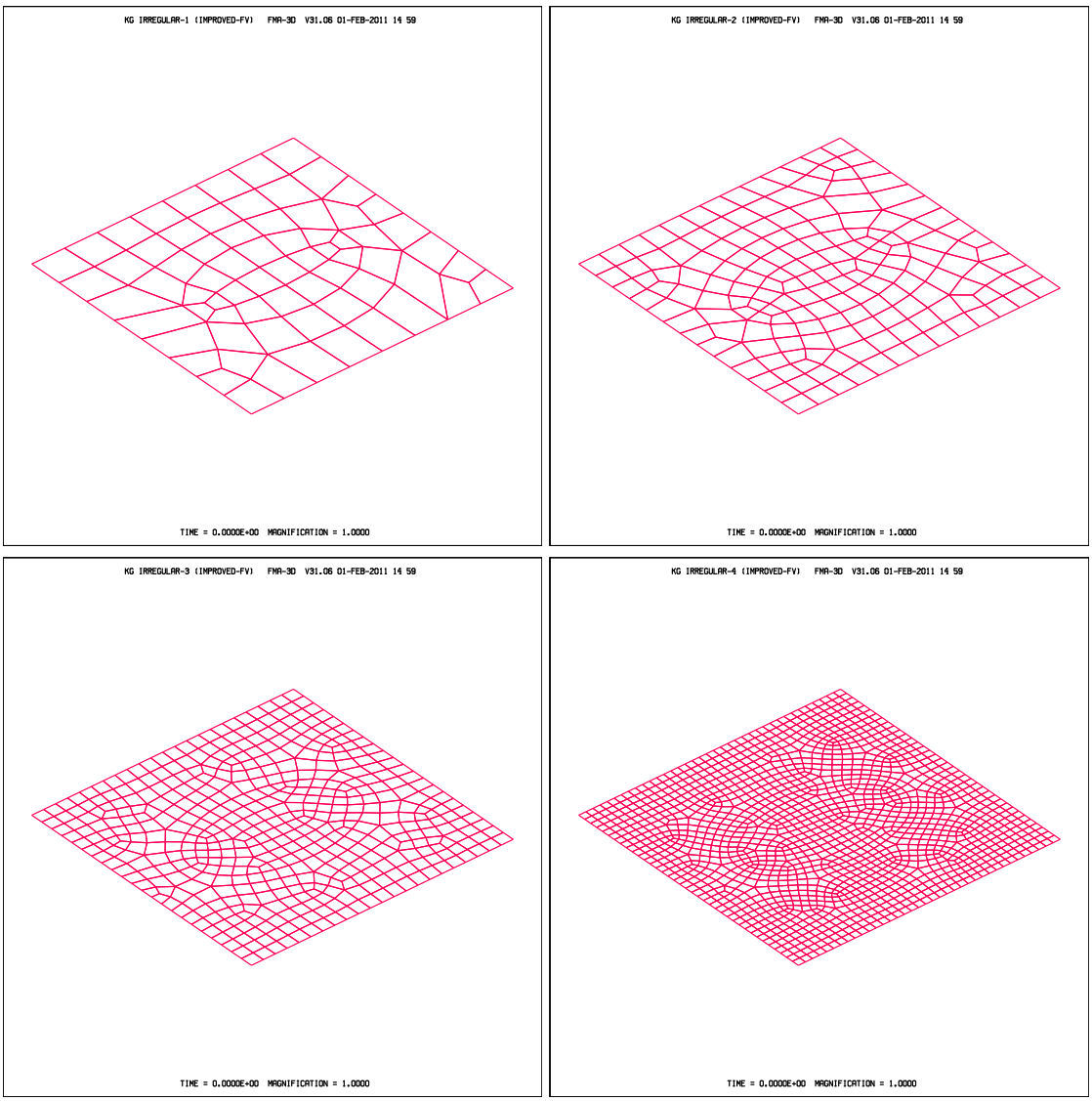

Figure 3.56. Square plate meshes with progressively finer resolution with their irregularity controlled by a fixed, interior elliptic boundary. The resolution sequence is nominally 8×8, 13×13, 22×22, 37×37.

The loading is a constant gravity loading of 100 g's applied at time equal to zero. (A "1 g" gravity loading equals a body force in lb_f/in^3 of $\rho \times 386.4$ in/sec^2.) The loading is zero at time $t = 0.0$ and is increased in time following a 10.0 ms duration cosine ramp to a value of 100.0 g's at which point the gravity forces are held constant until a time of $t = 40.0$ ms is reached. The static solution is obtained by using velocity damping at each nodal point. At $t = 40.0$ ms, the solution is fully damped to 4 significant digits.

The material is elastic with a Young's modulus of $E = 30.0 \times 10^{+6}$ psi, a Poisson's ratio of $\nu = 0.3$, and a density of $\rho = 5.0 \times 10^{-4}$ lb_f-sec^2/in^4.

Test Problem Characteristics. The reference problem is a standard, uniformly loaded, thin, square plate with clamped boundary conditions. The loading is sufficiently low that the central deflection is -0.01222 inches, just slightly more than the plate's thickness of 0.01 inches. The solution is bending dominated, that is, membrane stiffening due to finite deflections normal to the plate are not yet significant. The irregular meshes are "defined" by a *fixed* elliptical contour followed by using a *paved* mesh, a technique for generating quadrilateral meshes that conform to irregular boundaries. Ordinarily, the elliptical contour would represent a part with an opening or hole in it. Here, one may think of the elliptical contour as a step along the way to defining an outer coarse mesh and an inner fine mesh. The ultimate question being, can an irregular mesh utilizing shell elements produce a smooth and accurate bending solution when such meshes are needed? This test problem was crafted by Crane [2010]. The resolution sequence is nominally 8×8, 13×13, 22×22, 37×37. The actual numbers of 4-node quadrilateral finite elements in the irregular meshes are 70, 197, 511, and 1461, respectively.

Test Problem Results. The results of the study are tabulated in Table 11-3. The KGQ4 Key-Gruda plane-stress 4-node quadrilateral shell finite element exhibits 1% or less departure from the reference solution for all four irregular mesh resolutions; it is minimally affected by the mesh irregularities tested. The KHQ4 Key-Hoff plane-stress 4-node quadrilateral shell finite element exhibits a decided and unsatisfactory sensitivity to this sequence of irregular meshes. Very few of the individual quadrilateral elements depart in significant ways from rectangles, nonetheless, the overall result is a 38% degradation in deflection at the finest irregular 37×37 mesh.

Figures 3.57 and 3.58 are comparisons of normal deflection contours for the irregular and the regular meshes for the 37×37 resolution. What is evident is that the KGQ4 Key-Gruda plane-stress 4-node quadrilateral shell finite element exhibits only a small amount of sensitivity due to the irregular mesh in deflection amplitude and deflection pattern. The KHQ4 Key-Hoff plane-stress 4-node quadrilateral shell finite element exhibits a significant amount of sensitivity due to the irregular mesh both in deflection amplitude and in deflection pattern. Both finite elements perform well on regular meshes.

Table 11-3
Plate Center Deflection u_z Due to a Uniform Gravity Loading
(The reference solution was obtained from a 37×37
uniform mesh using the KGQ4 finite element.)

Irregular Mesh	KHQ4	KGQ4
8×8	-0.01155	-0.01232
13×13	-0.01108	-0.01217
22×22	-0.00961	-0.01225
37×37	-0.00763	-0.01220
Reference Result	-0.01222	-0.01222

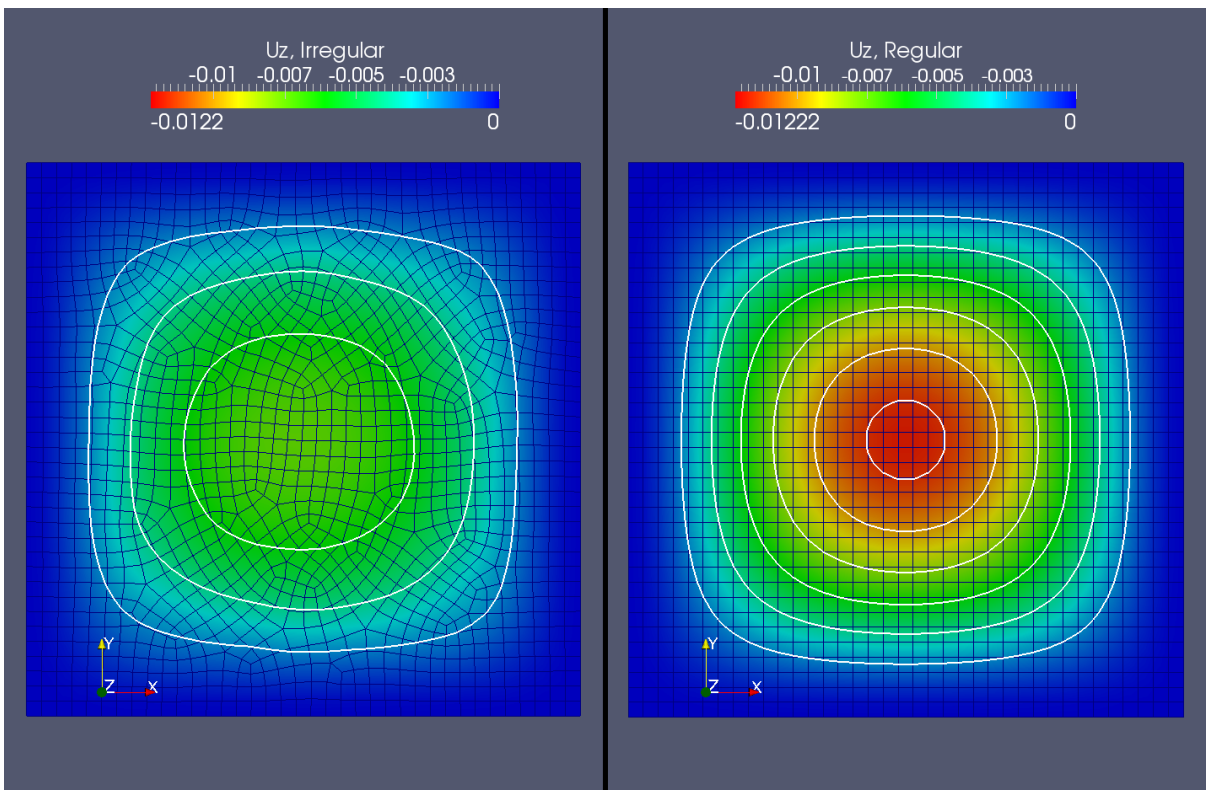

Figure 3.57. Irregular and regular fine mesh (37×37) solution contours for the KHQ4 shell finite element; contours are at the values of -0.0115, -0.010, -0.008, -0.006, -0.004, and -0.002 for displacement u_z. The irregular mesh (left panel) only exhibits the lowest three contours: -0.002, -0.004, and -0.006.

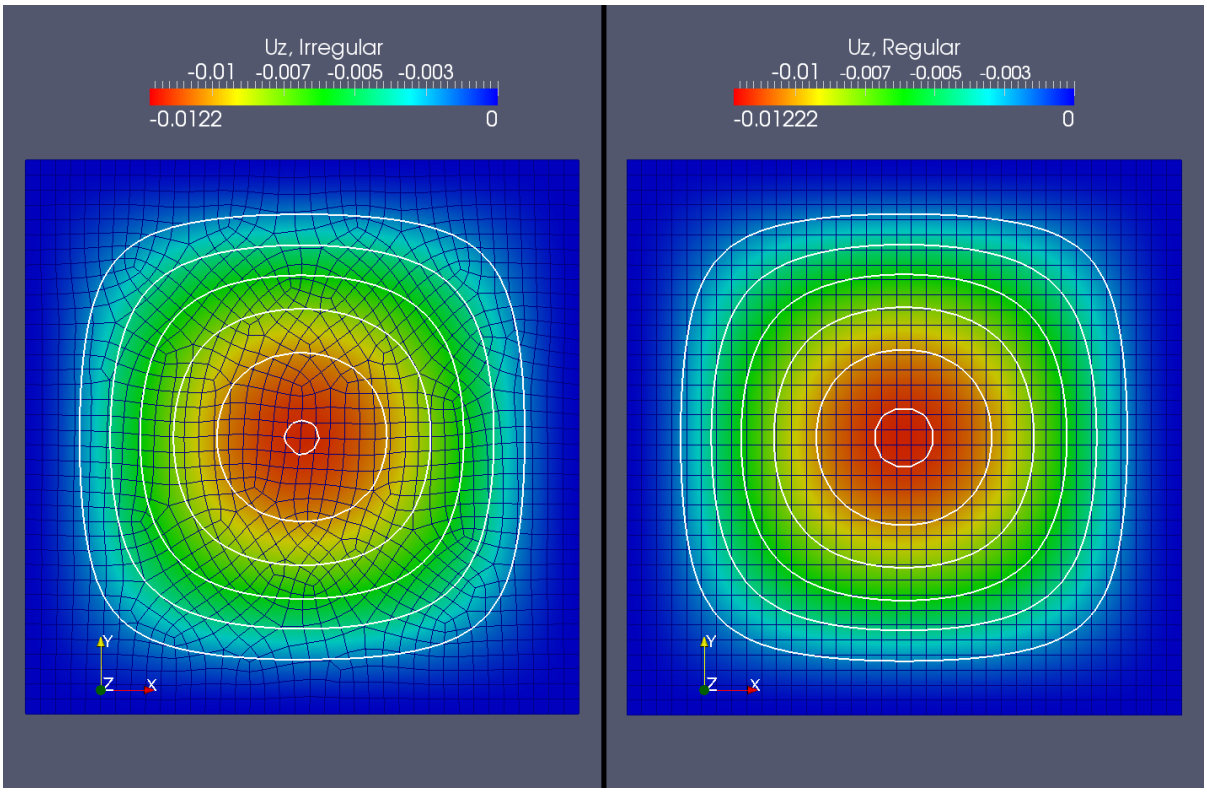

Figure 3.58. Irregular and regular fine mesh (37×37) solution contours for the KGQ4 shell finite element; contours are at the values of −0.0115, −0.010, −0.008, −0.006, −0.004, and −0.002 for displacement u_z.

3.12 Test Problem 12: Thick Shell to Thin Shell Transition

Test Problem Statement. The cantilever beam, pictured in Figure 3.59, has a length of 10 inches, a sequence of depths that varies from 5.0 inches to 0.1 inch, and a width of 1.0 inch. The boundary conditions are those of a cantilevered beam, namely, zero displacement and zero rotation at the root (far end), Figure 12.1.

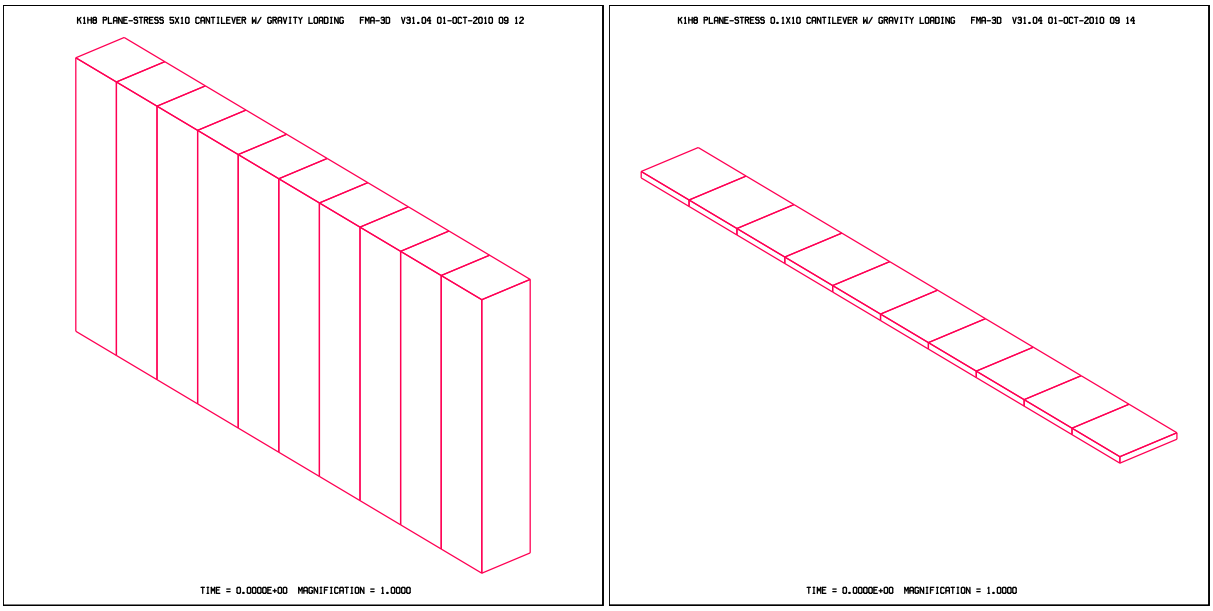

Figure 3.59. The end-members of a sequence of beam meshes consisting of a $1\times1\times10$ strip of 8-node hexahedral solid elements. The length to thickness ratio L/t varies from 2, the left panel, to 100, the right panel, the end-points of the L/t sequence (2, 5, 10, 20, 50, 100).

The loading is a constant gravity loading of 10 g's applied at time equal to zero. (A "1 g" gravity loading equals a body force in $\text{lb}_\text{f}/\text{in}^3$ of $\rho \times 386$ in/sec^2.) The static solution is obtained by nodal velocity damping.

The material is elastic with a Young's modulus of $E = 1.0 \times 10^{+6}$ psi, a Poisson's ratio of $\nu = 0.25$, and a density of $\rho = 2.61 \times 10^{-4}$ lb_f-sec^2/in^4.

Test Problem Characteristics. The test problem is a sequence of six beam geometries that vary in thickness (or 'depth' if one prefers) from 5 inches to 0.1 inch. At the *start* of the sequence the beam is deep compared to its length (10 to 5), and the continuum solution for the tip deflection due to a 10-g gravity load and a Timoshenko transverse-shear theory of bending with a 5/6 "correction" factor are very nearly equal. At the *end* of the sequence the beam is

thin compared to its length (10 to 0.1) and the tip deflection to a 10-g gravity load is given by a Kirchhoff bending theory. Between these two extremes the solution transitions from the transverse shear solution to the Kirchhoff solution. Here, the finite elements are based on a transverse shear formulation that incorporates the 5/6 correction factor.

A beam, plate, or shell transverse shear formulation has the characteristic that the strain energy density in the transverse shear term(s) grows faster than the bending strain energy density as the thickness goes to zero and, ultimately, approaches a Kirchhoff theory result. Computationally, a finite element based on a transverse shear formulation that becomes thin with respect to its in-plane dimension becomes quite ill-conditioned and "locks" giving erroneous results. The finite elements here (except ESH8) contain an anti-locking correction that limits the build-up of transverse shear strain energy density. Thus, the purpose of this test problem is to demonstrate that the finite elements give the transverse shear solution for a thick beam and properly transition to the classical Kirchhoff beam bending result as the beam becomes thin – without locking.

Test Problem Results. The results of the study are tabulated in Table 12-1.

Table 12-1
Cantilever Beam Tip Deflection Under a 10g Gravity Loading
(m,n) = (ranking for $L/t = 2$, ranking for $L/t = 100$)

Mesh	1×10	$1\times1\times10$	$1\times1\times10$	$1\times1\times10$	$2\times1\times10$
L/t	KHQ4 (2,2)	ESH8 (3,4)	K1H8 (1,3)	K2H8 (4,5)	TSH8 (5,1)
2*	-7.4773×10^{-4}	-7.4773×10^{-4}	-7.4773×10^{-4}	-7.4773×10^{-4}	-7.4773×10^{-4}
2	-7.5560×10^{-4}	-7.2997×10^{-4}	-7.5523×10^{-4}	-7.1646×10^{-4}	-9.2211×10^{-4}
5	-3.9291×10^{-3}	-3.8937×10^{-3}	-3.9163×10^{-3}	-3.6437×10^{-3}	-4.5963×10^{-3}
10	-1.5263×10^{-2}	-1.5130×10^{-2}	-1.5098×10^{-2}	-1.3622×10^{-2}	-1.6726×10^{-2}
20	-0.6060×10^{-1}	-0.5972×10^{-1}	-0.5875×10^{-1}	-0.4802×10^{-1}	-0.6250×10^{-1}
50	-0.3779×10^{-0}	-0.3677×10^{-0}	-0.3599×10^{-0}	-0.2693×10^{-0}	-0.3902×10^{-0}
100	-1.4865×10^{-0}	-1.4170×10^{-0}	-1.4173×10^{-0}	-1.0623×10^{-0}	-1.5185×10^{-0}
100*	-1.5112×10^{-0}	-1.5112×10^{-0}	-1.5112×10^{-0}	-1.5112×10^{-0}	-1.5112×10^{-0}

2*	Reference, $L/t = 2$: 2-D plane-stress solution (100×50 mesh)
100*	Reference, $L/t = 100$: 1-D Kirchhoff linear beam solution, Roark

All of the elements (except K2H8 and TSH8) exhibit a creditable response in modeling beam bending that ranges from thick ($L/t = 2$) to thin ($L/t = 100$) geometries. However, even with two TSH8 Wing Kam Liu Thick Shell finite elements through the thickness, the bending response for the thick beam example used here is 23% too great while for the thin beam example used here the bending response is quite close at 0.5% high. The K2H8 Key-Gullerud-Koteras multi-stress finite element while exhibiting a thick beam bending response of only 4% too stiff continues to stiffen as the beam becomes thin to the point where it is 30% too stiff.

Simulation Notes. This test problem leaves the mesh fixed while reducing the beam's depth. No exploration has been done regarding convergence with respect to mesh refinement.

Chapter 4

Evaluation Summary

4.0.1 Overview

While the text in Chapter 3 for each test problem contains details about how well each finite element formulation satified the objectives of the test problem, it remains to provide an overall summary from which one can rank, at least in an average sense, how well the individual formulations can be expected to perform in applications encountered year in and year out. To that end, a letter grade has been assigned albeit sometimes subjectively for each test problem. The number of A's, B's, C's, *et cetera* assigned have been totalled, and a grade point average (GPA) has been computed, based on a 4.0-system.

The test problems are suffciently varied that even the "best" formulation (KGQ4) received three B grades, and the "second best" formulation (K1H8) received two C grades. Unfortunately, the K1H8 finite element is the least practical formulation tested since it requires rigid links at the corners, a feature that can easily lead to "dueling" kinematic boundary conditions in everyday applications, and, hence, is a finite element that analysts will quickley come to avoid. In defence of the K1H8 finite element, its formulation and results, in an acdemic setting, are quite useful.

The following two tables, Tables 4-1 and 4-2, contain the aggragated results. Regarding the hexahedral solid finite elements in Table 4-1, they line up as follows in order of GPA: K1H8(3.54), ESH8(2.69), TSH8(2.15), K2H8(2.08), and SDH8(1.45). Regarding the quadrilateral and triangular shell finite elements in Table 4-2, they line up as follows in order of GPA: KHQ4(3.73), KHQ4(3.00), NCT3(2.8), and ECT3(1.20). Note that both the SDH8 Selective Deviatoric 8-node, hexehedral solid finite element and the ECT3 Element Centered 3-node triangular shell finite element were expected to perform poorly overall and did so even though they each collected several "A" ratings.

Summary Table 4-1
Test Result Letter Grade *vs* Solid Element Formulation

Test Problem	ESH8	K1H8	K2H8	TSH8	SDH8
1. Cantilever Beam	A	A	D	E	E
2. Twisted Beam	A	A	E	C	F
3. Point-Loaded Hemisphere	E	C	B	A	F
4. Raasch Hook	A	A	B	A	A
5. Beam Bent into a Ring	E	A	B	E	A
6. Membrane Patch Test	A	A	A	B	A
7. Sphere Patch Test	A	A	A	A	A
8. Pinched Cylinder	C	A	B	E	F
9. Vibrating Plate	B	B	D	B	E
10. Crushed Spherical Shell	C	B	E	C	C
11. Shape Sensitivity	B	A	C	C	D
12. Thick Shell Shear Limit	B	A	C	E	-
12. Thin Shell Shear Limit	C	C	D	A	-
Number of A's (+4.0)	5	9	2	4	4
Number of B's (+3.0)	3	2	4	2	0
Number of C's (+2.0)	3	2	2	3	1
Number of D's (+1.0)	0	0	3	0	1
Number of E's (+0.0)	2	0	2	4	2
Number of F's (-1.0)	0	0	0	0	3
Grade Point Average (GPA)	2.69	**3.54**	2.08	2.15	1.45

Briefly,

- **ESH8** Better for thick shells than for thin shells.
- **K1H8** Generally good, but impractical due to required corner constraints.
- **K2H8** Does not readily produce a plane-stress result.
- **TSH8** Can't be expected to be reliable; requires double-layer meshes when bending is important.
- **SDH8** Poor, not formulated for good bending results.

Summary Table 4-2
Test Result Letter Grade *vs* Shell Element Formulation

Test Problem	KHQ4	KGQ4	NCT3	ECT3
1. Cantilever Beam	A	A	D	E
2. Twisted Beam	A	A	C	F
3. Point-Loaded Hemisphere	A	B	B	F
4. Raasch Hook	F	A	C	B
5. Beam Bent into a Ring	A	A	A	A
6. Membrane Patch Test	A	B	A	A
7. Sphere Patch Test	A	A	A	A
8. Pinched Cylinder	A	A	C	E
9. Vibrating Plate	B	B	C	D
10. Crushed Spherical Shell	B	A	A	F
11. Shape Sensitivity	F	A	-	-
12. Thick Shell Shear Limit	A	-	-	-
12. Thin Shell Shear Limit	B	-	-	-
Number of A's (+4.0)	8	8	4	3
Number of B's (+3.0)	3	3	1	1
Number of C's (+2.0)	0	0	4	0
Number of D's (+1.0)	0	0	1	1
Number of E's (+0.0)	0	0	0	1
Number of F's (-1.0)	2	0	0	4
Grade Point Average (GPA)	3.00	**3.73**	2.8	1.20

Briefly,

- **KHQ4** Generally good except for the Raasch Hook and Shape sensitivity test problems.
- **KGQ4** Best overall performer, reliable and consistent.
- **NCT3** Based on a mixing rule with ECT3; does not have a reliable coefficent rule.
- **ECT3** Poor. (At best, it is a "place-holder" finite element.)

4.0.2 Comments on Individual Formulations

The following comments focus on the individual formulations to add insite for the tabulated ratings contained in the above Tables 4-1 and 4-2.

ESH8. The ESH8 Simo-Rifai Enhanced Strain 8-node hexahedral solid finite element is a formulation that introduces incompatible strain modes element-by-element to produce the

bending response characteristically associated with 1-D finite elements formulated from beam bending theory. The formulation has no preferred orientation and uses 3-D stress-strain constitutive material models. As a result, it can be meshed without concern for a plane-stress thickness direction. However, the ESH8 finite element is not ideally shape insensitive, test problem 11, nor can it model thin shells where it appears to develop shear locking, test problems 3 and 12. Its inelastic buckling capabilities are limited, test problems 8 and 10. It does satisfy the 2-D Irons patch test used here, test problem 6, and can be shown to satisfy a 3-D Irons patch test.

K1H8. The K1H8 Key-Gullerud-Koteras plane-stress, 8-node hexahedral solid finite element is a formulation that starts with a Taylor-series expansion of the stress field and obtains a set of exact analytically evaluated discrete gradient/divergence operators, that is, the operators take into account the finite element's exact geometrical shape irrespective of the departure from a regular hexahedron. The numerical quadrature is used to "sample" the stress field and project it onto the respective operator subspaces. Only constant membrane and bending *stress resultants* are retained when applying the divergence operators that produce the nodal point forces that drive the motion, or, in the case of a static solution are combined to satisfy equilibrium. The plane-stress material modeling means that there is a preferred element orientation which must be observed when generating a mesh. The K1H8 finite element reaches its limit of usefulness in the case of very thin shells, test problems 3 and 12. From a practical standpoint, it requires rigid links at the corners, a feature that can easily lead to "dueling" kinematic boundary conditions in everyday applications.

K2H8. The K2H8 Key-Gullerud-Koteras 3-D stress, 8-node hexahedral solid finite element is a formulation that parallels the development of the K2H8 finite element except that it uses full three-dimensional stress-strain constitutive models. Thus, the K2H8 finite element obviates the need for the kinematic constraints required by the K1H8 finite element's zero stiffness in the thickness direction engendered by the plane-stress constitutive models. The K2H8 finite element always has a *mean quadrature* thickness stress, and, consequently, tends toward a thick-shell solution, test problem 7.

TSH8. The TSH8 Wing Kam Lui 3-D stress, 8-node hexahedral solid finite element is a formulation that utilizes a *mean quadrature* core and retains a selected number of non-locking higher-order strain modes that provides a three-dimensional stress field without zero-energy hourglass modes. In its published form it relies on a four-point quadrature (a decimated $2\times2\times2$ Gauss quadrature) for efficiency. However, the element's response becomes sufficiently non-symmetric that only full $2\times2\times2$ Gauss quadrature results are used here. In a single-layer mesh (a $1\times m\times n$ mesh), the element's bending response is nonminally a factor of two too soft, and as a result all of the meshes used in the test problems were two-layer meshes. Even with the advantage of a two-layer mesh, it performed very poorly in a number of cases, namely, test problems 1, 5, 8, and 9.

SDH8. The SDH8 Selective Deviatoric 3-D stress, 8-node hexahedral solid finite element is a formulation that was *not* designed with superior bending performance in mind. The SDH8

finite element is a reduced integration element in that it has a *mean quadrature* bulk strain and pressure field also referred to in the literature as a "constant pressure" finite element. A user-selectable scaling is available that allows a reduction in the non-constant deviatoric stress and strain fields such that the finite element can be reduced to a pure *mean quadrature* formulation, however, for all of the work presented here the scaling was set to its default value of 1.0. The poor results in many of these test problems were predictable; the SDH8 was included in the test suite to document what would happen should it by chance be employed to model shells.

KHQ4. The KHQ4 Key-Hoff plane-stress 4-node quadrilateral shell finite element is a formulation that starts with the Mindlin-Reissner transverse shear plate bending theory and introduces the warped geometry that occurs with quadrilateral surfaces and focuses on constant membrane and bending stress *resultants* as its objectives (in place of a flat geometry approximation and a reduction to constant stress). The derivation elucidates the subtle transpose relationship between the gradient operator that produces the strain rates and the divergence operator that produces nodal forces and torques from the membrane and bending stress resultants. The KHQ4 finite element performs admirably well except for test problem 4, the Raasch Hook, the details of which can be found in the discussion of test problem 4, and test problem 11, Shape Sensitivity, the details of which can be found in the discussion of test problem 11. (It should be noted that a shell element with the sobriquet Key-Gruda, a 4-node quadrilateral finite element with internals obtained from the K1H8 plane-stress 8-node hexahedron has brought to light a need for converting the existing shell finite elements from using element-based vertex normal vectors to using globally defined nodal-based shell-surface fiber vectors. Some discussion of this is found in the comments of test problem 4.)

KGQ4. The KGQ4 Key-Gruda plane-stress 4-node quadrilateral shell finite element is a formulation that employs the hexahedral solid shell internals of the K1H8 solid 8-node finite element. However, it escapes the need to use nettlesome through-thickness kinematic constraints. In addition, it employs nodal-based surface unit-fiber vectors in the time-step-by-time-step reconstruction of the internal hexahedral frame. (Some discussion of the reason for using surface fiber vectors, as opposed to element-based corner normal vectors is found in the discussion of test problem 4.) The efficacy of this shell finite element is evident from it 3.73 GPA with only 'A' and 'B' ratings, Table 4-2 above. While at this stage of its development the KGQ4 finite element is computationally more expensive than the KHQ4 shell finite element, the KGQ4 shell finite element is consistently more accurate than all of the other solid and shell finite elements that are evaluated here.

NCT3. The NCT3 Nodal Centered plane-stress, 3-node triangular shell finite element is a formulation that uses area-weighted nodal velocity gradients to produce nodal-based membrane and bending stress resultants. The intent being to avoid the overly stiff response found with the conventional element-centered, one-point integrated 3-node triangular shell finite element. To-date, the formulation is overly soft and requires an only partially adequate "mixing" parameter defined as a function of element aspect ratio. The "mixing" parameter is used to blend in the overly stiff response of the ECT3 finite element, thus, obtaining more accurate results. Ideally, the mixing parameter should be a fixed value and result in between 1% to 5%

usage of the overly stiff results from the conventional element-centered, one-point integrated 3-node triangular shell finite element. It remains to be seen if the nodal-centered concept can be advanced to the point where it can be used reliably and routinely in everyday applications.

ECT3. The ECT3 Element Centered plane-stress, 3-node triangular shell finite element is a formulation that is best described as a one-point quadrature to find the gradient/divergence operators and multipoint quadrature through the thickness to compute the membrane and bending stress resultants. From a programming perspective, the element is at best a place-holder for a proper triangular shell finite element. Its performance in the test problems with grades from "A" through "F," means it is not recommended for use in everyday applications. However, it is fine for modeling the geometry of shells (or enclosed volumes) that are going to be treated as rigid bodies.

Chapter 5

Supporting Literature

5.1 Finite Element Formulations

5.1.1 ESH8, Simo-Rifai Enhanced Strain Hexahedron

The ESH8 Enhanced Strain finite element is thoroughly documented in the publication by Simo and Rifai [1990]. The publication by Simo and Rifai is their summary and foundational presentation of the *enhanced strain* concept put forward by a number of other finite element researchers in the years before 1990. On the surface, the enhanced strain concept is not complicated. The traditional bilinear quadrilateral and trilinear hexahedral displacement finite elements do not possess complete quadratic displacement fields, and, therefore, have quite deficient linear strain descriptions. The bilinear and trilinear displacement fields of these finite elements are missing the ability to describe the "bending" behavior common to beam theory, Figure 5.1.

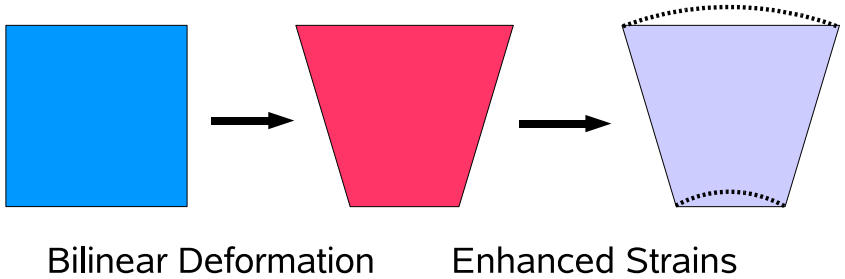

Figure 5.1. The bilinear deformation of a quadrilateral to which are added "enhanced strain" fields intended to provide the bending response embodied in beam bending theory.

The addition of enhanced strain fields is an element-by-element process and, therefore, produces slight implied discontinuities between neighboring finite elements due to spatial gra-

dients in the displacement field. If the enhanced strains are introduced as prescribed by Simo and Rifai, the discontinuities vanish as the mesh is refined since each finite element only needs to represent a *constant* stress state in the limit.

Within each finite element, the amplitudes of the enhanced strain modes are computed to minimize the strain energy density in the finite element. The minimization occurs at each load step in obtaining a static solution, and at each time step in computing a transient dynamic response. In the event that there is non-linear material behavior and/or nonlinear geometry changes included, the finite element's minimum energy solution requires an iteration sequence, generally, a Newton iteration.

The ESH8 Simo-Rifai enhanced strain hexahedron in spite of its elegant derivation is shape sensitive, that is, when it departs from an orthogonal hexahedron the efficacy of the enhanced strain modes noticeably diminishes.

Before reading the publication by Simo and Rifai [1990], it may be helpful to review the slides by Key [2007] where an overview of the the Simo and Rifai enhanced-strain, plane-stress quadrilateral formulation, the finite element internal numerical procedure, and example results are presented.

5.1.2 K1H8, Key-Gullerud-Koteras Plane-Stress Hexahedron

The K1H8 Key-Gullerud-Koteras plane-stress hexahedral finite element is documented in the publication by Key, Gullerud, and Koteras [2003]. The publication by Key, Gullerud, and Koteras starts by presenting and extending the *mean quadrature* concept to all of the stress-strain modes present in the trilinear displacement 8-node hexahedron. The publication then continues with adapting these ideas in a way that allows Reissner-Mindlin shell assumptions to be introduced, that is, only the stress components leading to constant membrane and bending stress resultants are retained. The balance of the stress-strain modes are retained with small coefficients multiplying them in order to control what would otherwise be zero-energy hourglass modes.

A particular advantage this finite element possesses is an exact set of gradient operators, the transpose of which are the divergence operators, that 'track' the finite element's shape and deformation exactly. Numerical quadrature is used only for sampling the element's stress state and projecting the stress state onto the respective stress-strain subspaces to obtain stress 'coefficients' for use with the subspace divergence operators. While the finite element is computationally expensive, it is the least shape sensitive of the finite elements tested here.

The KGQ4 Key-Gruda plane-stress 4-node quadrilateral below, uses this derivation and these same algorithms.

Because of plane-stress material modeling common in plate and shell theories, the element

requires rigid links in the thickness direction between the *lower surface* quadrilateral and the *upper surface* quadrilateral. From an every-day application perspective, the required introduction of these kinematic constraints makes the finite element rather unattractive.

5.1.3 K2H8, Key-Gullerud-Koteras Multi-Stress Hexahedron

The K2H8, Key-Gullerud-Koteras multi-stress hexahedron differs from the K1H8 finite element only in that it uses three-dimensional constitutive models and has no need of the rigid kinematic constraints connecting the upper and lower surface quadrilaterals. To date, however, the finite element does not use any numerical schemes to achieve a *plane-stress* solution, and, as a result, exhibits an undesirable, overly stiff response.

5.1.4 TSH8, Wing Kam Liu Thick Shell Hexahedron

The TSH8, Wing Kam Liu Thick Shell hexahedron finite element is documented in the publication by Liu, *et al* [1998]. There are missing important details for implementation, but the publication explains the major aspects of the finite element's derivation. The basic concept centers on an element that is nominally a mean quadrature element that retains a selected set of non-constant strain modes in terms of isoparameteric coordinates. The selection is based on omitting locking modes. It utilizes a local, physical r,s,t-coordinate system that has the r-coordinate and the s-coordinate directions while orthogonal, as nominally diagonal directions in the 'middle-surface' plane of the hexahedron. Further, as presented, the finite element uses a decimated $2\times2\times2$ Gauss quadrature that has only four integration points, and, as a result, has a slightly non-symmetric response. The implementation tested here uses a full $2\times2\times2$ Gauss quadrature as an improvement over the published finite element. The element is shape sensitive.

5.1.5 SDH8, Selective Deviatoric Hexahedron

The SDH8 Selective Deviatoric hexahedron has no publication associated with it. However, it is an ordinary mean quadrature bulk strain, mean quadrature pressure, but otherwise fully-integrated trilinear hexahedral finite element. In the technical literature, the finite element is sometimes called a B-bar ($\bar{B}$) finite element or a *reduced integration* finite element. As part of its implementation, it has a scale factor that allows the user to selectively reduce (hence the initials SD) the remaining non-constant deviatoric stress field; the factor can have values between 0.0 and 1.0, with the default value being 1.0. When the the selective deviatoric factor has a value of 0.0, the element becomes a *mean quadrature* hexahedron with no hourglass control. Because of the constant pressure feature the finite element does not have an artificially high stiffness in bending distortions, but it is *not* tuned to have the correct stiffness in bending. The

selective deviatoric finite element has no preferred orientations in the sense that the preceding finite elements have plane-stress orientations and traditional shell 'middle-surfaces,' even if implicitly.

Here, all of the testing of the SDH8 Selective Deviatoric element is conducted using a value for the SD factor of 1.0.

5.1.6 KHQ4, Key-Hoff Plane-Stress Quadrilateral

The KHQ4 Key-Hoff plane-stress 4-node quadrilateral finite element is documented in the publication by Key and Hoff [1995]. Using the current geometry of the finite element the vertex translational and rotational velocities are interpolated with bilinear shape functions. The derivation of the shell finite element centers on capturing the true geometric shape of the element by constructing normal vectors at the corner nodal points that are then interpolated over the surface with bilinear shape functions. The gradient and divergence operators are constructed in closed form through projections using a constant stress over the area of the quadrilateral plus linearly varying stress through the thickness, and, in addition, the transverse shear stress has components that vary linearly over the finite element's surface to capture the essential details needed to obtain a proper warping component for the bending stress resultant. The element performs very well in all of the test problems except for Test Problem 4, the Raasch Hook. The shortcomings of the finite element with respect to this test problem are discussed there.

The implementation details can be found in the Fma-3D Theoretical Manual, FMA Development, LLC [2010].

5.1.7 KGQ4, Key-Gruda Plane-Stress Quadrilateral

The KGQ4 Key-Gruda plane-stress 4-node quadrilateral finite element uses the same internal mechanics as the K1H8 Key-Gullerud-Koteras plane-stress, 8-node hexahedron, but without the need for kinematic constraints controlling the thickness dimension. Internally, the KGQ4 has a preamble, if you will, that sets up a hexahedral frame after which the same computations used in the K1H8 element are initiated. The gradient operator preamble carries out the following operations.

Element-by-Element KGQ4 Gradient Preamble

a) Gather nodal point coordinates, and translational and rotational velocities at the half-step time $t_{n+1/2}$.

b) Construct a local r,s,t-coordinate system with associated base vectors r_i, s_i, t_i.

c) Convert element geometry and kinematic variables to the local r,s,t-coordinate system.

d) Using the finite element's quadrilateral shape in three dimensions, numerically compute an accurate current surface area.

e) Using the initial volume and a constant-volume rule, compute the element's current thickness.

f) Using nodal-based surface common fiber vectors (initially surface normal vectors that have been rotated in time using nodal point rotational rates), construct an 8-node hexahedral frame. (Why the use of nodal-based common fiber vectors is important in the reconstruction of the hexehedral frame can be found in the discussion of results for Test Problem 4.)

g) Convert traditional shell finite element kinematic nodal variables to translational velocity at the eight nodal points of the hexahedron.

h) Initiate the three-dimensional finite element calculations on which the K1H8 hexahedral shell is based.

A similar preamble is used for the divergence operator construction at the end of the time step at time t_{n+1}. Thus, the KGQ4 finite element has all of the advantages offered by the K1H8 hexahedral shell, but does not require the use of rigid corner links to control the lack of stiffness in the thickness direction.

The results of the test problems used here have placed this formulation at the top of the list in terms of quality, however, it is computationally expensive. There is every indication that its expense can be reduced.

5.1.8 NCT3, Node-Centered Plane-Stress Triangle

The NCT3 Node Centered plane-stress 3-node triangular finite element has yet to be documented, however, its construction is easily outline as follows:

1. **Loop Over Elements**

a) Gather nodal point coordinates, and translational and rotational velocities at the half-step time $t_{n+1/2}$.

b) Construct the element-centered gradient operators in element-local r,s,t-coordinates.

c) Construct the element-centered velocity gradient $v_{i,j}$ at the half-step time $t_{n+1/2}$.

d) Transform the velocity gradient to global x,y,z-coordinates.

e) Disburse an area-weighted velocity gradient to the element's respective nodal points.

f) Update the element-centered stress from time t_n to t_{n+1}

2. **Loop Over Nodal Points**

a) Construct nodal-centered r,s,t-base vectors.

b) Transform the velocity gradient to r,s,t-coordinates.

c) Construct nodal-centered stretching D_{rs}

d) Update the nodal-centered stress from time t_n to t_{n+1}

e) Transform nodal-centered membrane and bending stress resultants to global x,y,z-coordinates and store.

3. **Loop Over Elements**

a) Copy element's nodal-centered stress resultants and transform to local r,s,t-coordinates at time $t_{n+1/2}$.

b) Blend in element-centered stress resultants to control short wave length modes that are too soft.

c) Gather nodal point coordinates, and translational and rotational velocities at the full-step time t_{n+1}.

d) Construct element-centered r,s,t-base vectors at time t_{n+1}

e) Construct divergence operators at time t_{n+1}.

f) Compute divergence of blended stress resultants.

g) Rotate forces and moments to global x,y,z-coordinates, store locally for subsequent nodal-pull assembly.

There are a couple of items to note in this computational sequence. First, the nodal-centered surface normal base vector t_i in Step 2.a is constructed from area-weighted normal base vectors obtained from the attached finite elements. Second, the nodal-centered stress resultants are converted to global x,y,z-coordinate components using nodal base vectors at time $t_{n+1/2}$ in Step 2.e and are pulled to the element's configuration in Step 3.a at tine $t_{n+1/2}$ and transformed to local element r,s,t-coordinates at time $t_{n+1/2}$, thus, the blending in Step 3.b with the element-centered stress resultants occurs in the same configuration where both were generated.

The blending of membrane and bending stress resultants is done separately and both are based on $(\alpha, 1-\alpha)$-rules. The objective is to take advantage of the too-stiff element-centered behavior of the ECT3 finite element to ameliorate the overly soft, short wave length modes

found in the pure nodal-centered formulation described above. Ideally, fixed factors in the range of 1% to 5% of the element-centered stress resultants are sought. To date, however, tuning done on the test problems here, have required a wide range in values for the blending factors that have no discernible pattern with respect to something such as finite element Aspect Ratio.

If the NCT3 formulation is going to see widespread acceptance in practical applications, some method of internally generating these blending factors will be required.

5.1.9 ECT3, Element-Centered Plane-Stress Triangle

The ECT3 Element Centered plane-stress, 3-node triangular finite element is based on following a "standard textbook" formula for deriving a finite element. The geometry is a simplex triangle in three-dimensional space within which the displacement and rotational degrees of freedom of a Reissner-Mindlin shell theory are linearly interpolated. Because the finite element is a simplex, the strain field is constant over the area of the triangle and, thus, the concepts of *one-point quadrature* and *mean quadrature* are indistinguishable. The only variation in strain and stress within the finite element is through the thickness due to bending. The constitutive evaluations through the thickness at a series of Gauss points is for the purpose of obtaining membrane and bending stress resultants. The integration through the thickness occurs *only* conceptually at the center of the finite element. There is nothing that can be done with under integration to improve the finite element's performance at the element level. The ECT3 finite element is overly stiff, and at best, is a placeholder waiting to be replaced with a more capable finite element. Nonetheless, this finite element is more than adequate for modeling the geometry of rigid bodies to which has been added an inertia tensor.

5.2 Reference Solutions

The majority of the test problems qualify as verification problems for which there is either an analytic solution or an independent source of results, possibly based on inference from assorted other attemps to quantify the result. Test Problem 10 is a validation calculation in that the expected results are from a rather complete suite of experimental results.

The publications from which the reference soulitions were obtained are listed here by test problem.

Test Problem 1: Cantilever Beam

Roark, R.J., "Formulas for Stress and Strain," 4th Edition, McGraw-Hill Book Company (1971).

Test Problem 2: Twisted Beam

MacNeal, R.H., and R.L. Harder, "A ProposedStandard Set of Problems to Test Finite Element Accuracy," *Journal of Finite Elements in Analysis and Design*, **Vol. 1**, 3-20 (1985).

Test Problem 3: Point-Loaded Hemisphere

MacNeal, R.H., and R.L. Harder, "A ProposedStandard Set of Problems to Test Finite Element Accuracy," *Journal of Finite Elements in Analysis and Design*, **Vol. 1**, 3-20 (1985).

Test Problem 4: Rassch Hook

Schoop H., J. Hornig, and T Wenzel, " Remarks on Raasch's Hook," *Technische Mechanik* **Band 22** Heft 4 259-270 (2002)

Wlassow, W.S., "Dünnwandige Elastische Stäbe", **Band 2** VEB Verlag für das Bauwesen Berlin (1964).

Knight Jr., N.F., "The Raasch Challange Problem for Shell Elements," *AIAA Journal* **Vol. 35** 375-381 (1997).

Kemp, B.L., C. Cho, and S.W. Lee, "A Four-Node Solid Shell Element Formulation with Assumed Strain," *International Journal of Numerical Methods in Engineering*, **Vol. 43** 909-924 (1998).

Hibbitt, Karlsson & Sorensen, Inc., *ABAQUS Theory Manual*, Version 6.2 (2001)

Test Problem 5: Beam Bent into a Ring

There is no reference for this test problem. The results are self-evident, that is, the initially straight beam is deformed into a circular ring by clamping one end and rotating the other end by 360 degrees. The exact answer is that the rotated end "arcs over" to match exactly the clamped end forming a perfect circle.

Test Problem 6: Irons Membrane Patch Test

MacNeal, R.H., and R.L. Harder, "A ProposedStandard Set of Problems to Test Finite Element Accuracy," *Journal of Finite Elements in Analysis and Design*, **Vol. 1**, 3-20 (1985).

Test Problem 7: Inflated Sphere Patch Test

Roark, R.J., "Formulas for Stress and Strain," 4th Edition, McGraw-Hill Book Company (1971).

Test Problem 8: Pinched Cylinder

Hauptmann, R., K. Schweizerhof, and S. Doll, "Extension of the Solid-Shell Concept for Application to Large Elastic and Large Elastoplastic Deformations," *International Journal for Numerical Methods in Engineering*, **Vol. 49** Issue 9, 1121-1141 (2000).

Test Problem 9: Vibrating Plate

Roark, R.J., "Formulas for Stress and Strain," 4th Edition, McGraw-Hill Book Company (1971).

Test Problem 10: Crushed Sphereical Shell

Pepin, J.E. and B.H. Thacker, "A Probabilistic Analysis to Quantify the Uncertainty in the Collapse Loading of Spherical Marine Floats," 44th AIAA/ASME/ASCE/AHS Structures, Structural Dynamics, and Materials Conference, 7-10 April 2003, Norfolk, Virginia, USA, **Paper No. AIAA 2003-1485** (2003).

Test Problem 11: Element Shape Sensitivity

Roark, R.J., "Formulas for Stress and Strain," 4th Edition, McGraw-Hill Book Company (1971).

Crane, N.K., Personal communication, Sandia National Laboratories, Albuquerque, New Mexico (2011).

Test Problem 12: Thick Shell to Thin Shell Transition

Roark, R.J., "Formulas for Stress and Strain," 4th Edition, McGraw-Hill Book Company (1971).

References

Crane, N.K., Personal communication, Sandia National Laboratories, Albuquerque, New Mexico (2011).

Fma Development, LLC, "Fma-3D Theoretical Manual," Version 30.0 (2009).

Hauptmann, R., K. Schweizerhof, and S. Doll, "Extension of the Solid-Shell Concept for Application to Large Elastic and Large Elastoplastic Deformations," *International Journal for Numerical Methods in Engineering*, **Vol. 49** Issue 9, 1121-1141 (2000).

Hibbitt, Karlsson & Sorensen, Inc., *ABAQUS Theory Manual*, Version 6.2 (2001).

Kemp, B.L., C. Cho, and S.W. Lee, "A Four-Node Solid Shell Element Formulation with Assumed Strain," *International Journal of Numerical Methods in Engineering*, **Vol. 43** 909-924 (1998).

Key, S. W. and C. C. Hoff, "An improved constant membrane and bending stress shell element for explicit transient dynamics," CMAME, Volume 124, Issues 1-2, Pages 33-47 (1995).

Knight Jr., N.F., "The Raasch Challange Problem for Shell Elements," *AIAA Journal* **Vol. 35** 375-381 (1997).

Liu, W.K., Y. Guo, S. Tang, T. Belytschko, "A Multiple-Quadrature Hexahedral Finit Element for Large Deformation Elastoplastic Analysis," CMAME, **Vol. 154**, 69-132 (1998).

MacNeal, R.H., and R.L. Harder, "A ProposedStandard Set of Problems to Test Finite Element Accuracy," *Journal of Finite Elements in Analysis and Design*, **Vol. 1**, 3-20 (1985).

Pepin, J.E. and B.H. Thacker, "A Probabilistic Analysis to Quantify the Uncertainty in the Collapse Loading of Spherical Marine Floats," 44th AIAA/ASME/ASCE/AHS Structures, Structural Dynamics, and Materials Conference, 7-10 April 2003, Norfolk, Virginia, USA, **Paper No. AIAA 2003-1485** (2003).

Roark, R.J., "Formulas for Stress and Strain," 4th Edition, McGraw-Hill Book Company (1971).

Schoop H., J. Hornig, and T Wenzel, " Remarks on Raasch's Hook," *Technische Mechanik* **Band 22** Heft 4 259-270 (2002).

Simo, J. C. and M.S. Rifai, “A Class of Mixed Assumed Strain Methods and the Method of Incompatible Modes,” IJNME, Vol. 29, pp 1595-1638 (1990).

Wlassow, W.S., “Dünnwandige Elastische Stäbe”, **Band 2** VEB Verlag für das Bauwesen Berlin (1964).

DISTRIBUTION:

1	MS 0372	J. G. Lupe Arguello Jr., 1525 (electronic)
1	MS 0372	Molly Bailey, 1525 (electronic)
1	MS 0824	James Bean, 1525 (electronic)
1	MS 0824	Joseph Bishop, 1525 (electronic)
1	MS 0372	Nicole Breivik, 1524 (electronic)
1	MS 9042	Arthur Brown, 8249 (electronic)
1	MS 9042	Michael Chiesa, 8249 (electronic)
1	MS 0372	Edmundo Corona, 1526 (electronic)
1	MS 0824	James Cox, 1526 (electronic)
1	MS 0380	Nathan Crane, 1542 (electronic)
1	MS 9042	Jeffrey Crowell, 8249 (electronic)
1	MS 0372	J. Franklin Dempsey, 1526 (electronic)
1	MS 9042	Jay Dike, 8249 (electronic)
1	MS 0372	Kristin Dion, 1525 (electronic)
1	MS 0380	John Dolbow, 1542 (electronic)
1	MS 0372	John Emery, 1524 (electronic)
1	MS 0372	Eliot Fang, 1524 (electronic)
1	MS 0372	Timothy Fuller, 1525 (electronic)
1	MS 0372	Jhana Gorman, 1524 (electronic)
1	MS 0372	Spencer Grange, 1524 (electronic)
1	MS 0372	Jeffrey Gruda, 1525 (electronic)
1	MS 1185	Arne Gullerud, 5417 (electronic)
1	MS 0372	Kenneth Gwinn, 1524 (electronic)
1	MS 0372	Shivonne Haniff, 1525 (electronic)
1	MS 0380	Martin Heinstein, 1542 (electronic)
1	MS 0372	Terry Hinnerichs, 1524 (electronic)
1	MS 0824	John Holland, 1524 (electronic)
1	MS 0372	Ryan Jamison, 1526 (electronic)
1	MS 0380	Joseph Jung, 1542 (electronic)
1	MS 0372	Jacob Koester, 1524 (electronic)
1	MS 9042	Timothy Kostka, 8249 (electronic)
1	MS 9042	Alex Lindblad, 8249 (electronic)
1	MS 0372	Chi (David) Lo, 1524 (electronic)
1	MS 0372	Kevin Long, 1524 (electronic)
1	MS 9409	Mark Merewether, 1542 (electronic)
1	MS 0372	Kurt Metzinger, 1524 (electronic)

1	MS	0380	Kyran Mish, 1542 (electronic)
1	MS	0346	Matthew Neidigk, 1526 (electronic)
1	MS	0824	Pania Newell, 1524 (electronic)
1	MS	9042	Jacob Ostein, 8246 (electronic)
1	MS	0380	Kendall Pierson, 1542 (electronic)
1	MS	0380	Vicki Porter, 1542 (electronic)
1	MS	0824	John Pott, 1525 (electronic)
1	MS	0824	Jonathon Rath, 1525 (electronic)
1	MS	0380	Nathan Roehrig, 1542 (electronic)
1	MS	0372	William Scherzinger, 1524 (electronic)
1	MS	0372	Jeffrey Smith, 1525 (electronic)
1	MS	0380	Benjamin Spencer, 1542 (electronic)
1	MS	9042	Nathan Spencer, 8249 (electronic)
1	MS	0380	Timothy Shelton, 1542 (electronic)
1	MS	0380	Jesse Thomas, 1542 (electronic)
1	MS	0824	Doug VanGoethem, 1526 (electronic)
1	MS	9042	Michael Veilleux, 8249 (electronic)
1	MS	0372	Gerald Wellman, 1525 (electronic)
1	MS	0380	David Womble, 1540 (electronic)
1	MS	0899	Technical Library, 9536 (electronic)

Sandia National Laboratories